



Multi-layer Cooperative Adaptive Cruise Control Subject to Heterogeneous Dynamic Limitations

DC 2018.075

A. Molina Acosta
Student ID: 1036456

Master Thesis

Coaches:

ir. J. Zegers (TNO)

dr. ir. M. Alirezaei (TNO)

Supervisors:

prof. dr. ir. N. van de Wouw

dr. ir. E. Lefeber

Eindhoven University of Technology
Department of Mechanical Engineering
Dynamics and Control

TNO
Technical Sciences
Department of Integrated Vehicle Safety

Eindhoven, September 2018

Declaration concerning the TU/e Code of Scientific Conduct for the Master's thesis

I have read the TU/e Code of Scientific Conduct¹.

I hereby declare that my Master's thesis has been carried out in accordance with the rules of the TU/e Code of Scientific Conduct

Date

August 24th, 2018

Name

Angel Molina Acosta

ID-number

1036456

Signature



Submit the signed declaration to the student administration of your department.

¹ See: <http://www.tue.nl/en/university/about-the-university/integrity/scientific-integrity/>
The Netherlands Code of Conduct for Academic Practice of the VSNU can be found here also.
More information about scientific integrity is published on the websites of TU/e and VSNU

Abstract

Cooperative Adaptive Cruise Control (CACC) is an innovative and promising vehicle technology that increases safety and road throughput, while decreasing traffic jams and fuel consumption. In real-life scenarios, vehicles in a platoon are likely to have heterogeneous longitudinal dynamics, which poses a challenge to the design of a CACC system. In this regard, a control strategy has been developed in the Integrated Vehicle Safety department at TNO intended to improve platoon cohesion when the vehicles have heterogeneous and dynamic acceleration limits. Using a multi-layer control approach, the control scheme prevents the platoon leader from accelerating beyond the capabilities of the following vehicles. In this thesis, the asymptotic stability of such a control strategy is thoroughly analyzed using a piecewise affine modelling framework, combined with classical frequency domain analysis, numerical methods for semi-definite programming, and computer simulations. Furthermore, an alternative control scheme is proposed, for which a stability analysis is conducted as well. The proposed control scheme is designed to overcome limitations of the existing multi-layer CACC strategy in terms of scalability and transient performance. The results from numerical analyses and computer simulations confirm stable responses and adequate performance of these control schemes.

Acknowledgements

This master thesis is the culmination of a yearlong project that I developed in collaboration with Eindhoven University of Technology and TNO's Integrated Vehicle Safety department. During this period of time, I received constant support from various coaches at TNO to whom I express my gratitude. Elham Semsar-Kazerooni, Jeroen Zegers, Mohsen Alirezaei, and Mauro Fusco, I am grateful for your time, patience, and useful feedback.

From the TU/e, I received invaluable support as well. Thank you prof. Nathan van de Wouw for the opportunity to collaborate with you, for your constant guidance, and accurate advice. Thank you dr. Erjen Lefeber for joining this project and for the time you invested in discussing and reviewing this report. Thanks to my classmates for sharing their knowledge, traditions, and cultures.

Finally, I would like to thank the people that, even when overseas, offered their support as if they were here with me. Thanks mom for your indefatigable care throughout almost 30 years. Thanks dad for helping me in the hard times. Thanks brother for all your advice. Thanks Richie for being my closest friend and for your editing expertise. Finally, thanks Irene for your love, patience, and courage that helped me to overcome my fears and got me through the tough times.

*"If I have seen further, it is by standing upon the shoulders of giants."
Isaac Newton, 1675.*

Contents

Contents	ix
Nomenclature	xi
1 Introduction	1
1.1 Literature survey	2
1.1.1 Heterogeneous actuation dynamics	2
1.1.2 Heterogeneous resistance forces	3
1.1.3 Heterogeneous constraints	3
1.2 Research approach	4
1.3 Outline	5
2 Multi-layer CACC strategies	7
2.1 Problem description	7
2.1.1 Vehicle model	7
2.1.2 Spacing policy and platoon model	9
2.1.3 Control objectives	9
2.2 Baseline multi-layer CACC strategy	10
2.3 Alternative multi-layer CACC strategy	12
3 Stability analysis	15
3.1 Preliminaries	15
3.1.1 Piecewise affine systems	15
3.1.2 Piecewise quadratic Lyapunov functions	16
3.2 Translating static non-linearities into a PWA system	20
3.3 Stability analysis for the baseline control scheme	23
3.3.1 A frequency domain approach to analyze the stability of a particular operation mode	23

3.3.2	Parametric stability analysis	27
3.4	Stability analysis for the proposed control scheme	31
3.4.1	Frequency domain analysis	31
3.4.2	Parametric stability analysis	32
4	Simulation study	35
4.1	Simulations for a 3-vehicle platoon	35
4.2	Simulations for larger platoons	40
4.2.1	4-vehicle platoon	41
4.2.2	10-vehicle platoon	46
5	Conclusions and recommendations	51
	Bibliography	53
	Appendices	55
A	Matrices used in the stability analysis of piecewise affine systems	55
A.1	Continuity matrices	55
A.2	Cell bounding matrices and the S-procedure	56
B	Additional parametric stability studies	59
C	Other attempts to improve the baseline multi-layer CACC strategy	63
C.1	A non-linear feedback in the coordination layer	63
C.2	A dynamic feedback in the coordination layer	65
C.3	Designing a full state-feedback for the coordination layer	67

Nomenclature

Acronyms

CACC	Cooperative Adaptive Cruise Control
PWA	piecewise affine
PWQLF	piecewise quadratic Lyapunov function

Roman symbols

t	time
a_i	acceleration of vehicle i
$a_{max,i}$	acceleration limit of vehicle i
$\hat{a}_{max,i}$	approximated acceleration limit of vehicle i
A_j	system matrix for j -th subsystem
\bar{A}_j	augmented system matrix for j -th subsystem
A_{rl}	road friction coefficient
b_j	affine term for j -th subsystem
\bar{B}_{rl}	internal friction coefficient
C_{rl}	air drag coefficient
d_i	inter-vehicle distance of vehicle i
e_i	spacing error of vehicle i
\bar{E}_j	cell bounding matrix for region j
\bar{F}_j	continuity matrix for region j
g	gravitational constant
g_j	hyperplane offsets for j -th subsystem
G_j	hyperplane matrix for j -th subsystem
\bar{G}_j	augmented hyperplane matrix for j -th subsystem
h	spacing policy timegap
i	vehicle index
\mathcal{I}	set of vehicle indices
i_d	driveline ratio
j	state space region index
\mathcal{J}	set of state space region indices
J_e	driveline mass moment of inertia
J_w	combined mass moment of inertia of the wheels
k	index of the vehicle with the lowest acceleration limit
k_p	CACC proportional gain
k_d	CACC derivative gain
k_v	cruise controller proportional gain
L_i	length of vehicle i
m_i	mass of vehicle i
m_{eq}	equivalent mass of rotating components

n	number of vehicles in the platoon
n_x	dimension of the state space
N	number of regions in the state space partition
P_j	symmetric matrix for quadratic function of region j
\bar{P}_j	augmented symmetric matrix for quadratic function of region j
q_i	position of vehicle i
r	standstill distance
R_w	wheel radius
T	unknown symmetric matrix
T_i	engine/brake torque of vehicle i
$T_{ref,i}$	desired engine/brake torque of vehicle i
$T_{max,i}$	maximum engine torque of vehicle i
u_i	intended CACC desired acceleration of vehicle i
$u_{ref,i}$	desired acceleration of vehicle i
U_j	unknown symmetric matrix with positive entries for region j
v_i	velocity of vehicle i
v_{des}	desired cruising speed
V	piecewise quadratic Lyapunov function
W_j	unknown symmetric matrix with positive entries for region j
x_i	state vector for vehicle i
x	lumped state vector
\bar{x}	augmented lumped state vector
\mathcal{X}_j	region of the state space partition
y_i	information vector of vehicle i
z_i	shifted state vector for vehicle i
z	shifted lumped state vector
\bar{z}	augmented, shifted, lumped state vector
\mathcal{Z}_j	region of the state space partition for shifted state vector

Greek symbols

α_i	rate of decrease for acceleration limit of vehicle i
β_i	maximum acceleration from rest of vehicle i
γ_p	coordination variable proportional gain
γ_d	coordination variable derivative gain
δ_{a_1, a_k}	performance index for the transient acceleration response
η_T	driveline efficiency parameter
θ_c	inter-vehicle communication time delay
θ_g	actuation time delay
ϕ_r	slope angle of the road
ξ_i	coordination variable of vehicle i
σ_i	coordination variable of vehicle i
τ	actuation dynamics constant

Chapter 1

Introduction

In present days, vehicle automation is attracting a considerable amount of attention from the automotive industry and the scientific community around the globe. Automation in passenger and commercial vehicles is expected to increase road safety by preventing traffic accidents related to human error [1]. Furthermore, as automated vehicles progressively replace manually driven ones, traffic congestion is expected to decrease [5]. In addition, vehicle automation can also contribute to reduce fuel consumption and, consequently, exhaust emissions [22].

Cooperative Adaptive Cruise Control (CACC) is an example of such vehicle automation of the longitudinal vehicle motion. The purpose of CACC is to automatically control the acceleration and deceleration of the vehicle in order to maintain a desired distance to the preceding vehicle. To achieve this, a CACC system relies on measurements of relative distance and relative speed with respect to the predecessor, which are acquired for example with a radar and cameras. Additionally, CACC employs wireless communication between vehicles to transmit relevant signals between platoon members. This communication allows the host vehicle to react faster to changes in acceleration of the predecessor.

In the field of vehicle automation, the term vehicle platoon is often used to refer to a set of vehicles that follow each other, while interacting through a sensing and (possibly) a communication network. Vehicles driving in a platoon while employing CACC can follow each other at a short inter-vehicle distance [13], which is beneficial in terms of road throughput (i.e., more vehicles can fit on the road). Moreover, when the vehicles drive sufficiently close to each other, the aerodynamic drag is reduced [22]. This can provide a significant reduction of fuel consumption, in particular for heavy-duty trucks.

An additional benefit of CACC is its potential to attenuate disturbances as these propagate upstream through the platoon. As expressed in [14], the notion of string stability refers to the evolution of disturbances across the vehicular platoon. Disturbances might originate, for example, from variations in the acceleration of the leading vehicle. String stable behavior is desired because it achieves smoother traffic flow (i.e., with less accelerating and decelerating) and prevents the so-called ghost traffic jams.

Still, various challenges need to be addressed before CACC becomes a mature technology that can be commercially available. For instance, the fact that vehicles in a platoon might have different longitudinal dynamics is a key aspect that has motivated several research studies. Designing a CACC system for platoons of heterogeneous vehicles is a complex task because one must consider that different vehicles might have very different responses to the same input. Moreover, vehicles have a limited engine torque, which restricts their acceleration capabilities. If the vehicles in a platoon have heterogeneous torque limitations, the cohesion of the platoon might be compromised if the CACC system does not take into account the limitations in acceleration.

To the best of the author's knowledge, a comprehensive study addressing the issues mentioned previously has not been conducted yet. The present thesis intends to design and analyze a CACC strategy that provides adequate performance, focusing particularly on platoon cohesion, while considering heterogeneities in the acceleration capabilities of the platoon members.

1.1 Literature survey

A vast amount of literature addresses the design, asymptotic stability, and string stability properties of CACC controllers. In various studies, the authors assume all vehicles in the platoon to have identical longitudinal dynamics (cf. [12], [13], [24]). However, in reality, even for a platoon of vehicles of the same brand and model, differences in the longitudinal dynamics can be expected. To broaden its scope of application, a CACC system should be able to deal with heterogeneous vehicles. To identify what solutions have been proposed to address heterogeneities in the vehicle platoon, a literature survey is conducted and the relevant findings are presented here.

1.1.1 Heterogeneous actuation dynamics

In various publications that deal with vehicular platooning, the longitudinal dynamics of the vehicle are represented with a third-order linear dynamic model that describes the position, velocity, and acceleration of the vehicle, with the input being a desired acceleration. In such models, the actuation dynamics is modelled as a first-order lag filter characterized by a certain time constant. As explained in [13], to arrive at this linear model, it is assumed that a low-level controller is used to achieve input-output linearization of a more complex, non-linear model for the driveline dynamics, which considers the engine and (possibly) the braking dynamics.

It could be assumed that all vehicles in the platoon employ a low-level controller that linearizes the driveline dynamics in such a way that all vehicles behave as if they all had the same time constant for the actuation dynamics. This approach might not have wide acceptance from the drivers, since the potentially fast driveline dynamics of a sports car would be hindered by the slow dynamics of other platoon members. Alternatively, various authors have proposed CACC controllers considering heterogeneous time constants. For instance, in [18] a decentralized control strategy is proposed with a one-vehicle look ahead topology, i.e., the desired acceleration of the preceding vehicles serves as a feedforward signal for the host vehicle. The host vehicle must be informed about the actuation dynamics of the predecessor to compensate for the difference with respect to its own actuation dynamics, which is done using a lead/lag filter.

A different approach to handle heterogeneous actuation dynamics can be found in [3], where the authors represent the heterogeneous time constants as an uncertainty around a nominal value and propose an adaptive controller to estimate the actual value of the time constant. The authors also propose a switching mechanism to alternate from CACC to Adaptive Cruise Control (ACC), in case the inter-vehicle communication fails.

Yet another example can be found in [15], where the authors consider heterogeneous actuation dynamics and they evaluate various communication topologies, such as one-vehicle look-ahead, leader-following, and a combination of these two. The authors propose decentralized feedback controllers where the control gains are chosen differently for each vehicle in the platoon, depending on its actuation dynamics. Additionally, the authors define string stability for a heterogeneous platoon as the property of maintaining bounded spacing errors, regardless of the platoon size and vehicle ordering (i.e., whether a vehicle with slow actuation dynamics is followed by a vehicle with faster dynamics or vice-versa).

1.1.2 Heterogeneous resistance forces

Turning now to other sources of heterogeneity, some authors have considered heterogeneous resistance forces acting on the vehicles. For example, these forces can be related to the inertia, i.e., vehicle mass, aerodynamic drag, rolling resistance, and gravitational forces due to the slope of the road. Some relevant examples found in the literature that focused on heterogeneity with respect to these forces are described next.

Already in the 1960's, vehicular platooning for passenger transportation was being analyzed. For instance, [8] used optimal control theory to design a controller that regulates the spacing and velocity errors of a string of vehicles with heterogeneous masses and drag coefficients. However, the authors point out that their approach is limited because each vehicle needs information from all the other platoon members to determine its control input. Another example dating from the 90's can be found in [16], where the authors discuss a decentralized feedback control designed using a pole-placement approach where heterogeneity with respect to aerodynamic drag and vehicles mass is treated as an external perturbation. However, these authors do not address the problem of platoon cohesion.

The effect of heterogeneous resistance forces has also been modelled as uncertainty in the longitudinal dynamics or as external disturbances. For instance, in [2] and [9] the authors use robust control techniques to design a CACC controller for vehicles with uncertain dynamics, considering distinct actuation dynamics for the engine and braking system of the vehicle. On the other hand, in [21] sliding mode control is used to deal with the uncertainty in the air drag coefficient, slope of the road, and rolling resistance.

1.1.3 Heterogeneous constraints

Apart from vehicle heterogeneity, an additional challenge in the design of CACC arises from possible constraints in velocity or acceleration, as a consequence of limited actuator capabilities, e.g., limited engine or braking torque. The work of some authors that have considered constraints on the control inputs are discussed next.

Some CACC controllers have been proposed to deal with actuator saturation. In [6], a method is proposed to determine acceptable control gains, depending on the initial conditions of the vehicle (i.e., initial velocity, acceleration, and spacing error), to prevent the control input for the vehicle from exceeding a certain saturation level. A different approach can be found in [19], where an error-governor methodology is used to prevent integral windup when the vehicle reaches its saturation level. However, the main limitation of these studies is that the saturation level is assumed to be the same for all platoon members, which implies they are capable of reaching the same maximum acceleration. Furthermore, these authors do not explore the effect of actuator saturation on platoon cohesion when one or more vehicles are in saturation.

In [24], the authors employ consensus control to handle a constraint in the velocity of one of the platoon members. The authors propose a decentralized controller with a bidirectional communication topology, where the desired acceleration for each vehicle is determined based on the input of the preceding vehicle, the spacing error of the following vehicle, and the spacing error of the host. The authors do not analyze the case where more than one vehicle has a velocity constraint and no acceleration constraints are considered, which limits the scope of their technique.

An interesting control approach is proposed in [25], where the authors consider vehicles with heterogeneous actuation dynamics and input constraints. In this work, model predictive control is used to deal with heterogeneous constraints on the driving/braking torque of the vehicles. However, the authors only present results for the case when the heterogeneous constraints on the driving torque still allow all the vehicles to develop the same acceleration levels. No discussion of

heterogeneous acceleration limits is offered therein.

Yet another example can be found in [17], where the authors consider a platoon of vehicles subject to a dynamic acceleration limit defined as a function of the vehicle velocity and the slope of the road. Furthermore, the authors consider vehicles with different power-to-weight, meaning the acceleration limits among the platoon members are heterogeneous. The authors use a leader-predecessor following topology so that the desired acceleration for all vehicles is influenced by the leader's and the predecessor's input. With this topology, when a vehicle reaches its acceleration limit, the vehicle behind it might crash into the former in an attempt to follow the leader's motion. The control strategy proposed therein aims to prevent collisions in such a scenario, which is achieved by means of an adaptive spacing policy. However, their approach is not designed to guarantee platoon cohesion when one of the vehicles reaches its acceleration limit.

1.2 Research approach

The various publications encountered in the literature review in Section 1.1 indicate that extensive research on vehicle platooning has been conducted, considering various types of heterogeneity. However, few authors have considered vehicles with heterogeneous constraints in acceleration, let alone dynamic acceleration constraints, i.e., constraints that dependent on the vehicle's velocity. Moreover, to the best of the author's knowledge, the adverse effect of acceleration limits on the cohesion of the platoon has not been addressed. To this end, in [23] the authors propose a novel multi-layer CACC strategy that improves platoon cohesion when the vehicles are subject to heterogeneous and dynamic acceleration limits.

In [23], the authors present results from simulations and experiments that indicate an adequate performance of the control strategy proposed therein. However, the authors do not analyze the stability of the platoon dynamics, neither do they explore the scalability of their technique nor the influence of the vehicle parameters and control gains on performance. These open issues motivate the research described in this thesis.

The objectives for this project are as follows. First, we aim to derive mathematical models for the closed-loop platoon dynamics of vehicles subject to heterogeneous and dynamic acceleration limits, when applying the CACC strategy proposed in [23]. Then, using these models, we aim to perform stability analyses in order to provide further insight on the behavior observed in the simulation results from [23]. A further objective is to assess the scalability of this strategy and analyze the influence of the vehicle parameters, control gains, and the spacing policy on stability and performance. A final objective is to develop an improved CACC strategy that achieves better performance in face of dynamic acceleration limits.

As will be explained later, the control scheme proposed in [16] involves various non-linearities that can be represented as a switching system. This makes the stability analysis a complex task. To address this problem, in this report the platoon dynamics are modelled as piecewise affine (PWA) systems, for which asymptotic stability can be proven using piecewise quadratic Lyapunov functions (PWQLF) that are derived from linear matrix inequalities (LMI), which can be solved via numerical methods [4]. In addition to the analytical and numerical tools used to model and assess the stability of the platoon dynamics, computer simulations are also conducted to evaluate the performance of the control algorithms in different scenarios, including more realistic phenomena such as time delays in communication, gear-shifting, and non-linear, dynamic acceleration limits.

1.3 Outline

The content of this report is organized as follows. Chapter 2 formally describes the platooning problem being addressed, including the model used for the vehicle dynamics and the dynamic acceleration limitation. Additionally, in Chapter 2 the multi-layer CACC strategy from [23] is presented, together with an alternative strategy that intends to improve performance and extend the scalability of this platooning technique. In Chapter 3, the mathematical theory employed to model the platoon dynamics and analyze asymptotic stability is presented and is applied to the multi-layer CACC strategies, while considering different values for the parameters in the model. Chapter 4 presents simulation results that compare the benefits and limitations of the control strategies when applied to platoons of various sizes. Finally, Chapter 5 offers conclusions and recommendations for future work.

Chapter 2

Multi-layer CACC strategies

The structure of this chapter is as follows. Section 2.1 presents the control problem. Hereto, the model used to represent the longitudinal vehicle dynamics is described, together with the dynamic acceleration limit that results from a limitation in engine torque. In Section 2.2, the multi-layer CACC strategy proposed in [23] is described. An alternative CACC design is proposed in Section 2.3.

2.1 Problem description

2.1.1 Vehicle model

A platoon of n vehicles is considered. For all vehicles in the platoon, the longitudinal dynamics are described with the following non-linear dynamics:

$$\begin{cases} \dot{q}_i(t) = v_i(t) \\ \dot{v}_i(t) = \frac{1}{m_i + m_{eq}(v_i)} \left(\frac{\eta_T i_d(v_i)}{R_w} T_i(t) - C_{rl} v_i^2(t) - B_{rl} m_i v_i(t) - A_{rl} m_i \cos(\theta_r(t)) - m_i g \sin(\phi_r(t)) \right) \\ \dot{T}_i(t) = -\frac{1}{\tau_i} T_i(t) + \frac{1}{\tau_i} T_{ref,i}(t - \theta_g), \end{cases} \quad \forall i \in \mathcal{I}, \quad (2.1)$$

where i denotes the vehicle index and the set $\mathcal{I} = \{1, \dots, n\}$ collects all vehicle indices. Herein, t denotes time, q_i is the position of vehicle i , defined at the rear bumper as illustrated in Figure 2.1), v_i is the velocity, and T_i is the engine torque. The input to the system is $T_{ref,i}$, the desired torque, which is subject to the actuation delay θ_g . The parameter τ_i corresponds to the driveline time-constant.

In (2.1), m_i is the (heterogeneous) vehicle mass, η_T is the transmission efficiency parameter, R_w is the wheel radius, $i_d(v_i)$ is the driveline ratio, and $m_{eq}(v_i)$ is the equivalent mass of the rotating components in the driveline, defined as

$$m_{eq}(v_i) = \frac{i_d^2(v_i) J_e + J_w}{R_w^2}, \quad (2.2)$$

where J_e and J_w are the moments of inertia of the engine and wheels, respectively. The coefficients C_{rl} , B_{rl} , and A_{rl} are associated to aerodynamic drag, internal friction, and road friction, respectively. The slope of the road is defined by the angle $\phi_r(t)$ and the gravitational constant is denoted with g . In general, all the vehicle parameters in (2.1) and (2.2) could be different between

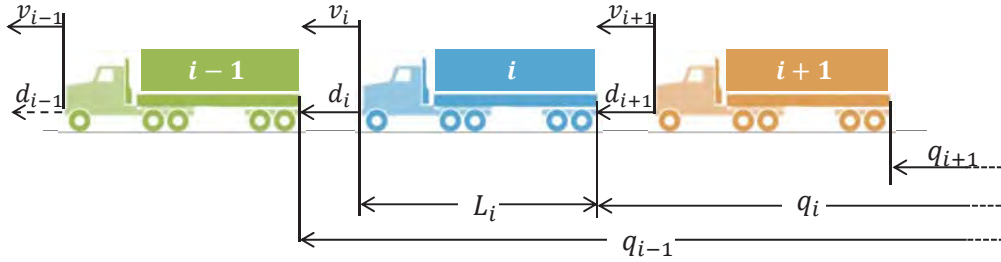


Figure 2.1: Schematic of a vehicle platoon.

platoon members, i.e., the parameters could be considered as being heterogeneous. However, in this report only the vehicle mass is considered to be heterogeneous as this parameter may vary significantly from one vehicle to another, especially when dealing with commercial vehicles due to changes in their cargo. The effect of heterogeneity with respect to other vehicle parameters is considered to be beyond the scope of this research.

In order to model the effect of gear-shifting, the driveline ratio $i_d(v_i)$ is defined as a piecewise-constant function of velocity. In other words, $i_d(v_i)$ takes different constant values for different velocity ranges, based on a simplistic gear-shifting strategy (an example of this strategy is provided later in the report). Notice that, as the driveline ratio $i_d(v_i)$ appears in expression (2.2), the equivalent mass $m_{eq}(v_i)$ is also a piecewise-constant function of velocity.

Assuming that the engine torque is subject to an upper-bound $T_{max,i}$, then the vehicle is only able to develop a certain maximum acceleration. In fact, setting $T_i = T_{max,i}$ in the second equation in (2.1) leads to the following expression for the maximum acceleration of vehicle i :

$$a_{max,i}(v_i) = \frac{1}{m_i + m_{eq}} \left(\frac{\eta T^{i_d}}{R_w} T_{max,i} - C_{rl} v_i^2 - B_{rl} m_i v_i - A_{rl} m_i \cos(\phi_r(t)) - m_i g \sin(\phi_r(t)) \right), \quad \forall i \in \mathcal{I}. \quad (2.3)$$

As the velocity of the vehicle appears in (2.3), the function $a_{max,i}(v_i)$ represents a dynamic acceleration limit for the vehicle. Moreover, as the driveline ratio i_d and equivalent mass m_{eq} are piecewise-constant in v_i , the function $a_{max,i}(v_i)$ is piecewise-continuous in v_i . As stated previously, in this study it is assumed that the vehicle mass m_i can differ between vehicles in the platoon, which results in heterogeneous acceleration limits. Notice that the driveline time-constant τ_i does not influence the acceleration limit defined in (2.3). Since this study focuses primarily on the effect of limitations in acceleration, in the remainder of this work the driveline time-constant is assumed to be homogeneous for all vehicles in the platoon (i.e., $\tau_i = \tau, \forall i \in \mathcal{I}$).

As explained in [23], with a suitable control law for the desired torque $T_{ref,i}$, the dynamics in (2.1) can be linearized using an input-output feedback linearization technique. To apply this technique one takes the time derivative of the expression for \dot{v}_i in (2.1) and then an expression for the reference torque $T_{ref,i}$ can be derived such that the resulting expression for \dot{T}_i cancels out the non-linearities in the expression for \dot{v}_i . For the sake of simplicity, this linearization procedure is applied assuming the driveline ratio i_d and slope of the road θ_g are time invariant; this means that the expression for $T_{ref,i}$ is not able to linearize the dynamics during transients when the driveline ratio or the slope of the road are changing. The resulting linear dynamics are as follows [13]:

$$\begin{cases} \dot{q}_i(t) = v_i(t) \\ \dot{v}_i(t) = a_i(t) \\ \dot{a}_i(t) = -\frac{1}{\tau} a_i(t) + \frac{1}{\tau} u_{ref,i}(t - \theta_g) \end{cases}, \quad \forall i \in \mathcal{I}, \quad (2.4)$$

where a_i is the acceleration and the new input $u_{ref,i}$ corresponds to the desired acceleration that is subject to the actuation delay θ_g . To account for the limit in engine torque in the linearized

dynamics, the function $a_{max,i}$ as in (2.3) is used to restrict the input $u_{ref,i}$ with the following non-linear expression:

$$u_{ref,i} = \min [a_{max,i}(v_i) , u_i], \forall i \in \mathcal{I}, \quad (2.5)$$

where u_i is the desired acceleration prescribed by a controller defined later in this chapter. The restriction presented in (2.5) prevents the desired acceleration from reaching values that are beyond the capabilities of the vehicle. The linear system in (2.4) together with the restriction in (2.5) are used in this study to represent the longitudinal dynamics of a vehicle that is subject to a dynamic acceleration limit.

2.1.2 Spacing policy and platoon model

Consider a group of n vehicles that are following each other forming a platoon, as represented in Figure 2.1. Then, the inter-vehicle distance d_i (i.e., the gap between consecutive vehicles) can be defined as

$$d_i(t) = q_{i-1}(t) - q_i(t) - L_i, \forall i \in \mathcal{I} \setminus \{1\}, \quad (2.6)$$

where L_i is the length of vehicle i .

The vehicles should maintain a desired inter-vehicle distance d_{des} defined with the following spacing policy:

$$d_{des,i}(t) = r + hv_i(t), \forall i \in \mathcal{I} \setminus \{1\}, \quad (2.7)$$

where r is the standstill distance (i.e., the gap that should remain between vehicles if they come to a full stop) and h is the desired timegap (i.e., the time it takes to travel a certain distance at the current speed). As explained in [14], a velocity-dependent spacing policy can contribute to achieve string stability (i.e., disturbance attenuation in upstream direction). Combining (2.6) and (2.7), the spacing error between consecutive vehicles is defined as

$$e_i(t) = d_i(t) - d_{des}(t) = q_{i-1}(t) - q_i(t) - L_i - r - hv_i(t), \forall i \in \mathcal{I} \setminus \{1\}. \quad (2.8)$$

A state space representation of the open-loop platoon dynamics is provided next. Let the state vector for vehicle i be

$$x_i = (e_i \quad v_i \quad a_i)^T, \forall i \in \mathcal{I} \setminus \{1\}, \quad (2.9)$$

and for vehicle 1 the state vector is $x_1 = (v_1 \quad a_1)^T$. Combining the linear dynamics in (2.4) and the spacing error definition in (2.8), the open-loop platoon dynamics are described with the following set of differential equations:

$$\begin{cases} \dot{v}_1 = a_1 \\ \dot{a}_1 = -\frac{1}{\tau}a_1 + \frac{1}{\tau}u_{ref,1} \\ \dot{e}_i = v_{i-1} - v_i - ha_i \\ \dot{v}_i = a_i \\ \dot{a}_i = -\frac{1}{\tau}a_i + \frac{1}{\tau}u_{ref,i}, \end{cases} \quad (2.10)$$

for $i \in \mathcal{I} \setminus \{1\}$. The inputs for this system are the desired accelerations $u_{ref,i}$ for $i \in \mathcal{I}$ as defined in (2.5), which in turn depend on the acceleration limits $a_{max,i}$ defined in (2.3) and the intended desired accelerations u_i prescribed by a controller that will be presented later in this report. Because of the dynamic acceleration limit in (2.3) and the minimum function in (2.5), the platoon dynamics can be described as a non-linear, state-based switching system.

2.1.3 Control objectives

The first objective for the CACC controller is to guarantee that the platoon members follow each other while realizing the inter-vehicle distance specified by the spacing policy. Hence, the spacing errors should converge to zero (i.e., $\lim_{t \rightarrow \infty} e_i(t) = 0, \forall i \in \mathcal{I} \setminus \{1\}$).

The second objective is to guarantee stability for the closed-loop platoon dynamics. In other words, the states of all vehicles in the platoon, including internal states associated to the controller, should remain bounded. Furthermore, asymptotic stability of the platoon dynamics is desired, i.e., the states should converge to a desired equilibrium, which corresponds to a point where all vehicles drive at the same cruising speed, while the spacing errors, accelerations, and control inputs are equal to zero.

The objectives described before should be achieved for a platoon of vehicles that are subject to heterogeneous and dynamic acceleration limits as defined in (2.3).

2.2 Baseline multi-layer CACC strategy

This section describes the multi-layer CACC controller proposed in [23], which was developed to achieve the control objectives presented in Section 2.1.3. This multi-layer scheme is illustrated in Figure 2.2.

The lower layer of this control scheme consists of a CACC with one-vehicle look ahead topology based on [13], which defines the following dynamics for the desired acceleration u_i :

$$\dot{u}_i(t) = -\frac{1}{h}u_i(t) + \frac{1}{h}u_{ref,i-1}(t - \theta_c) + \frac{1}{h}(k_p e_i(t) + k_d \dot{e}_i(t)), \quad \forall i \in \mathcal{I} \setminus \{1\}, \quad (2.11)$$

where k_p and k_d are proportional and derivative gains, respectively. The signal $u_{ref,i-1}$ is the desired acceleration of the preceding vehicle as defined in (2.5), which serves as a feedforward term that improves vehicle following and contributes to string stability. Vehicle i receives the signal $u_{ref,i-1}$ from its predecessor via wireless communication, which introduces a communication delay, denoted as θ_c .

As discussed in [13], when the vehicles have no acceleration limit (i.e., $a_{max,i}(v_i)$ is unbounded $\forall v_i > 0$ and $i \in \mathcal{I}$), the control law (2.11) achieves asymptotically stable error dynamics for any positive value of the timegap h , as long as the gains satisfy $k_p > 0$ and $k_d > k_p \tau$. In [13], the authors also study for which combinations of communication delay and timegap the platoon exhibits string stability (i.e., disturbances are attenuated as these propagate upstream through the platoon). The interested reader may refer to [14] for a formal definition of string stability and for details on which values of h and θ_c achieve string stability.

Because the first vehicle has no predecessor, expression (2.11) does not apply to vehicle 1. Instead, the desired acceleration u_1 is prescribed by a simple cruise controller, as follows:

$$u_1(t) = k_v(v_{des} - v_1(t)), \quad (2.12)$$

where v_{des} is a constant desired speed and k_v is a positive gain.

As expressed in (2.5), the CACC input u_i defined in (2.11) is used together with the acceleration limit $a_{max,i}$ from (2.3) to define the desired acceleration $u_{ref,i}$. The signal $u_{ref,i}$ is the input to the linear system (2.4) that represents the longitudinal dynamics of the vehicle. The block-diagram in Figure 2.3 illustrates this relation.

The coordination layer

Turning now to the coordination layer in this control scheme, this is used to convey information about the acceleration limits of the platoon members. As illustrated in Figure 2.2, the vehicles behind the leader send the information vector $y_i \in \mathbb{R}^3$ to their corresponding node in the coordination layer. This vector is defined as $y_i = (a_{max,i}, e_i, \dot{e}_i)^T$. The coordination variable ξ_i , a

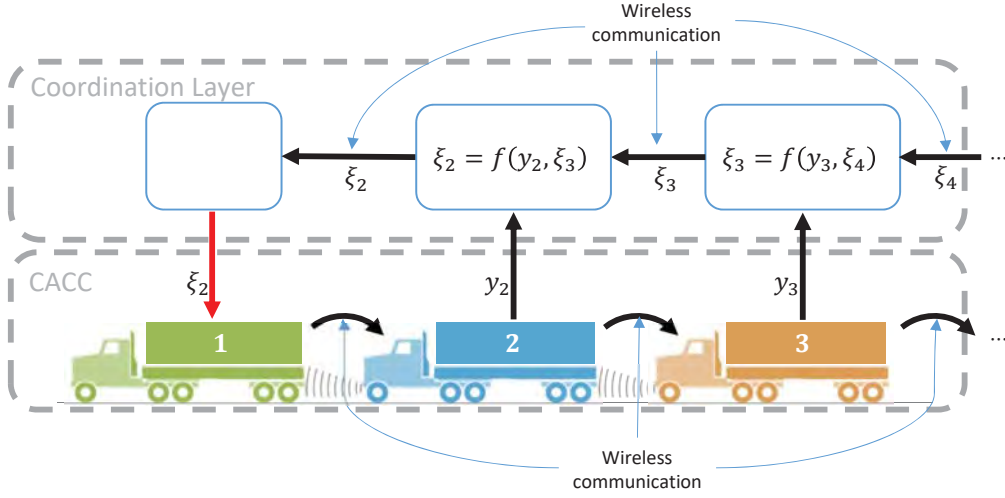
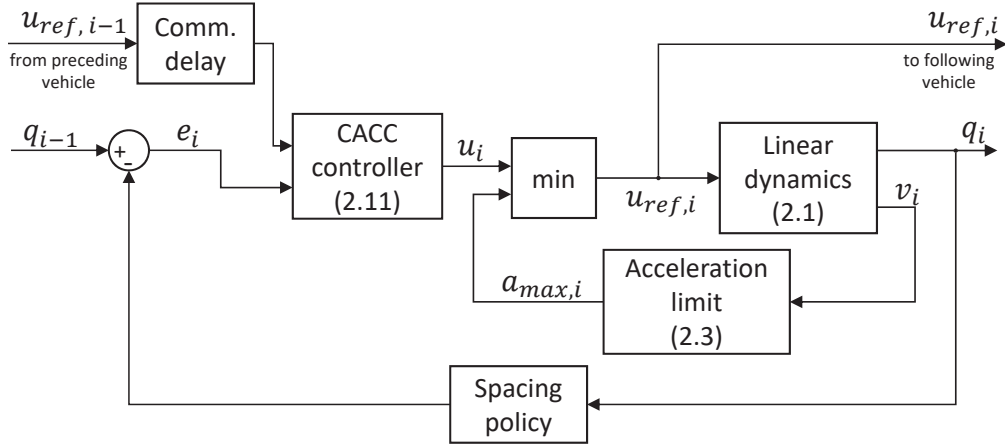


Figure 2.2: Schematic overview of a platoon with the multi-layer controller from [23].


 Figure 2.3: Block diagram of vehicle i , for $i \in \mathcal{I} \setminus \{1\}$, with the CACC controller (2.11) and dynamic acceleration limit (2.3).

scalar variable, is defined based on the vector y_i and the coordination variable from the following vehicle ξ_{i+1} , according to the following expressions:

$$\begin{aligned} \xi_i(t) &= f(y_i(t), \xi_{i+1}(t - \theta_c)) := \min [K y_i(t), \xi_{i+1}(t - \theta_c)], \quad \forall i \in \mathcal{I} \setminus \{1, n\} \\ \xi_n(t) &= K y_n(t), \end{aligned} \quad (2.13)$$

with gain vector $K = (1, -\gamma_p, -\gamma_d)$, where $\gamma_p > 0$ and $\gamma_d > 0$ are proportional and derivative gains, respectively. Notice that vehicle i uses the coordination variable from the following vehicle ξ_{i+1} which is transmitted via wireless communication, so that a time delay θ_c is considered in this transmission.

As a result of (2.13), the smallest of all $K y_i = a_{max,i} - \gamma_p e_i - \gamma_d \dot{e}_i$, for $i \in \mathcal{I} \setminus \{1\}$, is propagated downstream until it reaches the platoon leader via the variable ξ_2 . The platoon leader uses the information in ξ_2 to restrict its desired acceleration $u_{ref,1}$ as follows:

$$u_{ref,1}(t) = \min [u_1, a_{max,1}(v_1), \xi_2(t - \theta_c)], \quad (2.14)$$

where u_1 is the acceleration setpoint from the cruise controller in (2.12).

The restriction defined by (2.14) prevents vehicle 1 from accelerating beyond the capabilities of the slowest member in the platoon. Suppose that vehicle k is the one with the lowest value of Ky_i for a point in time at which this information is received by the lead vehicle. In this case, the coordination variable reaching the leader would take the value $\xi_2 = Ky_k(t - \theta_T)$, where θ_T corresponds to the total communication delay between vehicle k and vehicle 1. Then, in view of (2.14), the leader would not exceed the acceleration limit of vehicle k . Furthermore, if the spacing error of vehicle k starts to increase, then the term $-\gamma_p e_k$ in the coordination variable reduces the acceleration allowed for the platoon leader to a value below the feasible limit of vehicle k . In this way, the spacing error of the slowest member can be regulated when such vehicle reaches its acceleration limit. An example that illustrates this behavior is presented later in the report. As explained in [23], the term $-\gamma_d \dot{e}_i$ is included in the coordination variable as a damping factor which prevents a cyclic increase and decrease in the spacing error of a vehicle that is driving near its limit.

As illustrated in Figure 2.2, in this control scheme only the platoon leader uses information from the coordination layer to modify its behavior. In other words, the coordination layer does not interfere with the CACC controller that defines the acceleration setpoint for the vehicles behind the leader. This preserves, to some extent, the string stability properties of a nominal CACC, as explained next.

Suppose that only one of the vehicles has limited acceleration, let us say vehicle k . Then, with this multi-layer technique string stability can still be guaranteed for those vehicles between the leader and the limited one (i.e., vehicles 2 to $k - 1$) and also for those behind the slowest (i.e., vehicles $k + 1$ to n). This is true because vehicles 2 to $k - 1$ and $k + 1$ to n would be using the desired acceleration prescribed by a string-stable CACC (assuming the values for the timegap and communication delay guarantee string stability in the first place). A formal proof for the string stability properties of this multi-layer technique is beyond the scope of this work. A more important aspect is addressed first: asymptotic stability of the closed-loop platoon dynamics, thereby addressing the first and second control objectives formulated in Section 2.1.3.

The multi-layer controller described before is able to maintain platoon cohesion even when the vehicles have different acceleration capabilities and it also provides upstream disturbance attenuation. These properties are illustrated in Chapter 4 with results from computer simulations.

The main limitation of the baseline multi-layer CACC comes from the fact that only the desired acceleration of the platoon leader is affected directly by the coordination layer. When the platoon is accelerating and the slowest member, vehicle k , reaches its limit, then its spacing error starts to increase. In such case, there is a phase lag before the terms $\gamma_p e_k$ and $\gamma_d \dot{e}_k$ have an effect on the motion of vehicle $k - 1$. This actuation lag depends on the number of vehicles between the leader and vehicle k , the total communication delay between vehicle k and vehicle 1, and the chosen timegap for the spacing policy. The simulations presented later in this report indicate that when the slowest vehicle is located sufficiently back in the platoon, it becomes hard to tune the gains γ_p and γ_d to guarantee platoon cohesion and at the same time obtain a smooth transient response for the vehicles' acceleration. Hence, the scalability of this control approach is limited. This limitation is clarified with the analyses and simulation results in the following chapters of this report. In the following section, an alternative control strategy is proposed aimed at tackling this limitation.

2.3 Alternative multi-layer CACC strategy

This section describes an alternative multi-layer CACC strategy that is proposed to satisfy the control objectives presented in Section 2.1.3 and overcome the limitations of the CACC scheme discussed in the previous section. The proposed strategy consists of a lower layer where a CACC,

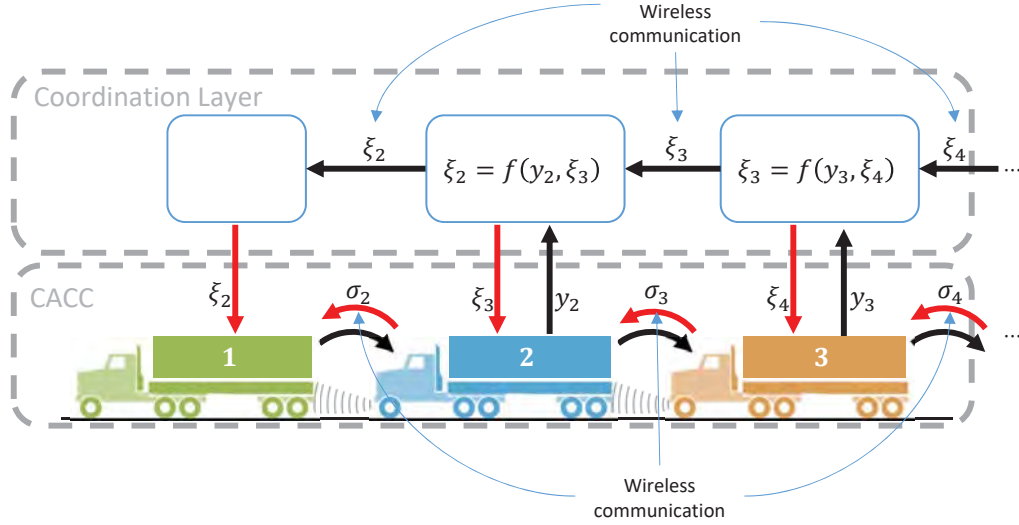


Figure 2.4: Schematic overview of a platoon with the proposed multi-layer controller.

with a control law defined as in (2.11), prescribes the desired acceleration to achieve the vehicle following objective, while a coordination layer is used to determine an acceleration level that is feasible for all the vehicles in the platoon. Compared to the baseline CACC strategy where only the platoon leader is affected by the coordination layer, in the control scheme proposed here the coordination variable directly influences the motion of all vehicles. The proposed control scheme is illustrated in Figure 2.4.

In this novel design, the coordination variable $\xi_i(t)$ is used to communicate only the acceleration limit of the vehicles, without including information on the spacing error. Now the signal y_i that each vehicle sends to its corresponding node in the upper layer is a scalar variable defined as $y_i(t) = a_{max,i}(v_i)$. Then, the coordination variable ξ_i is defined based on the variable y_i and the coordination variable from the following vehicle ξ_{i+1} , as follows:

$$\begin{aligned} \xi_i(t) &= f(y_i(t), \xi_{i+1}(t - \theta_c)) := \min [y_i(t), \xi_{i+1}(t - \theta_c)], \quad \forall i \in \mathcal{I} \setminus \{1, n\} \\ \xi_n(t) &= y_n(t), \end{aligned} \quad (2.15)$$

This definition ensures that $\xi_i = \min [a_{max,i}, \dots, a_{max,n}]$. The information in these coordination variables is then used to restrict the desired acceleration for every vehicle, as explained in the coming paragraphs, but first an additional communication variable is introduced.

In the novel coordination layer design, a second variable $\sigma_i(t)$ is used to transmit information of the spacing error of vehicle i to the preceding vehicle. The variable $\sigma_i(t)$ is defined as follows:

$$\sigma_i(t) = \gamma_p e_i + \gamma_d \dot{e}_i, \quad \forall i \in \mathcal{I} \setminus \{1\}, \quad (2.16)$$

where $\gamma_p > 0$ and $\gamma_d > 0$ are proportional and derivative gains, respectively. The variable $\sigma_i(t)$ is transmitted from vehicle i to vehicle $i - 1$ only. Now, with the variables ξ_i and σ_i , the control input for the vehicles, i.e., the desired acceleration, is defined as:

$$\begin{aligned} u_{ref,i}(t) &= \min [u_i, a_{max,i}(v_i), \xi_{i+1}(t - \theta_c) - \sigma_{i+1}(t - \theta_c)], \quad \forall i \in \mathcal{I} \setminus \{n\} \\ u_{ref,n}(t) &= \min [u_n, a_{max,n}(v_n)], \end{aligned} \quad (2.17)$$

with u_1 defined as in (2.12) and u_i for $i \in \mathcal{I} \setminus \{1\}$ as in (2.11). The block-diagram in Figure 2.5 illustrates the interaction defined in (2.17).

With the non-linear control law proposed in (2.17), assuming vehicle k to be the vehicle with the lowest acceleration limit, all vehicles from 1 to $k - 1$ are restricted directly by the acceleration

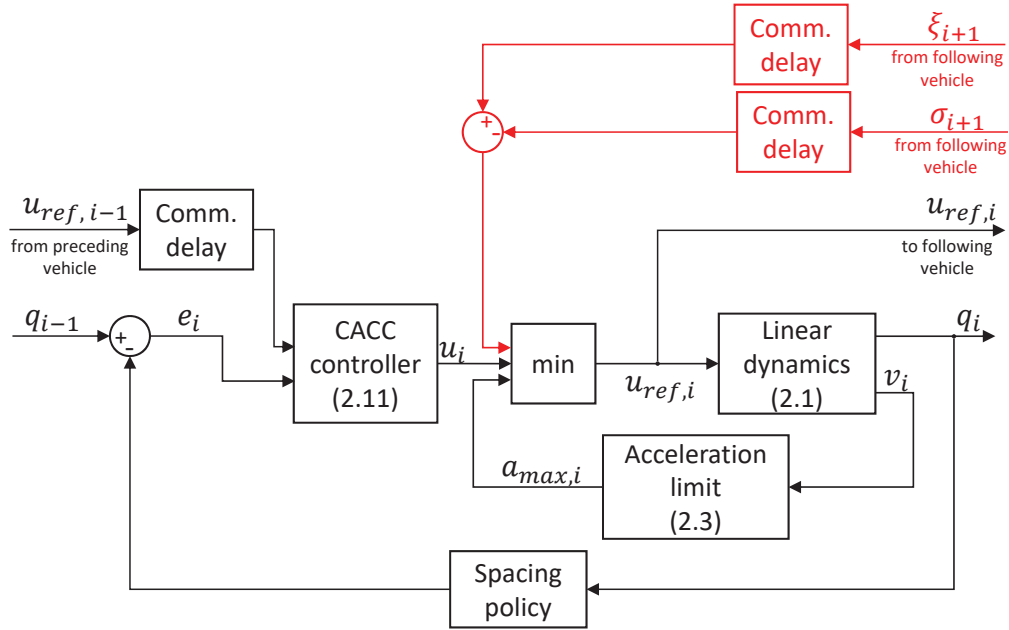


Figure 2.5: Block diagram of vehicle i , for $i \in \mathcal{I} \setminus \{n\}$, with acceleration limit from (2.3), desired acceleration as defined in (2.17), and coordination variables as in (2.15) and (2.16).

limit of vehicle k . This eliminates the phase lag that is present in the baseline multi-layer CACC, responsible for the poor performance in the case of large platoons or large values of the timegap h . It is important to mention that, if the variable σ_i were not to be included in this control scheme, then platoon cohesion would not be guaranteed. When the spacing error of vehicle i is increasing because it is being restricted either by its acceleration limit or by the expression $\xi_{i+1} - \sigma_{i+1}$, then vehicle $i - 1$ is forced to reduce its acceleration thanks to the variable $\sigma_i(t)$. It is more effective to regulate the spacing error of the host by slowing down the vehicle in front, instead of slowing down only the first vehicle in the platoon, as would be the case with the baseline controller

The proposed multi-layer scheme offers advantages with respect to the baseline technique describe in 2.2, in particular with respect to the size of the platoon that can be handled and it expands the range of timegap values for which platoon cohesion can be guaranteed. Nevertheless, as discussed in Chapter 3, the stability analysis for the proposed control scheme is more involved compared to the stability analysis for the baseline multi-layer controller. The benefits, disadvantages, and limitations of both control schemes are discussed throughout this report to help assess which control scheme performs better in a certain scenario.

It is worth mentioning that throughout this research project several attempts were made to design a multi-layer CACC strategy that would perform appropriately under various circumstances. The interested reader might refer to Appendix C, where alternative control strategies are described which offer some improvement with respect to the baseline approach, but still suffer from limitations compared to the algorithm described in this section.

Chapter 3

Stability analysis

Having presented two distinct multi-layer CACC strategies in Chapter 2, the resulting asymptotic stability of the closed-loop platoon dynamics is the focus of this chapter. First, the modelling framework and tools used for the stability analysis are introduced as preliminaries in Section 3.1. These tools are then applied to the control strategies in question and the results are presented in the following sections.

3.1 Preliminaries

The closed-loop platoon dynamics that result from the control strategies described in Chapter 2 can be formulated as piecewise affine systems. A piecewise affine (PWA) system indicates that the state space is partitioned into multiple regions where different linear or affine dynamics are active. This mathematical model is suitable to represent systems with static non-linearities, such as saturations, hysteresis, and relays. For instance, the *min* function used to define the coordination variables and desired acceleration in the previous chapter can be modelled with a PWA system. This section describes what a PWA system is and how a suitable Lyapunov function can be found to prove the stability properties of the system. The content of this section is based on [4].

3.1.1 Piecewise affine systems

A piecewise affine system can be expressed as

$$\dot{x}(t) = A_j x(t) + b_j \quad \text{for } x(t) \in \mathcal{X}_j, \quad j \in \mathcal{J} = \{1, \dots, N\}, \quad (3.1)$$

where $x \in \mathbb{R}^{n_x}$ is the state vector and n_x is the dimension of the state space. Then, $A_j \in \mathbb{R}^{n_x \times n_x}$ are the system matrices, and $b_j \in \mathbb{R}^{n_x}$ are affine terms in the dynamics. The sets $\mathcal{X}_j \subset \mathbb{R}^{n_x}$, referred to as cells, denote N different regions that compose the state space partition. The subscript j denotes the index of the cell, and the set \mathcal{J} collects the indices for the N cells.

The cells \mathcal{X}_j are convex, possibly unbounded, polyhedra that result from dividing the state space with a finite number of hyperplanes. The cells \mathcal{X}_j can be defined with a set of linear inequalities, as follows:

$$\mathcal{X}_j = \{x \in \mathbb{R}^{n_x} \mid G_j x + g_j \succeq 0\}, \quad \text{for } j \in \mathcal{J}, \quad (3.2)$$

with $G_j \in \mathbb{R}^{p_j \times n_x}$ and $g_j \in \mathbb{R}^{p_j}$. The number of rows in G_j and g_j , denoted by p_j , corresponds to the number of hyperplanes that delimit the cell \mathcal{X}_j . The symbol \succeq denotes an element-wise inequality.

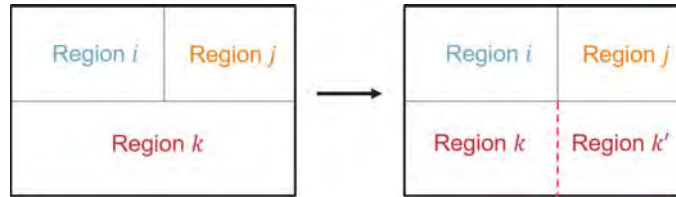


Figure 3.1: Schematic representation the state space partition, before (left) and after (right) extending the original boundaries. The solid black lines represent the original boundaries, while the red dashed line indicates the extension of a boundary. The dynamics are the same in regions k and k' .

In principle, the cells in the PWA model might be delimited by different numbers of hyperplanes. However, for the stability analysis described in the next section, it is important that the boundaries of all cells are extended globally, as represented schematically in Figure 3.1.

For a PWA system to have a well-defined solution, it is necessary (but not sufficient) for the cells \mathcal{X}_j to have a disjoint interior, meaning that adjacent cells may overlap only at the boundary. The common boundary between two adjacent cells corresponds to a collection of points that lie on one of the hyperplanes or on the intersection of multiple hyperplanes that are common to adjacent cells. The previous fact implies that the overlap between adjacent cells is a set of dimension less than or equal to $n_x - 1$.

The definition in (3.1) restricts dynamics that correspond to each cell to be continuous up to the cell boundary. However, in principle, the dynamics, i.e., the vector fields, from adjacent cells might not be continuous at their common boundary. This gives rise to the possibility of sliding modes, for which a unique solution might not exist. As explained in [4], the concept of Filippov solutions can be used to define a unique solution even in the presence of attractive sliding modes. Attractive sliding modes result in a more involved stability analysis. However, sliding modes are not discussed further in this report because, as explained in upcoming sections, the PWA models analyzed in this work have continuous dynamics.

3.1.2 Piecewise quadratic Lyapunov functions

For a PWA system, asymptotic stability of the origin, assuming this point is an equilibrium for the dynamics, can be proven with a piecewise quadratic Lyapunov function (PWQLF). Such a function can be (potentially) found by solving an optimization problem consisting of linear matrix inequalities (LMIs). The method proposed in [4] for this purpose is described next.

First, it is necessary to make a distinction between cells that contain the origin and those cells that do not. When referring to the origin, it corresponds to the point $x_0 = 0 \in \mathbb{R}^{n_x}$. With this in mind, let $\mathcal{J}_0 \subset \mathcal{J}$ be the set of indices for cells that contain x_0 , and $\mathcal{J}_1 \subset \mathcal{J}$ be the set of indices for cells that do not. Notice that x_0 lies on the common boundary of the cells with indices $j \in \mathcal{J}_0$ or in the interior of one cell in case \mathcal{J}_0 contains a single element.

For those cells \mathcal{X}_j that contain the origin, it is required that the corresponding dynamics have no affine terms, i.e., $b_j = 0, \forall j \in \mathcal{J}_0$, such that the origin is the equilibrium for the dynamics associated to those cells. On the other hand, for the cells with indices $j \in \mathcal{J}_1$, the dynamics are allowed to have affine terms, but in that case the point x that makes $A_j x + b_j$ equal to zero, if it exists, should not lie within the corresponding cell \mathcal{X}_j . The previous conditions are necessary, but not sufficient, to have global asymptotic stability of the origin.

To prove exponential stability of the origin for the system in (3.1), one can search for a piecewise

quadratic Lyapunov function of the form:

$$V(x) = \begin{cases} x^T P_j x, & \text{for } x \in \mathcal{X}_j, j \in \mathcal{J}_0 \\ [x^T \ 1] \bar{P}_j \begin{bmatrix} x \\ 1 \end{bmatrix}, & \text{for } x \in \mathcal{X}_j, j \in \mathcal{J}_1, \end{cases} \quad (3.3)$$

where $P_j \in \mathbb{R}^{n_x \times n_x}$ and $\bar{P}_j \in \mathbb{R}^{(n_x+1) \times (n_x+1)}$ are symmetric matrices. The matrices \bar{P}_j for $j \in \mathcal{J}_1$ have the following structure:

$$\bar{P}_j = \begin{bmatrix} P_j & p_j \\ p_j^T & r_j \end{bmatrix} = x^T P_j x + 2p_j^T x + r_j \quad (3.4)$$

with $P_j \in \mathbb{R}^{n_x \times n_x}$, $p_j \in \mathbb{R}^{n_x}$, and $r_j \in \mathbb{R}$.

The quadratic functions for $j \in \mathcal{J}_1$ in (3.3) have the following form:

$$[x^T \ 1] \bar{P}_j \begin{bmatrix} x \\ 1 \end{bmatrix} = x^T P_j x + 2p_j^T x + r_j. \quad (3.5)$$

The terms $2p_j^T x + r_j$ in the expression above allow to handle possibly affine dynamics in the cells \mathcal{X}_j with $j \in \mathcal{J}_1$. The expression in (3.3) indicates that the function $V(x)$ is composed of possibly different quadratic functions associated to each cell in the state space partition.

To ensure the function $V(x)$ is continuous at the boundary between cells, continuity matrices \bar{F}_j are used. These matrices have the following structure:

$$\bar{F}_j = [F_j \ f_j] = \begin{bmatrix} F_j' & f_j' \\ I_{(n_x)} & 0_{(n_x \times 1)} \end{bmatrix}, \text{ for } j \in \mathcal{J}, \quad (3.6)$$

with $F_j \in \mathbb{R}^{(n_x+m) \times n_x}$ and $f_j \in \mathbb{R}^{(n_x+m)}$, where m denotes the total number of hyperplanes used to define the state space partition. Here $I_{(n_x)}$ is the identity matrix of dimension $n_x \times n_x$, which is included to give full row rank to \bar{F}_j [4]. The matrices \bar{F}_j are constructed using the equations of the hyperplanes used to partition the state space with the procedure described in Appendix A, in such a way that these matrices satisfy the following expression:

$$[x^T \ 1] \bar{F}_j \begin{bmatrix} x \\ 1 \end{bmatrix} = [x^T \ 1] \bar{F}_k \begin{bmatrix} x \\ 1 \end{bmatrix}, \text{ for } x \in \mathcal{X}_j \cap \mathcal{X}_k, \forall j, k \in \mathcal{J}. \quad (3.7)$$

The expression above must be satisfied for any pair of cells that share a common boundary, regardless of whether they both contain the origin, only one contains the origin, or neither of them does. The continuity matrices \bar{F}_j are used to define the matrices P_j and \bar{P}_j in (3.3) as follows:

$$\begin{aligned} P_j &= F_j^T T F_j, \quad j \in \mathcal{J}_0 \\ \bar{P}_j &= \bar{F}_j^T T \bar{F}_j, \quad j \in \mathcal{J}_1, \end{aligned} \quad (3.8)$$

where T is a symmetric matrix and F_j is the submatrix of the corresponding \bar{F}_j , as defined in (3.6). In this way, continuity of the function $V(x)$ is guaranteed.

If the function $V(x)$ in (3.3) is indeed a Lyapunov function for the system (3.1), then it must be positive and its time derivative $\dot{V}(x)$ must be negative, except at the origin where both must be equal to zero. The individual quadratic functions that conform $V(x)$ need to satisfy these two conditions inside their corresponding regions of the state space, but not necessarily outside of it. A Lyapunov function with such characteristics proves asymptotic stability of the origin for a PWA system, assuming the system (3.1) has no sliding modes. A piecewise quadratic function with the aforementioned characteristics can be determined from a solution to the following set of LMIs [4]:

$$\begin{cases} P_j - E_j^T U_j E_j > 0 \\ A_j^T P_j + P_j A_j + E_j^T W_j E_j < 0 \end{cases}, \quad j \in \mathcal{J}_0, \quad (3.9)$$

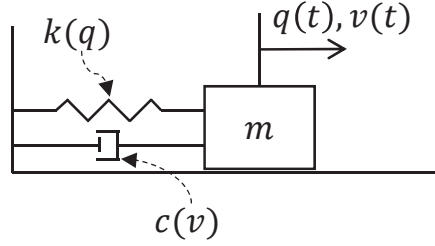


Figure 3.2: Mass-spring-damper system.

$$\begin{cases} \bar{P}_j - \bar{E}_j^T U_j \bar{E}_j > 0 \\ \bar{A}_j^T \bar{P}_j + \bar{P}_j \bar{A}_j + \bar{E}_j^T W_j \bar{E}_j < 0 \end{cases}, j \in \mathcal{J}_1, \quad (3.10)$$

with matrices P_j and \bar{P}_j as in (3.8), which means the matrix T is present in every LMI defined by the expressions above. The unknown matrices in the set of LMIs in (3.9) and (3.10) are T , U_j , and W_j , which must all be symmetric. Furthermore, matrices U_j and W_j must contain only non-negative elements. The reason for this restriction is explained in Appendix A. Moreover, the matrix \bar{A}_j is an augmented system matrix defined as:

$$\bar{A}_j = \begin{bmatrix} A_j & b_j \\ 0_{(1 \times n_x)} & 0 \end{bmatrix}. \quad (3.11)$$

The matrices E_j and \bar{E}_j are so-called cell bounding matrices which satisfy the following expressions:

$$\begin{aligned} E_j x &\succeq 0, & \text{for } x \in \mathcal{X}_j, j \in \mathcal{J}_0 \\ [x^T \quad 1] \bar{E}_j \begin{bmatrix} x \\ 1 \end{bmatrix} &\succeq 0, & \text{for } x \in \mathcal{X}_j, j \in \mathcal{J}_1. \end{aligned} \quad (3.12)$$

The matrices E_j and \bar{E}_j are known and are constructed with the algorithm described in Appendix A using the equations of the hyperplanes that bound the corresponding region.

The first expression in both (3.9) and (3.10) guarantees that the function $V(x)$ is positive definite, while the second expression guarantees that $\dot{V}(x)$ is negative definite. The terms containing U_j or W_j are introduced to relax the conditions for the individual quadratic functions in $V(x)$, meaning they are not required to be positive or strictly decreasing (along solutions of the PWA system) outside of the cell where they are used. This relaxation is known as the S-procedure and is explained in more detail in Appendix A.

It is important to point out that the feasibility of the LMIs presented before is only a sufficient condition for stability. In other words, it is not always possible to find a PWQLF for a PWA system that is asymptotically stable. Moreover, a stable PWA system might admit a PWQLF which cannot be derived from these LMIs [4].

The methodology explained in this section is applied to assess the asymptotic stability of the origin for a PWA model that describes the closed-loop platoon dynamics for the control schemes described in Chapter 2. But first a simple example is provided to clarify how this methodology is applied.

An illustrative example

Consider a mass-spring-damper system, as depicted in Figure 3.2. Both the spring and the damper are assumed to behave differently in the expansion and compression strokes, as follows:

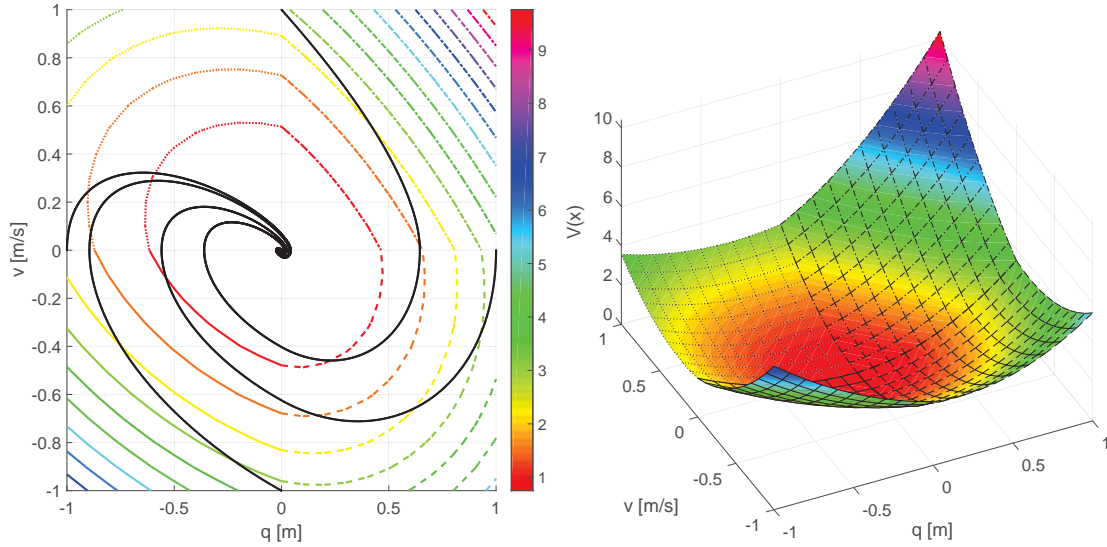


Figure 3.3: Computed Lyapunov function for the mass-spring-damper system. State trajectories for different initial conditions are shown (left), together with level curves for the Lyapunov function. The different line styles of the level curves indicate the four regions of the state space partition. The plot to the right illustrates the continuity of the PWQLF.

$$k(q(t)) = \begin{cases} k_1 & ; q(t) \leq 0 \\ k_2 & ; q(t) > 0 \end{cases} \quad (3.13)$$

$$c(v(t)) = \begin{cases} c_1 & ; v(t) \leq 0 \\ c_2 & ; v(t) > 0 \end{cases}, \quad (3.14)$$

where $q(t)$ denotes the horizontal position and $v(t)$ the horizontal velocity. This mechanical system can be modelled using a PWA system with a state-space partitioned into four regions, each with different linear dynamics. The equations of motion for the system are:

$$\begin{cases} \dot{q}(t) = v(t) \\ \dot{v}(t) = -\frac{1}{m} (k(q) \cdot q(t) + c(v) \cdot v(t)). \end{cases} \quad (3.15)$$

Choosing the state vector as $x(t) = [q(t), v(t)]^T$, four system matrices can be derived from (3.13), (3.14), and (3.15). In this example, the various dynamics have no affine terms, so that the origin is a common equilibrium for all regions. Two lines divide the state-space: $q(t) = 0$ and $v(t) = 0$. These equations are used to construct the matrices \bar{G}_j defined in (3.2).

Solving the LMIs in (3.9) using the YALMIP toolbox for MATLAB [10], a PWQLF can be found when the parameters are set to: $m = 1 \text{ kg}$, $k_1 = 0.5 \frac{\text{N}}{\text{m}}$, $k_2 = 1 \frac{\text{N}}{\text{m}}$, $c_1 = 0.5 \frac{\text{Ns}}{\text{m}}$, $c_2 = 1 \frac{\text{Ns}}{\text{m}}$. The obtained Lyapunov function is illustrated in Figure 3.3. The plot to the left shows various state trajectories for different initial conditions, which all converge to the origin. Furthermore, the plot contains level curves for the PWQLF. The plot to the right illustrates the Lyapunov function for a subset of the state-space, where it can be seen that the function is continuous at the boundary between regions. The obtained PWQLF proves global exponential stability of the origin for this PWA system. The procedure described here will also be applied to assess the stability of the platoon dynamics, but in that case it is not simple to visualize the obtained Lyapunov function because of the high dimension of the state space.

3.2 Translating static non-linearities into a PWA system

Deriving a PWA model for the closed-loop platoon dynamics can be a cumbersome task because of the multiple non-linearities associated to the *min* functions used to introduce the heterogeneous acceleration bounds as in (2.5) and to define the coordination variables as in (2.13) and (2.15). Each minimum function can be translated into inequalities which, in turn, define one or more hyperplanes that partition the state space. Furthermore, as the number of vehicles in the platoon increases, the number of hyperplanes required to represent the non-linearities increases rapidly.

Instead of manually writing the system matrices A_j and corresponding affine terms b_j , as well as the cell bounding matrices \bar{G}_j and offset terms g_j , required to describe the PWA model, a MATLAB script is developed to generate the complete set of matrices for a platoon with n vehicles. The rationale behind this script is described next, which clarifies why the PWA system becomes rather complex for platoons with more than two vehicles.

As explained in [4], when analyzing the stability of an equilibrium point for a PWA system, it is necessary to apply a state transformation such that the equilibrium point of interest lies at the origin of the transformed coordinates. In this case, the equilibrium of interest corresponds to a point where all vehicles drive with speed v_{des} , while the acceleration, desired acceleration, and spacing error for all vehicles are equal to zero. With this in mind, a shifted state vector for the vehicles is defined as follows:

$$z_i = (e_i, v_i - v_{des}, a_i, u_i)^T, \quad \forall i \in \mathcal{I} \setminus \{1\}, \quad (3.16)$$

where i is the vehicle index and n is the platoon size. Furthermore, $e_i(t)$ is the spacing error, $v_i(t)$ is the velocity, v_{des} is the desired constant speed for the platoon, $a_i(t)$ is the acceleration, and $u_i(t)$ is the unrestricted control input prescribed by the CACC in the lower layer (see (2.11)). The shifted state vector for vehicle 1 is defined as $z_1 = (v_1 - v_{des}, a_1)^T$. Then, introducing the lumped state vector $z = (z_1^T, z_2^T, \dots, z_n^T)^T$, the PWA system is expressed as

$$\dot{z}(t) = A_j z(t) + b_j, \quad \text{for } z \in \mathcal{Z}_j, \quad j \in \mathcal{J} = \{1, \dots, N\}, \quad (3.17)$$

where N is the number of regions that compose the state-space partition and j is the region index. The regions are defined as $\mathcal{Z}_j = \{z \mid G_j z + g_j \succeq 0\}$. The matrices A_j and vectors b_j in (3.17) are determined from the differential equations that describe the dynamics in cell \mathcal{Z}_j , while the matrices G_j and vectors g_j are determined from the hyperplanes that delimit the cell \mathcal{Z}_j .

Some assumptions must be made so that the platoon dynamics can be modelled with a PWA system. First, the aerodynamic drag is neglected, because it introduces a nonlinearity in the function $a_{max,i}(v_i)$ in (2.3). The acceleration limit of the vehicle is approximated with a linear function, as follows:

$$a_{max,i}(v_i) = \alpha_i v_i + \beta_i, \quad \forall i \in \mathcal{I}, \quad (3.18)$$

with constants $\alpha_i < 0$ and $\beta_i > 0$. The coefficient α_i indicates the rate of decrease in acceleration capability as the vehicle increases its velocity, and the constant β_i indicates the maximum acceleration from rest. A second assumption deals with the time-delays in the dynamics. It is assumed the delay θ_c for the wireless inter-vehicle communication and the actuation delays θ_g are negligible. With these two assumptions, the platoon dynamics can be represented as a collection of linear dynamics that are active in different regions of the state space.

Deriving a PWA model for the baseline control strategy

The closed-loop platoon dynamics that arise when applying the baseline control strategy described in Section 2.2 are described with the following set of differential equations in terms of the states

in the shifted state vector z :

$$\begin{cases} \frac{d}{dt}(v_1 - v_{des}) = a_1 \\ \dot{a}_1 = -\frac{1}{\tau}a_1 + \frac{1}{\tau}u_{ref,1} \\ \dot{e}_i = (v_{i-1} - v_{des}) - (v_i - v_{des}) - ha_i \\ \frac{d}{dt}(v_i - v_{des}) = a_i \\ \dot{a}_i = -\frac{1}{\tau}a_i + \frac{1}{\tau}u_{ref,i} \\ \dot{u}_i = -\frac{1}{h}u_i + \frac{1}{h}u_{ref,i-1} + \frac{1}{h}(k_p e_i + k_d \dot{e}_i), \end{cases} \quad (3.19)$$

for $i \in \mathcal{I} \setminus \{1\}$. These equations are derived by combining the linear dynamics in (2.4) and the CACC control law in (2.11). Furthermore, the desired acceleration for vehicle 1, $u_{ref,1}$, is defined as in (2.14) which, in turn, involves the cruise controller in (2.12). The desired acceleration $u_{ref,i}$ for vehicles 2 to n is defined with expression (2.5).

The *min* function in expression (2.5) is represented in the PWA system with the hyperplane $u_i - a_{max,i} = 0$. Then, $u_{ref,i} = u_i$ in those regions of the state space where $u_i - a_{max,i} \leq 0$, and $u_{ref,i} = a_{max,i}$ in the regions where $u_i - a_{max,i} \geq 0$. A total of $n - 1$ hyperplanes are required to represent the limited acceleration of vehicles 2 to n . These hyperplanes together divide the state-space into 2^{n-1} regions.

The coordination variable ξ_2 , which is involved in the expression for $u_{ref,1}$ in (2.14), is a non-linear function of the states of vehicles 2 to n , defined as:

$$\xi_2(t) = \min [Ky_2, \dots, Ky_n], \quad (3.20)$$

with $Ky_i = a_{max,i}(v_i) - \gamma_p e_i - \gamma_d \dot{e}_i$, with $a_{max,i}$ as in (3.18). Substituting (3.20) in (2.14) leads to the following expression for $u_{ref,1}$:

$$u_{ref,1}(t) = \min [u_1, a_{max,1}, Ky_2, \dots, Ky_n]. \quad (3.21)$$

To explain how (3.21) is represented in the PWA system, consider for example the case when u_1 is in fact the minimum of the variables in the right-hand side of (3.21). In other words, $u_1 \leq a_{max,1}$, $u_1 \leq Ky_2$, \dots , $u_1 \leq Ky_n$. In the region of the state-space where the previous inequalities hold, the control input for vehicle 1 is $u_{ref,1} = u_1$. This region is delimited by n hyperplanes, namely, $u_1 - a_{max,1} = 0$, $u_1 - Ky_2 = 0$, \dots , $u_1 - Ky_n = 0$.

Following the logic in the previous paragraph, the state-space partition requires a hyperplane for every possible pair of variables in the argument of the *min* function in (3.21), which results in $\frac{1}{2}n(n+1)$ hyperplanes. These hyperplanes define $(n+1)!$ regions, where $!$ denotes the factorial. To explain the previous statement, notice that a possible set of inequalities that describe a region where $u_{ref,1} = u_1$ can be $u_1 \leq a_{max,1}(v_1) \leq Ky_2 \leq Ky_3 \leq \dots \leq Ky_n$, which involves all $\frac{1}{2}n(n+1)$ hyperplanes. However, $u_{ref,1}$ also takes the value of u_1 in the region where $u_1 \leq Ky_2 \leq Ky_3 \leq \dots \leq Ky_n \leq a_{max,1}(v_1)$. Hence, a different cell in the state space is defined for every possible permutation of the variables in $\{u_1, a_{max,1}, Ky_2, \dots, Ky_n\}$, which gives $(n+1)!$ distinct cells.

Combining the hyperplanes required to represent expressions (2.5) and (3.21), the total number of regions in the partition is $N = 2^{n-1} \times (n+1)!$. Table 3.1 illustrates the rapid increase in number of regions as the platoon size increases. A MATLAB script is developed with the logic described above, which automatically enumerates all the possible regions for a given platoon size and constructs the corresponding system matrices A_j and (possible) affine terms from the equations in (3.19), and the matrices G_j and offset terms g_j for the inequalities that delimit these regions. The output of the script is a set of matrices defined with symbolic variables that can be stored into a file and then retrieved to evaluate the matrices for some values of vehicle parameters and control gains.

The advantage of constructing the PWA system as described before is that such a system can be used to represent platoons with different vehicle ordering, meaning the slowest member can

Table 3.1: Number of regions in the PWA system for various platoon sizes with the baseline multi-layer scheme.

Platoon size n	2	3	4	5
Regions in the state-space partition	12	96	960	11,520

Table 3.2: Number of regions in the PWA system for various platoon sizes with the proposed control scheme.

Platoon size n	2	3	4	5
Regions in the state-space partition	12	288	34,560	24,883,200

be located in any position in the platoon. Furthermore, the acceleration limits of the platoon members can be arbitrarily close to each other, such that the coordination variable ξ_2 in (3.20) might contain information from a different vehicle at different time instants, such that the control input for the leading vehicle might be restricted by a different platoon member at different times.

Deriving a PWA model for the newly proposed control strategy

Next, we consider the control strategy proposed in Section 2.3, the non-linearities in that high-level control scheme translate into an even more involved PWA system. The rationale presented before is used to design a MATLAB script that automatically generates the matrices for the PWA system of the proposed multi-layer scheme.

The main difference between the baseline and the newly proposed control strategies is that in the latter all vehicles are directly influenced by the coordination variables. As defined in (2.17), the expression for the desired acceleration $u_{ref,i}$ consists of a *min* function with three arguments, as follows:

$$\begin{aligned} u_{ref,i} &= \min [u_i, a_{max,i}(v_i), \xi_{i+1} - \sigma_{i+1}] \\ &= \min [u_i, a_{max,i}(v_i), \min [y_{i+1}, \dots, y_n] - \sigma_{i+1}], \forall i \in \mathcal{I} \setminus \{n\}, \\ &= \min [u_i, a_{max,i}(v_i), y_{i+1} - \sigma_{i+1}, \dots, y_n - \sigma_{i+1}] \end{aligned} \quad (3.22)$$

where the expression for ξ_i in (2.15) was used, with σ_i as in (2.16), and $y_i = a_{max,i}(v_i)$. The *min* function defining $u_{ref,n}$ has only two arguments: u_n and $a_{max,n}(v_n)$, which translates into a single hyperplane. However, for vehicles 1 to $n - 1$ the number of hyperplanes required to describe $u_{ref,i}$ depends on the value of i . To determine the total number of cells defined by these hyperplanes, one must look at all the possible permutations of the variables in the argument of (3.22), one vehicle at a time. The product of the permutations for each value of i gives the total number of cells, as follows:

$$N = \prod_{i=1}^n ((2 + n - i)!). \quad (3.23)$$

Table 3.2 shows the number of cells for platoons of 2 to 5 vehicles. Comparing Tables 3.1 and 3.2, it can be seen that the proposed control scheme is harder to analyze and in fact it is only feasible to conduct the stability analysis for platoons with up to 3 vehicles. From an analysis point of view, this is a disadvantage of the newly proposed multi-layer strategy when compared to the baseline control scheme, but this is not necessarily a disadvantage from a performance point of view.

It is important to mention that, because the non-linearities in the platoon dynamics that make these piecewise affine are equivalent to a saturation function, continuity of the dynamics at the boundary between regions is guaranteed. In other words, the minimum functions in expression (3.21) and (3.22) lead to continuous functions, such that the vector fields that arise from (3.19) are also continuous. In this way, sliding modes are discarded from the dynamics and the stability analysis based on PWQLF, as described in Section 3.1.2, is applicable.

The rationale used to construct PWA models for the platoon dynamics has been described. In the next section, global asymptotic stability of the origin is assessed via piecewise quadratic Lyapunov functions.

3.3 Stability analysis for the baseline control scheme

The method to assess stability described in Section 3.1.2 requires to solve LMIs, for which numerical procedures are available in the form of MATLAB toolboxes for semidefinite programming (c.f. [10], [7]). A disadvantage of this numerical approach is that one must choose certain parameter values before attempting to find a Lyapunov function. Various control gains are involved in the PWA model. It would be useful to have an additional tool that provides insight on how to choose these gains. Computer simulations can serve this purpose, but these are time-consuming. To this end, an analysis in the frequency domain is discussed next, which can be used as a guideline to choose the control gains for the coordination layer. This analysis is based on inspecting the stability of the individual subsystems that compose the PWA model describing the closed-loop platoon dynamics. As the control gains influence the stability of these subsystems, it is useful to derive conditions for which the subsystems are (marginally) asymptotically stable.

3.3.1 A frequency domain approach to analyze the stability of a particular operation mode

Consider a platoon of n vehicles under the nominal CACC proposed in [13], i.e., where the desired acceleration is defined with (2.11) and when the vehicles have no bound on acceleration. Assuming homogeneous engine dynamics for all vehicles, the transfer function from v_{i-1} to v_i corresponds to [13]:

$$\Gamma(s) = \frac{1}{H(s)} \frac{D_c(s) + G(s)K(s)}{1 + G(s)K(s)}, \quad (3.24)$$

where $s \in \mathbb{C}$ is the Laplace variable. Then, $H(s) = hs + 1$ is the spacing policy transfer function. $G(s) = ((\tau s + 1)s^2 e^{-\theta_a s})^{-1}$ is the vehicle transfer function from the desired acceleration $u_{ref,i}(s)$ to the position of the vehicle $q_i(s)$; in $G(s)$, the actuation delay θ_a is considered. Next, $K(s) = k_d s + k_p$ corresponds to the PD controller associated to the feedback of the spacing error. Finally, $D_c(s) = e^{-\theta_c s}$ corresponds to the inter-vehicle communication delay. As explained in [13], for the case of homogeneous vehicle strings, $\frac{q_i(s)}{q_{i-1}(s)} = \frac{v_i(s)}{v_{i-1}(s)} = \frac{a_i(s)}{a_{i-1}(s)} = \Gamma(s)$.

If the actuation delay θ_a is neglected, the transfer function $\Gamma(s)$ has stable poles when $h > 0$, $\tau > 0$, $k_p > 0$, and $k_d > k_p \tau$ [13]. From (3.24), it is evident that the spacing policy acts as a low-pass filter which introduces phase lag. The higher the value of the timegap h , the more sluggish the response of the platoon to an input applied to the leading vehicle.

Now consider the case in which vehicle k is the slowest in the platoon. Then, when applying the baseline multi-layer strategy, the acceleration limit of the vehicle k and its spacing error are used to define the desired acceleration for the platoon leader. A particular operation mode is analyzed here: vehicle k is driving at its limit, vehicle 1 is restricted by the coordination variable ξ_2 , and all other vehicles are applying the input prescribed by the CACC. It is particularly relevant to analyze the dynamics in this operation mode because, from the numerous simulations conducted along this research, it has been observed that undesired transient performance can arise when the dynamics in this operation mode are unstable as a result of the control gains in the coordination layer.

The operation mode in question is illustrated with the block scheme in Figure 3.4, where the acceleration limit of vehicle k is considered to be an exogenous input. In reality, the limit $a_{max,k}$

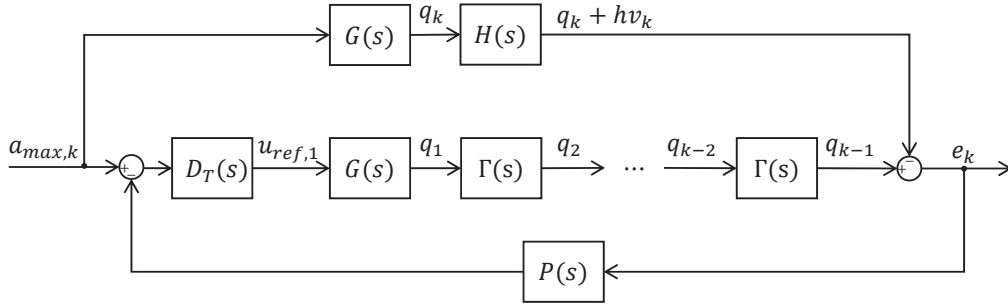


Figure 3.4: Block scheme of the closed-loop platoon dynamics subject to the baseline control strategy, when vehicle k is driving at its acceleration limit and vehicle 1 is limited by the coordination variable ξ_2 .

is a function of v_k , but this is not relevant for the analysis presented next. Furthermore, it is not necessary to analyze the dynamics of vehicles $k + 1$ to n because in this operation mode those vehicles are being controlled by a stable CACC and do not influence the dynamics of the preceding vehicles.

In Figure 3.4, $P(s) = \gamma_d s + \gamma_p$ is the error feedback in the coordination layer, while $D_T(s)$ corresponds to the total communication delay in the coordination layer between vehicle k and the platoon leader.

From the block scheme in Figure 3.4, the closed-loop transfer function from $a_{max,k}(s)$ to $e_k(s)$ is

$$CL(s) = \frac{e_k(s)}{a_{max,k}(s)} = \frac{D_T(s)G(s)\Gamma^{k-2}(s) - G(s)H(s)}{1 + D_T(s)G(s)\Gamma^{k-2}(s)P(s)}. \quad (3.25)$$

This transfer function is relevant for the stability analysis because the dynamics of all vehicles in the platoon play a role in this transfer function as well as the the control gains in the coordination layer. Moreover, it is useful to analyze the spacing error dynamics for vehicle k during the operation mode in question.

Now, to simplify the analysis, the communication and actuation delays are assumed to be zero. In such case, (3.24) simplifies to $\Gamma(s) = 1/H(s)$; this simplification is valid because the actuation time constant τ is assumed to be homogeneous for all vehicles in the platoon. Substituting the simplified expression for $\Gamma(s)$ in (3.25), the transfer function $CL(s)$ becomes

$$CL(s) = \frac{GH^{-(k-2)} - GH}{1 + GPH^{-(k-2)}} = \frac{1 - (hs + 1)^{k-1}}{(hs + 1)^{k-2}(\tau s + 1)s^2 + \gamma_d s + \gamma_p}. \quad (3.26)$$

The dynamics for some regions in the PWA system are related to the transfer function (3.26). In fact, the denominator of (3.26) appears in the characteristic polynomial for the system matrices of some subsystems in the PWA model. Therefore, if the transfer function above is unstable, also the dynamics in some regions of the state space would be unstable. Notice that, as explained in [4], for a PWA system to have a stable equilibrium, the various subsystems in it need not be stable. As long as the region containing the equilibrium of interest has stable dynamics, it might be possible to find a PWQLF for a PWA system that has unstable dynamics in some regions of the partition.

To illustrate the influence of the gains γ_p and γ_d on the stability properties of this operation mode, the poles of (3.26) are computed for two values of the timegap h , $0.3s$ and $0.6s$, with the actuation time constant set to $\tau = 0.1s$. In Figure 3.5, the shaded areas indicate the region in the design space $\gamma_p \times \gamma_d \in \mathbb{R}^2$ for which (3.26) has only poles in the open left half-plane. In this figure, the shaded areas are overlapping, i.e., the area for k lies within the area for $k - 1$. Notice that

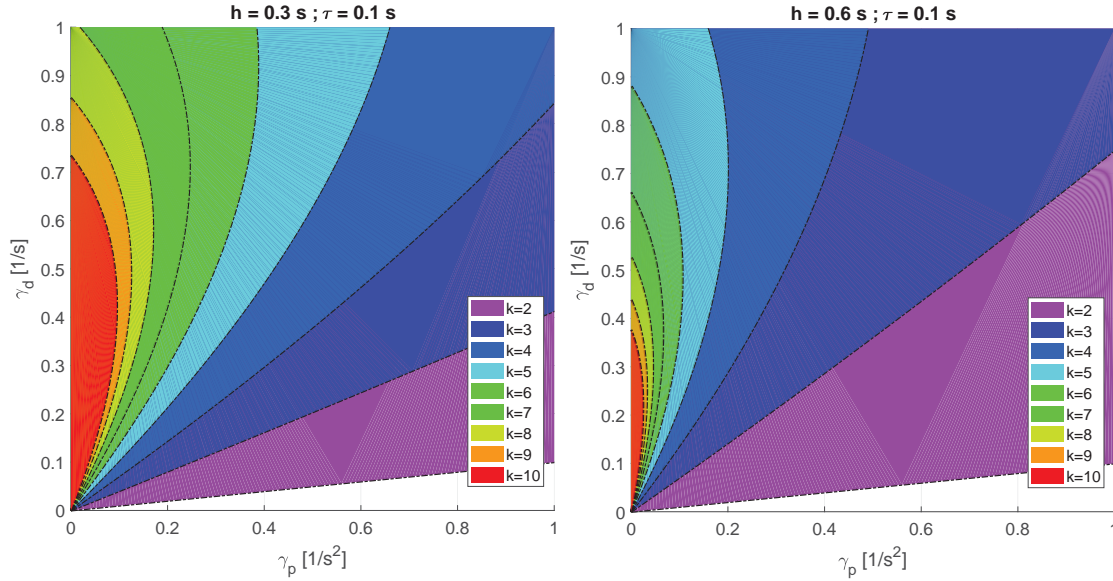


Figure 3.5: Boundary for the values of γ_p and γ_d that achieve stable poles in (3.26), with $\tau = 0.1$ s, for two values of h , 0.3s (left) and 0.6s (right), and various values of the index k , associated to the index of the saturated vehicle. The shaded areas correspond to the gain values that lead to stable poles.

the regions that achieve stable poles reduce considerably in size as the index k increases and also when the value of the timegap increases. Although not illustrated here, increasing the value of the time constant τ also reduces the size of the stable region. When the gains are chosen exactly at the boundary of the stable region, the transfer function has a pair of marginally stable poles, i.e., lying on the imaginary axis, which in the time domain translates into undamped oscillations.

For the control problem discussed here, it has been observed in simulations that the desired equilibrium might be reached for some cases in which the gains γ_p, γ_d are such that the function (3.26) has unstable poles. However, in such cases the performance is rather poor, meaning that the acceleration of the vehicles shows oscillations which would be inefficient in terms of fuel consumption and even uncomfortable for the passengers. Hence, the stability of the transfer function (3.26) can serve as a guideline to choose the control gains in the coordination layer.

The frequency domain analysis discussed here shows the limitation of the baseline control strategy in terms of scalability and versatility with respect to the timegap. Of course, even if the poles in (3.26) are stable, stability of the origin for the full PWA system remains to be proven.

The influence of the acceleration limit on the stability of a particular subsystem

In this section, a different operation mode is analyzed to determine the influence of the dynamic acceleration limits on the stability of the platoon dynamics. Once again, a platoon of n vehicles is considered, where vehicle k has the lowest acceleration capability. This time, the operation mode corresponds to the case when vehicle 1 is restricted by the coordination variable, such that it uses the acceleration limit of vehicle k together with the spacing error e_k to determine its desired acceleration. In contrast to the dynamics analyzed in the previous section, in this operation mode vehicle k is not in saturation, meaning it is following the desired acceleration prescribed by the CACC in (2.11). The dynamics of this operation mode are illustrated with the block diagram in Figure 3.6. Here, the acceleration limit of vehicle k is assumed to be a linear function of its velocity, as defined in (3.18).

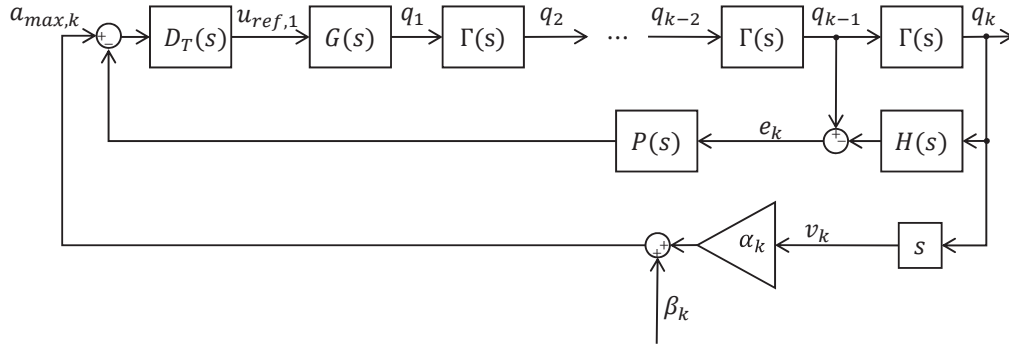


Figure 3.6: Block scheme of the closed-loop platoon dynamics subject to the baseline control strategy, when vehicle 1 is limited by the coordination variable ξ_2 . Vehicle k , the slowest in the platoon, has not reached its acceleration limit.

To assess the stability of this dynamics, the communication and actuation delays are neglected. In such case, and assuming homogeneous vehicles, the transfer function $\Gamma(s) = q_i(s)/q_{i-1}(s)$ simplifies to $H^{-1}(s)$. With this in mind, the transfer function from $\beta_k(s)$ to $q_k(s)$ is derived:

$$\frac{q_k(s)}{\beta_k(s)} = \frac{G\Gamma^{-(k-1)}}{1 + G\Gamma^{-(k-2)}P(1 - \Gamma H)} \cdot \left(1 - \frac{G\Gamma^{-(k-1)}\alpha_k s}{1 + G\Gamma^{-(k-2)}P(1 - \Gamma H)}\right)^{-1} = \frac{1/s}{(hs + 1)^{k-1}(\tau s + 1)s - \alpha_k}, \quad (3.27)$$

where the fact that $(1 - \Gamma(s)H(s)) = 0$ was used. This transfer function is relevant for the stability analysis because it involves the dynamics of all vehicles in the platoon. Moreover, the polynomial in the denominator of this transfer function appears as a factor in the characteristic polynomial for the system matrix associated to this operation mode, indicating that the coordination layer has an influence in the stability of the platoon dynamics.

The parameter α_k , the rate of change of the acceleration limit as a function of velocity, has a direct influence on the stability of the transfer function (3.27). The values for the parameters h and α_k that guarantee stable poles for this transfer function are illustrated in Figure 3.7 for two values of τ . In this figure, the shaded areas are overlapping, i.e., the area for k lies within the area for $k - 1$. Notice that as the index k increases, the range of values for α_k and h that lead to stable poles reduces.

From the analysis above, it can be concluded that instability might occur during this operation mode if the acceleration limit of the slowest vehicle decreases sufficiently fast. If that is the case, then it might not be possible to find a PWQLF to prove stability of the origin for the PWA system. The coefficient α_i can be estimated from the non-linear function for $a_{max,i}$ in (2.3). For the vehicle parameters considered in this research, which are presented later in this report, the values of α_i are always within the stable regions depicted in Figure 3.7.

Following the design guidelines derived from the previous frequency domain analyses, parametric stability studies are presented in the next section for the PWA closed-loop system dynamics corresponding to the baseline multi-layer CACC.

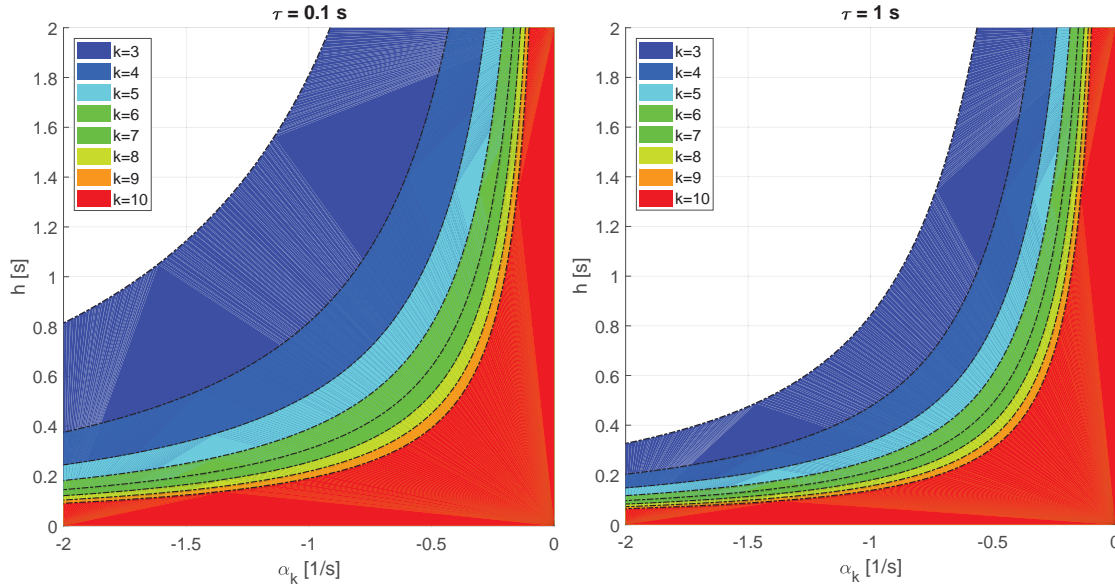


Figure 3.7: Boundary for the values of α_k and h that achieve stable poles in (3.27), for two values of τ , 0.1s (left) and 1s (right), and various platoon sizes. The values for the parameters that lead to stable poles, for each value of index k , lie in the corresponding shaded area.

3.3.2 Parametric stability analysis

In this section, the results of a parametric stability analysis are discussed. In this study, exponential stability of the origin is attempted to be proven for the PWA system that describes closed-loop platoon dynamics for the baseline control scheme. To this end, the method described in Section 3.1 is used to search for a piecewise quadratic Lyapunov function. Due to the complexity of the PWA models derived for the platoon dynamics, only the case of a 3-vehicle platoon is analyzed here. Nevertheless, analyzing a 3-vehicle platoon is relevant because it can provide insight on the influence that the control parameters have on the feasibility of the LMIs in (3.9) and (3.10).

Table 3.3: Vehicle parameters [23].

Parameter	Value	Unit	Parameter	Value	Unit	Parameter	Value	Unit
R_w	0.45	m	A_{rl}	0.039	m/s^2	ϕ_r	0	rad
J_w	232	$kg \cdot m^2$	B_{rl}	0.0037	$1/s$	g	9.81	m/s^2
J_e	2.5	$kg \cdot m^2$	C_{rl}	1.25	kg/m	r	2	m
$T_{max,i}, \forall i$	2500	$N \cdot m$	τ	0.1	s	h	0.3	s
η_T	1	-	θ_g	0.12	s	k_p	0.2	-
$L_i, \forall i$	18	m	θ_c	0.02	s	k_d	0.7	-

For this parametric study, a set of three trucks with identical drivelines is chosen. The masses of the trucks are set to $(m_1, m_2, m_3) = (20, 20, 40) \cdot 10^3 \text{ kg}$, so that vehicles 1 and 2 have a higher acceleration limit than vehicle 3. The acceleration limit is estimated with expression (2.3) using the parameters in Table 3.3, but setting the air-drag coefficient C_{rl} and the time delays θ_g, θ_a equal to zero. Furthermore, the driveline ratio i_d is fixed to the value corresponding to the highest velocity range, as shown in Table 3.4.

The following linear functions are used to describe the heterogeneous acceleration limits of the

Table 3.4: Driveline ratios i_d [23].

Velocity range [km/h]	Driveline ratio i_d [-]
0 - 10	24
10 - 20	14.75
20 - 30	8.75
30 - 45	5.25
45 - 70	3
> 70	2.5

trucks:

$$\begin{aligned}
 a_{max,1} &= -0.0035v_1 + 0.6177 \text{ [m/s}^2\text{]} \\
 a_{max,2} &= -0.0035v_2 + 0.6177 \text{ [m/s}^2\text{]} \\
 a_{max,3} &= -0.0036v_3 + 0.2991 \text{ [m/s}^2\text{]}.
 \end{aligned} \tag{3.28}$$

Notice that the coefficients of v_i in (3.28) are rather small, which is explained by the fact that the air drag is assumed to be zero at all driving speeds and only internal and road friction are considered to affect the acceleration limit. The maximum acceleration from rest, i.e., the constant terms in (3.28), is small because it is assumed that the trucks are driving with the highest gear available in the gearbox (see Table 3.4). In this research, it was observed that the acceleration limits do not have a crucial role in the stability of the PWA system, provided that the parameters α_i in (3.18) satisfy the stability conditions discussed in Section 3.3.1. In Appendix B, a more detailed parametric study is presented in which stability is assessed for various values of the acceleration limit.

The feasibility of the LMIs in (3.9) and (3.10) is verified for several points in the design space $\gamma_p \times \gamma_d \times h \times \tau \in \mathbb{R}^4$ using the YALMIP toolbox in MATLAB [10]. The values for the gains γ_p and γ_d are chosen between 0.01 and 1; the desired timegap h is set between 0.1 and 3 s; the actuation time constant τ is chosen between 0.1 and 1 s. The ranges for these parameters are defined in accordance to the frequency domain analysis in Section 3.3.1, such that some of the parameter combinations provide stable eigenvalues for the transfer functions (3.26) and (3.27), while some combinations result in unstable eigenvalues for these transfer functions.

For this study, the desired cruising speed is set to $v_{des} = 80 \text{ km/h}$, which is a feasible speed for the three vehicles in the platoon, in view of the acceleration limits in (3.28). The control gains k_p and k_d used for the CACC in the lower layer are fixed to the values shown in Table 3.3, which achieve a stable transfer function $\Gamma(s)$ in (3.24).

Figure 3.8 presents the results of this study. In this figure, cross-sections of the four-dimensional design space are depicted, choosing three values for h and three values for τ . The values for γ_p and γ_d that lead to feasible LMIs are shown as green dots. The red crosses correspond to parameter combinations that lead to infeasible LMIs. The dashed line in the plots indicates the bound for the region of the design space for which all subsystems in the PWA model have (marginally) stable dynamics. This boundary was determined based on the analysis presented in Section 3.3.1.

Notice in Figure 3.8 that, for the plots with $h = 0.3s$, some of the feasible points lie beyond the boundary for which the subsystems in the PWA are stable. This confirms a prior statement: for a PWA system, even when the dynamics in some regions of the partition are unstable, it might be possible to find a PWQLF that proves global exponential stability of the origin.

On the other hand, notice in Figure 3.8 that, except for the plot with $h = 3s$ and $\tau = 1s$, all the infeasible points lie to one side of the dashed line. This is a useful results because, for most values of h and τ , the stability of the individual subsystems in the PWA model serves as a good indicator of the feasibility of the LMIs. For the exceptional case with $h = 3s$ and $\tau = 1s$, the infeasibility of the LMIs for most combinations of γ_p and γ_d does not indicate that the origin is unstable. As explained in Section 3.1, the feasibility of the LMIs is only a sufficient condition to prove

exponential stability of the origin for a PWA system, but it is not necessary. In fact, simulations indicate a stable behavior for those parameter combinations that lead to stable subsystems even if the LMIs are not feasible, but in such case the performance is not adequate. An example of parameter combinations that lead to a stable PWA system but for which a Lyapunov function could not be found is presented in Chapter 4.

In Appendix B, the parametric study described here is repeated for a platoon with 4 vehicles, exploring the same subset of the design space discussed above. The results are consistent with those presented here: for most parameter combinations that achieve stable subsystems in the PWA model, a PWQLF function can be derived. For the 4-vehicle platoon, the number of parameter combinations for which a Lyapunov function can be found is significantly lower compared to the results in Figure 3.8, which is to be expected in view of the stability analysis discussed in Section 3.3.1.

The parametric studies and frequency domain analyses presented in this section provide useful insight on how to design the control gains for the coordination layer such that the platoon dynamics that arise from the baseline control scheme are stable. By proving the feasibility of the LMIs in (3.9) and (3.10), global asymptotic stability of the desired equilibrium for the closed-loop platoon dynamics has been proved for several combinations of control parameters. Furthermore, these studies allow to conclude that, for the baseline multi-layer CACC scheme the stability of the individual subsystems that compose the PWA model is a good indicator of the feasibility of the LMIs used to derive a PWQLF. In Chapter 4, computer simulations are presented that confirm the stability results discussed here.

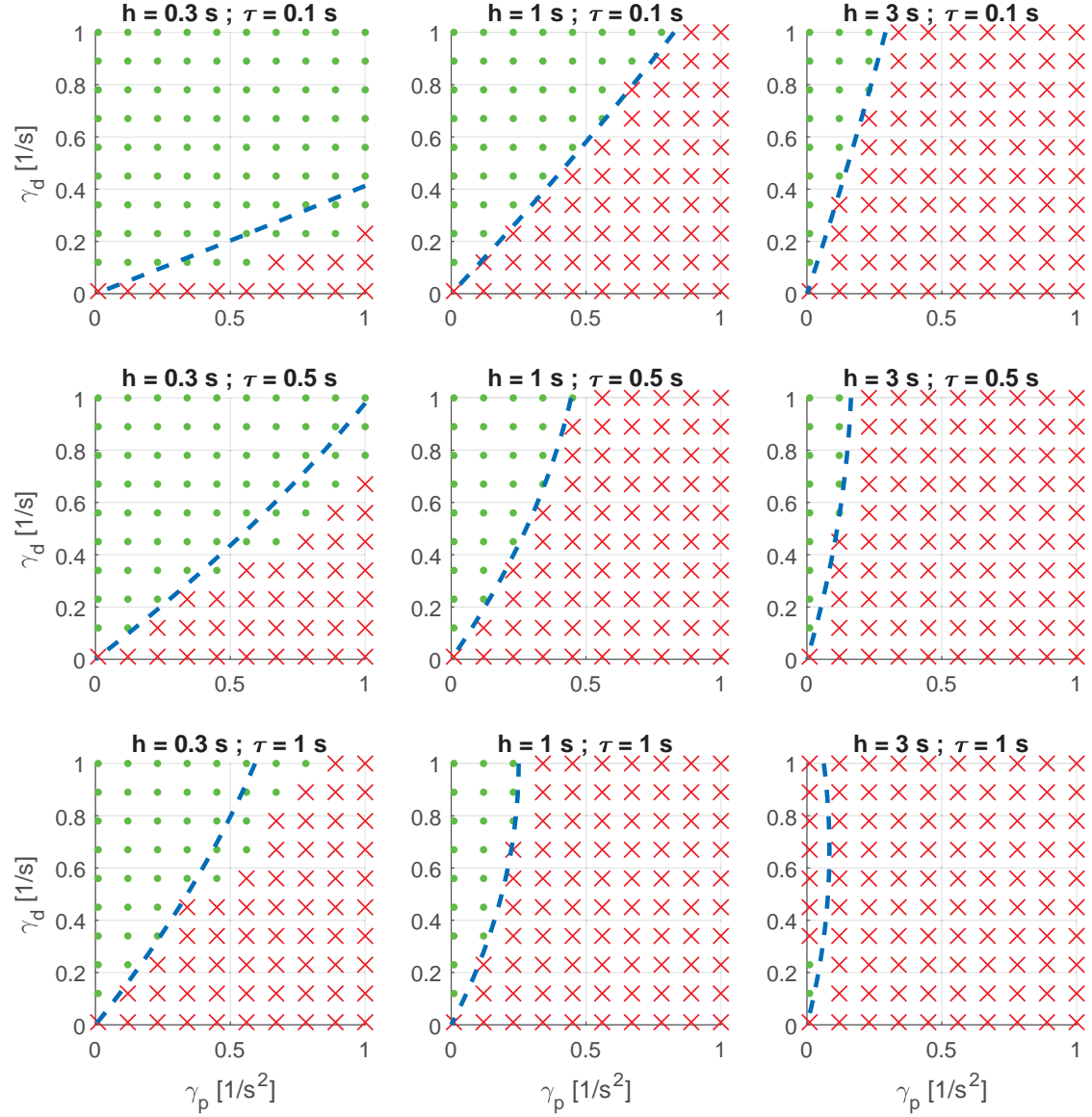


Figure 3.8: Parametric stability analysis for a three-vehicle platoon subject to the baseline control scheme, varying γ_p , γ_d , h , and τ . The green dots indicate points in the design space for which the LMIs (3.9) and (3.10) are feasible. The red dots indicate parameter combinations that lead to infeasible LMIs. The dashed line bounds the region for which (marginally) stable eigenvalues are obtained for all the subsystems in the PWA model.

3.4 Stability analysis for the proposed control scheme

After analyzing the stability properties of the baseline control scheme, the same tools are applied to the multi-layer strategy proposed in Section 2.3. Similar to the procedure in the previous section, first the dynamics of a particular operation mode is analyzed using a frequency domain approach. Then, a parametric study is conducted to assess the stability of the corresponding PWA model. The results presented in this section illustrate some of the advantages of the proposed control scheme when compared to the baseline.

3.4.1 Frequency domain analysis

As discussed in Section 3.3.1, analyzing the stability of the individual subsystems in a PWA model can provide insight on how to choose the control gains in order to increase the chances of finding a PWQLF that proves stability of the PWA system. To this end, the subsystems in the PWA model for the proposed control strategy are analyzed to identify which of those might become unstable when changing the gains γ_p and γ_d used in the variables σ_i , as defined in (2.16).

Consider a platoon of n vehicles under the proposed multi-layer strategy. Furthermore, assume that vehicle k has the lowest acceleration limit in the platoon. With the proposed control scheme, the acceleration limit of vehicle k is used to restrict the desired acceleration of vehicles 1 to $k - 1$, while taking into account the spacing error of the vehicle behind.

To assess which subsystems are most sensitive to the control gains γ_p and γ_d , the characteristic polynomials of the various system matrices are computed with the help of the Symbolic Math Toolbox in MATLAB [11]. From this procedure, a particular operation mode is identified as the most critical one: the case when vehicle k is driving at its acceleration limit and vehicles 1 to $k - 1$ are all restricted by the coordination variable ξ_i . The block scheme in Figure 3.4 illustrates the dynamics of this operation mode. In Figure 3.4, the function $P(s) = \gamma_d s + \gamma_p$ is the error feedback implemented with the variables σ_i ; the transfer functions $D_c(s)$, $G(s)$, and $H(s)$ are as defined in Section 3.3.1.

To analyze the stability of this operation mode, the transfer function from $a_{max,k}$ to $u_{ref,k-1}$ is derived:

$$\Theta_{k-1}(s) := \frac{u_{ref,k-1}(s)}{a_{max,k}(s)} = \frac{D_c(s) (1 + G(s)P(s)H(s))}{1 + D_c(s)G(s)P(s)}. \quad (3.29)$$

If one extends the block diagram in Figure 3.9 to include vehicles 1 to $k - 3$ the transfer function from $a_{max,k}$ to $u_{ref,i}$ can be derived as follows:

$$\Theta_i(s) := \frac{u_{ref,i}(s)}{a_{max,k}(s)} = \frac{D_c(s) (D_c^{k-i-1}(s) + \Theta_{i+1}(s)P(s)H(s))}{1 + D_c(s)G(s)P(s)}, \forall i \in \{1, \dots, k - 2\}. \quad (3.30)$$

This transfer function is relevant because it illustrates how the input $a_{max,k}$ propagates downstream from vehicle k towards vehicle 1, as a result of the coordination layer in the proposed control scheme. The transfer function from $a_{max,k}$ to e_i could have been analyzed instead; in that case the poles turn out to be defined by the same polynomial in the denominator of (3.30).

If one computes the full expression for $\Theta_i(s)$ a pattern can be identified: the denominator of $\Theta_i(s)$ is $(1 + D_c(s)G(s)P(s))^{k-i}$, for $i \in \{1, \dots, k - 1\}$. Now, for the sake of simplicity, the communication and actuation delays are neglected. In such a case, the denominator for $\Theta_i(s)$ simplifies to $(\tau s^3 + s^2 + \gamma_d s + \gamma_p)^{k-i}$. This polynomial is included as a factor in the characteristic polynomial for the system matrix that describes the dynamics in this operation mode. This polynomial allows to conclude that the stability of this operation mode is independent of the timegap h and of the value of the index k . If the time delays are neglected, the transfer functions

the parameter combinations identified here that violate the previous statement, it might still be possible to find a Lyapunov function. As suggested in [4], refining the state space partition by subdividing the initial regions provides additional flexibility in the search for a PWQLF. However, this refinement is not attempted here because it is extremely time-consuming and the results might not add significant value to this report.

The stability analyses discussed in this chapter concern only platoons with 3 vehicles. Although, in principle, it is possible to analyze stability of PWA models for larger platoons, in practice it is not feasible to conduct such numerical analyses due to limitations in computational power. An alternative to analyze the stability for platoons with more than 3 vehicles is to consider some additional assumptions that simplify the PWA model. For instance, the number of regions in the state space partition reduces considerably if it is assumed that some vehicle k has an acceleration limit that is sufficiently low compared to the limit of all other platoon members. Under this assumption, vehicle k prescribes, at all times, the acceleration limit for the platoon through the coordination layer. The other vehicles would not reach their own saturation point, assuming their initial spacing errors are sufficiently small.

Yet another alternative to assess the stability of the platoon dynamics is to conduct computer simulations. This approach is used in the following chapter, considering platoons with more than three vehicles and also more realistic phenomena in the dynamics.

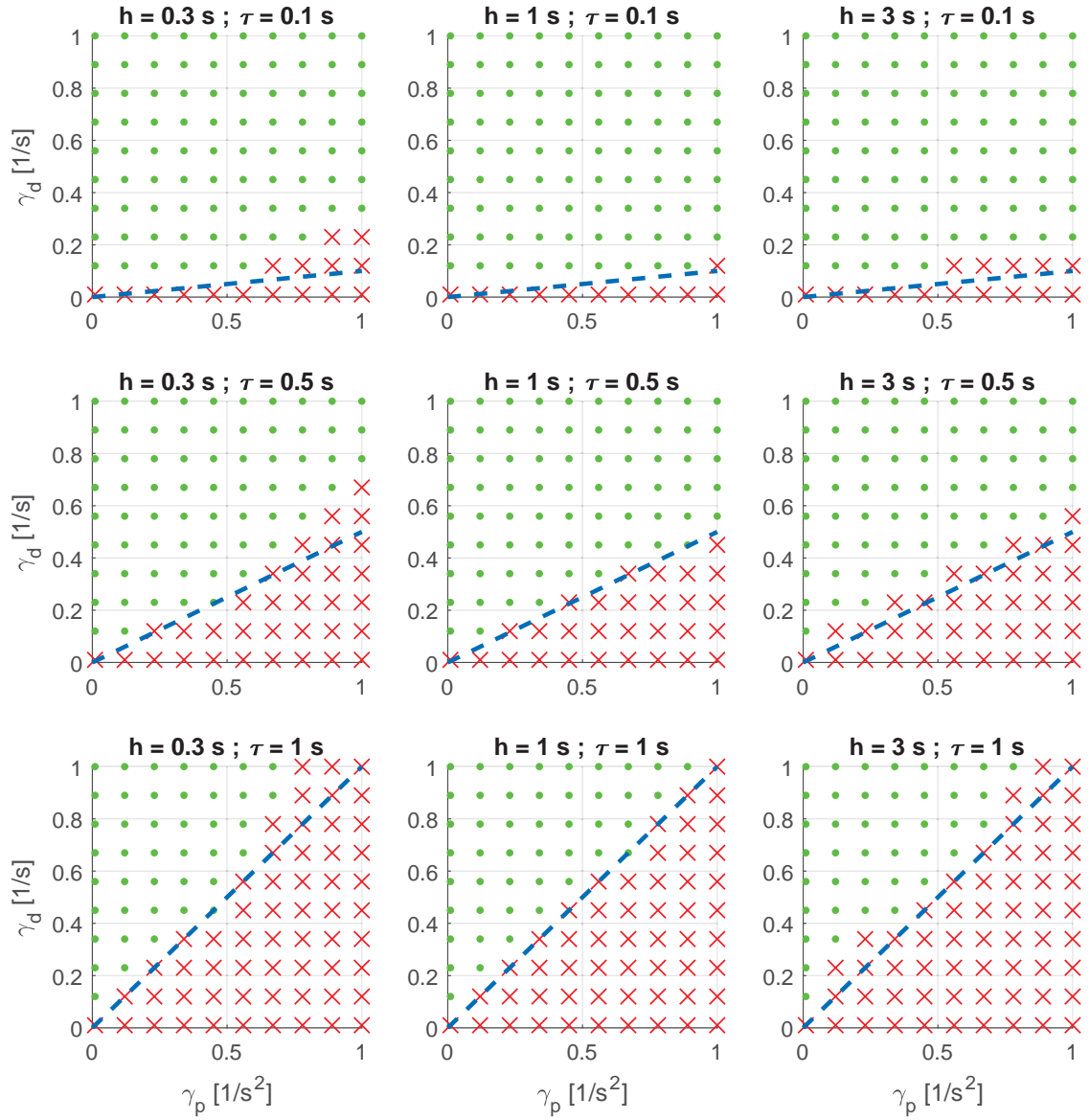


Figure 3.10: Parametric stability analysis for a three-vehicle platoon subject to the proposed control scheme, varying γ_p , γ_d , h , and τ . The green dots indicate points in the design space for which the LMIs (3.9) and (3.9) are feasible. The red dots indicate parameter combinations that lead to infeasible LMIs. The dashed line bounds the region for which (marginally) stable eigenvalues are obtained for all the subsystems in the PWA model.

Chapter 4

Simulation study

As explained in Chapter 3, assessing the stability of the platoon dynamics via PWA models is computationally feasible for platoons of up to four vehicles, for the case of the baseline control scheme, and for up to three vehicles for the newly proposed scheme. Nevertheless, the PWA models for larger platoons can be used to conduct simulations and assess stability using such simulation results. This chapter presents the results of a simulation study comparing the control strategies described in Chapter 2, both with piecewise linear and non-linear simulation models.

The purpose of this simulation study is to illustrate the limitations of the baseline control scheme and how the proposed algorithm overcomes those limitations. Moreover, the effects of vehicle parameters and control gains on the performance of the control schemes are illustrated here. Simulations are conducted with some peculiar parameter combinations identified in Chapter 3 to illustrate why it is not always possible to find a PWQLF for a PWA system that exhibits stable behavior in simulations.

The results in this chapter were obtained using two different simulation models. The first model is based on piecewise-linear (affine) systems, as described in chapters 2 and 3. The simulations with this model confirm the stability results presented in Chapter 3. However, the analysis based on PQA models was limited to platoons of up to three vehicles. To this end, a non-linear simulation model is used to simulate larger platoons which includes more realistic phenomena such as time delays and gear shifting. Both the PWA and non-linear simulation models are developed in MATLAB-Simulink.

For the simulations presented in this chapter, the vehicle parameters from Tables 3.3 and 3.4 are used, unless specified otherwise. These parameters correspond to trucks with homogeneous driveline dynamics. The heterogeneity is introduced by choosing different vehicle masses so that the acceleration capabilities are not homogeneous. The critical case for both control schemes analyzed in this report corresponds to the scenario when the last vehicle in the platoon has the lowest acceleration limit, so the vehicle masses in the simulations below are chosen accordingly.

4.1 Simulations for a 3-vehicle platoon

This section compares simulation results based on PWA models derived with the rationale in Section 3.2. Examples of the computed PWQLF functions are also provided to illustrate that these indeed meet the characteristics of a Lyapunov function, thus proving asymptotic stability of the origin. Furthermore, the differences in performance between the two control algorithms are illustrated.

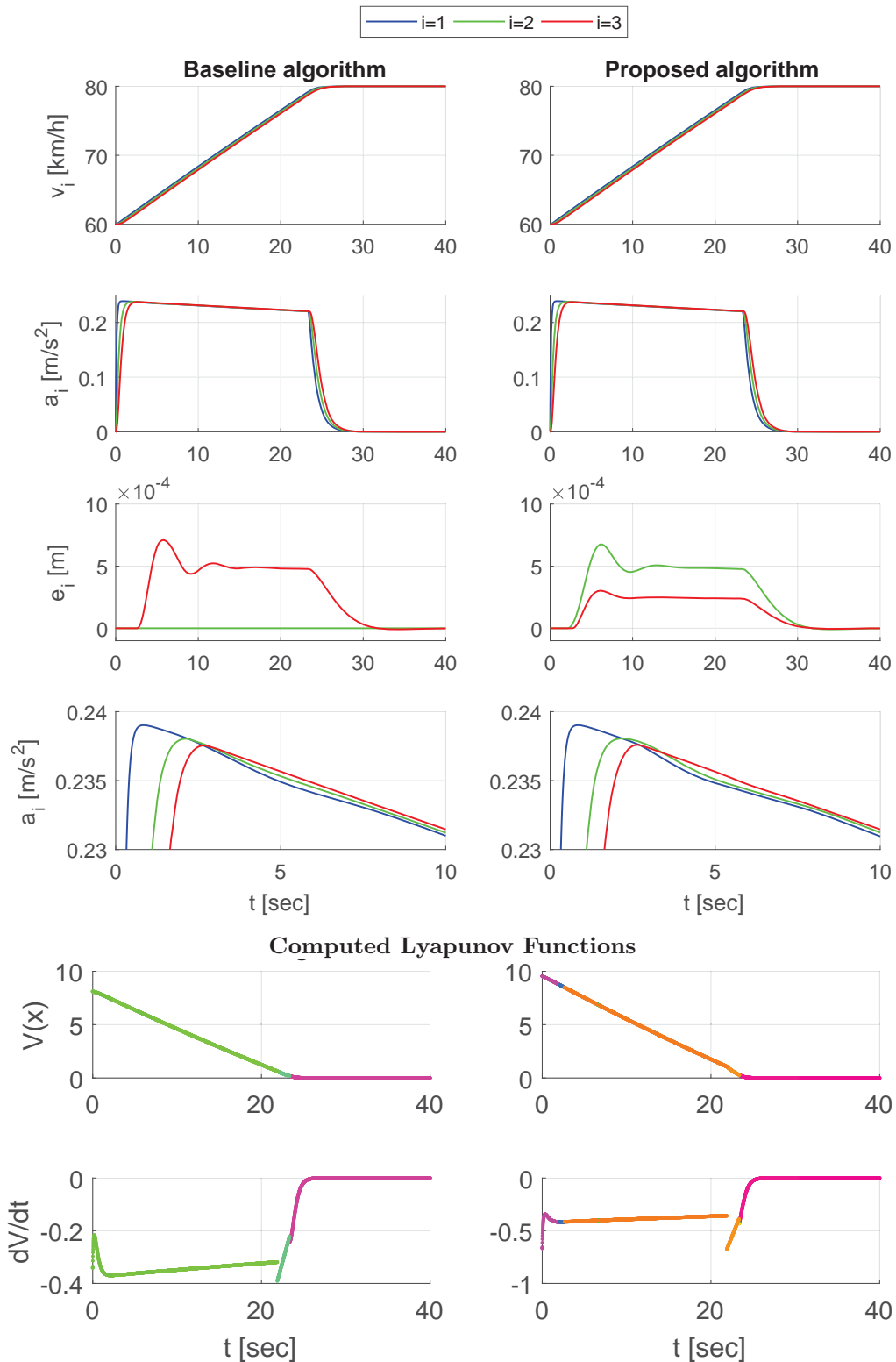


Figure 4.1: Time response for velocity, acceleration, and spacing error of a 3-vehicle platoon (top), and the computed Lyapunov functions evaluated for the state trajectories (bottom). The different colors in the plots for $V(x)$ and dV/dt indicate different regions of the state space partition. The simulations are based on PWA models. The plots to the left correspond to the baseline control scheme. The plots to the right correspond to the proposed control scheme.

The first simulation scenario consists of a 3-vehicle platoon with masses

$$(m_1, m_2, m_3) = (20, 20, 40) \cdot 10^3 \text{ kg}. \quad (4.1)$$

The scenario corresponds to a platoon transitioning from a medium to a high cruising speed, i.e., from 60 to 80 km/h . A step input is applied to the desired velocity v_{des} in the cruise controller of vehicle 1. The spacing errors and accelerations are initially equal to zero for the three vehicles. Gear-shifting, time delays, and air drag are not considered in this simulation. The cruise controller in vehicle 1 is tuned so that the vehicles are forced to drive at their acceleration limit, which is achieved by setting the proportional gain k_v in the cruise controller (2.12) equal to 1. This particular choice for k_v allows to illustrate the benefits of the control schemes.

The control gains for the coordination layer of the two control schemes are set to $\gamma_p = \gamma_d = 1$. The timegap is chosen as $h = 0.3 \text{ s}$ and the driveline time constant as $\tau = 0.1 \text{ s}$. As discussed in Chapter 3, for these parameter values a Lyapunov function can be found both for the baseline and proposed control schemes. The plots in Figure 4.1 show the time response for the velocity, acceleration, and spacing error of the 3-vehicle platoon.

The plots in Figure 4.1 show that the velocity and acceleration responses are very similar for both control schemes. The three vehicles accelerate from the initial speed to the desired one, while the platoon leader sets an acceleration level that is feasible for vehicle three. Notice that the order of magnitude of the spacing error is in millimeters, which confirms that platoon cohesion is guaranteed with any of the two control schemes. In this simulation, the conspicuous difference between the two control schemes is in the spacing error response. With the baseline control scheme, only vehicle 3, the slowest in the platoon, has an increase in spacing error during the accelerating phase. On the other hand, with the proposed algorithm, vehicles 2 and 3 exhibit an increase in their spacing error, which can be explained as follows.

With the proposed control strategy, the desired acceleration of vehicle 2 is limited by the expression $\xi_3 - \sigma_3 = a_{max,3} - \gamma_p e_3 - \gamma_d \dot{e}_3$ (see (2.17)), such that vehicle 3 is not left behind due to its lower acceleration limit. During the time when the desired acceleration of vehicle 2 is $u_{ref,2} = \xi_3 - \sigma_3$, this vehicle it is not able to regulate its spacing error down to zero because it is not following the intended desired acceleration u_2 prescribed by the CACC controller (2.11). However, as vehicle 1 receives the coordination variable $\xi_2 = a_{max,3}$ and the variable $\sigma_2 = \gamma_p e_2 + \gamma_d \dot{e}_2$, this vehicle limits its desired acceleration to $u_{ref,1} = \xi_2 - \sigma_2$, such that it respects the acceleration limit of vehicle 3, while compensating for the spacing error of vehicle 2. Vehicle 2 has a positive spacing error during the transient because it takes some time for vehicle 1 to respond to the change in e_2 . At around $t = 20 \text{ s}$ the spacing error of vehicles 2 and 3 starts to decrease, although very slowly. In fact, if the desired cruising speed v_{des} were set higher, it would be possible to observe how the spacing errors e_2 and e_3 continue to decrease after the initial transient period.

The detailed view for the acceleration response at the bottom of Figure 4.1, a particular formation can be identified: when vehicle 3 reaches its limit, vehicles 1 and 2 eventually reduce their acceleration slightly below that of vehicle 3. In both control schemes, this driving formation is achieved by the coordination variable and the terms associated to the spacing error. Notice also the subtle differences between the two control schemes in the acceleration profiles. With Zeger's algorithm, the acceleration of vehicles 1 and 2 exhibit slightly more undershoot with respect to the acceleration limit of vehicle 3. On the other hand, with the proposed control scheme, the acceleration of the vehicles is slightly more smooth.

The plots at the bottom of Figure 4.2 illustrate the computed Lyapunov functions $V(x)$ and the time derivative $\dot{V}(x)$ for both control schemes. These functions are evaluated for the state trajectory obtained in the aforementioned simulation. Notice that the Lyapunov functions are indeed positive definite and their time derivatives are negative. When the vehicles have reached the equilibrium, i.e., around $t = 35 \text{ s}$, both $V(x)$ and $\dot{V}(x)$ are equal to zero. Even when the state trajectories traverse various regions of the state space partition, the computed PWQLFs are continuous. On the other hand, the time derivative of the Lyapunov functions are discontinuous.

The LMIs presented in Chapter 3 do not guarantee continuity of the time derivative, but this is not required to prove stability of the origin for a PWA system, provided the dynamics contains no sliding modes [4].

The fact that both vehicles 2 and 3 exhibit an increase in spacing error when using the proposed algorithm could be considered a disadvantage because in this case the total space occupied by the platoon on the road is larger during the transient. From this simulation, it can be concluded that, for a platoon of three vehicles, with a sufficiently low timegap h , and a sufficiently low time constant τ , the baseline control strategy offers better performance in terms of platoon cohesion compared to the proposed control scheme. Nevertheless, as discussed later in this report, other simulation scenarios indicate that this is not always the case.

Simulations with parameter values that lead to stable response but poor performance

The simulation illustrated in Figure 4.1 is repeated but this time setting the gains in the coordination variables to $\gamma_p = 0.89$ and $\gamma_d = 0.23$. For these values, some subsystems in the PWA model for the baseline control approach are unstable. Nevertheless, a PWQLF can be found, as indicated in Figure 3.8. On the contrary, these gain values guarantee marginally stable subsystems in the PWA model for the proposed control scheme, but the LMIs turn out to be infeasible. This particular tuning for the control gains allows to illustrate why in some cases it is not possible to find a PWQLF for a PWA model composed of stable subsystems and also what is the effect of the control gains on the transient performance.

The simulation results using the gain values discussed before are shown in Figure 4.2, where only the accelerations and spacing errors are depicted. Notice that both control strategies cause oscillations in the acceleration of vehicles 1 to 3. In fact, vehicle 3 is periodically switching in and out of its acceleration limit, which explains the periodic increase and decrease in spacing error. In both cases, the platoon reaches the desired equilibrium at $t = 40$ s and platoon cohesion is guaranteed. However, from a performance point of view, this controller tuning is worse than the tuning used in Figure 4.1.

For the PWA model corresponding to the baseline control scheme, in spite of the oscillatory behavior associated to unstable subsystems, it is possible to derive a PWQLF. Figure 4.3 illustrates the computed Lyapunov function $V(x)$ together with the time derivative $\dot{V}(x)$, evaluated for the state trajectory obtained in the simulation illustrated in Figure 4.2. The Lyapunov is positive definite and its time derivative is negative definite, thus proving asymptotic stability for the baseline controller with the aforementioned parameters.

The control gains chosen for the simulation in Figure 4.2 achieve stable subsystems in the PWA model for the proposed control strategy. However, it is not possible to construct a Lyapunov function from the LMIs presented in Chapter 3. The simulation offers a possible explanation for the infeasibility of the LMIs. Notice in the spacing error plot to the right of Figure 4.2 that both signals e_2 and e_3 show oscillations that fade out when the platoon reaches the equilibrium. These indicate that vehicles 2 and 3 are switching periodically between the desired acceleration prescribed by the CACC and the limit imposed by $a_{max,3}$. Hence, the state trajectory is circling around various regions in the state-space partition. As suggested in [4], refining the state-space partition might allow to find a PWQLF for this peculiar combination of control gains, but in any case the poor performance observed in Figure 4.2 does not make the refinement worthy of the time it would require.

The simulations discussed in this section confirm the results obtained in the numerical analyses of Chapter 3. Furthermore, the influence of the control gains on the transient performance is also illustrated. The fact that a Lyapunov function can be found does not guarantee an adequate performance, since the acceleration and spacing error of the vehicles might exhibit sustained oscillations while the platoon accelerates.

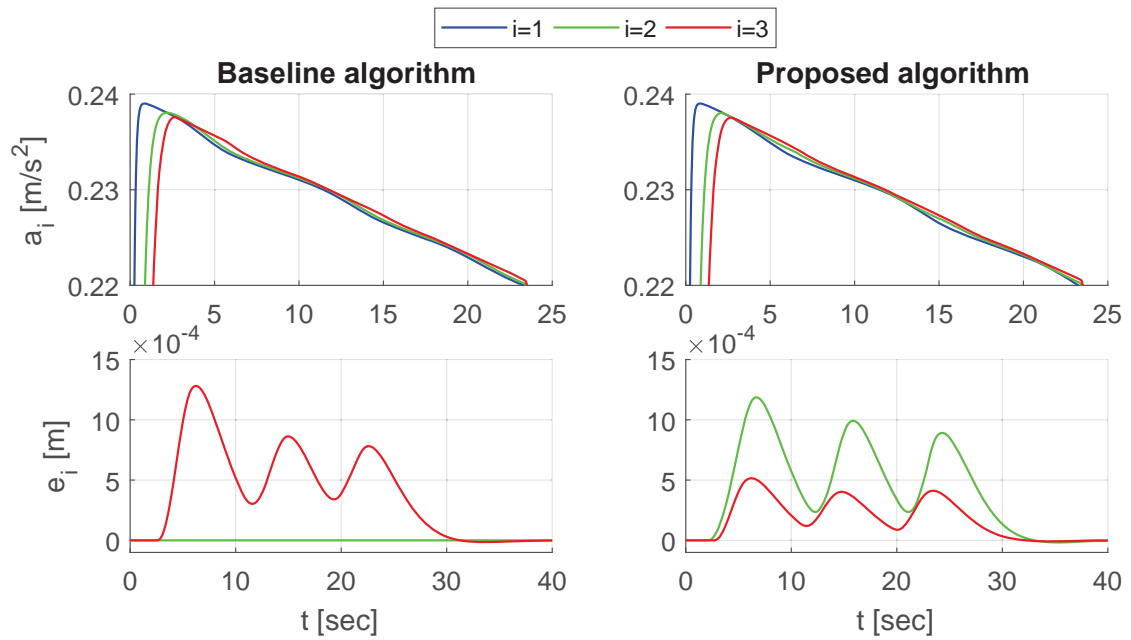


Figure 4.2: Time response for acceleration and spacing error of a 3-vehicle platoon. The plots to the left correspond to the baseline control scheme. The plots to the right correspond to the proposed control scheme. The chosen control gains induce transient oscillations in the acceleration of the vehicles

For the simulation scenario discussed here, the advantages of the proposed control scheme are not evident. To this end, in the next section the simulation study is extended to larger platoons.

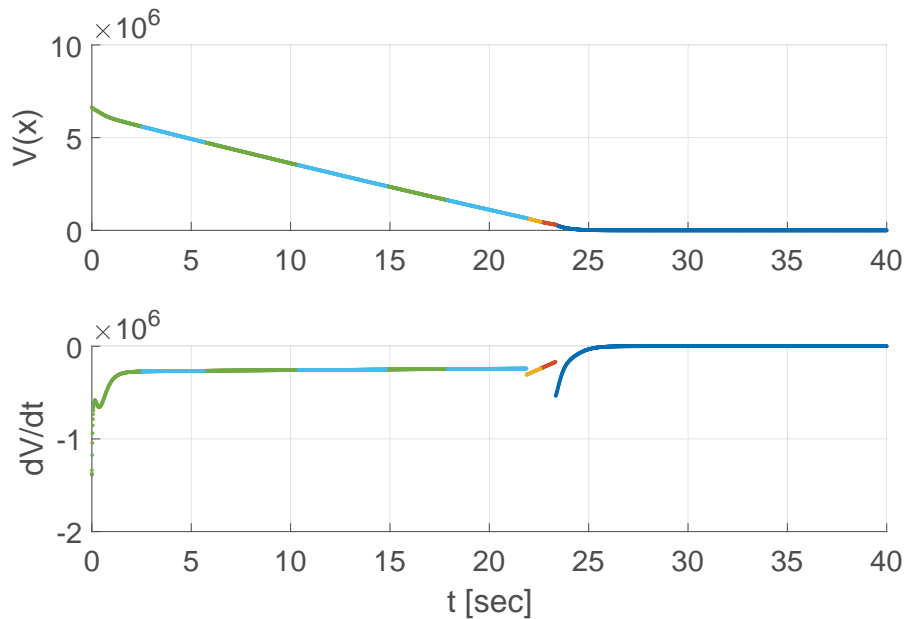


Figure 4.3: Computed Lyapunov function for the PWA system corresponding to the baseline control scheme. The function is evaluated for the state trajectory depicted in Figure 4.2. The line colors indicate different regions of the state space partition.

4.2 Simulations for larger platoons

Although the stability analysis in Chapter 3 is limited to platoons with 3 vehicles, PWA models for the platoon dynamics can be derived for larger platoons. Instead of conducting simulations based on PWA models, in this section a non-linear simulation model is used to assess the asymptotic stability and performance of the control schemes in question when applied to platoons with more than 3 vehicles.

The simulation model used here was developed by the department of Integrated Vehicle Safety at TNO. It considers time delays in the inter-vehicle communication, in the radar measurements, and in the actuation dynamics, which were determined from real hardware and sensors. This simulation model was customized to implement the control strategies discussed in this report, together with the dynamic acceleration limitation that includes the effect of aerodynamic drag and a simple gear-shifting strategy. With this complex simulation model, the robustness of the control schemes is assessed in face of more realistic dynamics and disturbances.

Simulation scenarios for platoons of 4 and 10 vehicles are discussed in this section. Two values of timegap for the spacing policy are used to illustrate the strong influence of this parameter on the performance of the control schemes. In the simulations below, the last vehicle in the platoon has the lowest acceleration limit as a consequence of its higher vehicle mass.

It is worth mentioning that simulations were also conducted for a 10-vehicle platoon in which the slowest vehicle is not at the rear but somewhere in between the platoon. As no remarkable distinguishing phenomenon was observed in those simulations, the results are not presented here. Once again, the critical scenarios correspond to those in which the last vehicle in the platoon has the lowest acceleration capabilities. Simulations for even larger platoons were not attempted because for the case of 10 vehicles the computation time required is already quite considerable. Moreover, from the simulation scenarios with 4 and 10 vehicles, it is possible to infer how the control schemes might behave for even larger platoons.

4.2.1 4-vehicle platoon

The scenario discussed in Section 4.1 is simulated now considering a 4-vehicle platoon. The vehicle mass distribution is the following:

$$(m_1, m_2, m_3, m_4) = (20, 20, 20, 40) \cdot 10^3 \text{ kg}. \quad (4.2)$$

In this scenario, the platoon starts driving at a constant speed of 60 km/h with no spacing errors. The desired cruising speed is set to $v_{des} = 80 \text{ km/h}$. The timegap is set to $h = 0.3 \text{ s}$, and the actuation constant to $\tau = 0.1 \text{ s}$. Other vehicle parameters, including time delays in communication and actuation, are listed in Table 3.3. The gear-shifting strategy is described in Table 3.4.

To choose adequate values for the control gains in the coordination layer, the stability of the poles in the transfer functions (3.25) and (3.30) is assessed. Recall that these transfer functions describe the closed-loop platoon dynamics for a particular operation mode of the control schemes in question. These operation modes were identified as critical because of their sensitivity to the tuning of the control gains. Notice that the simulation model does contain time delays, which affect the stability of the aforementioned transfer functions. However, for the sake of simplicity and because the time delays considered here are rather small, the stability of the poles in these transfer functions is verified while neglecting the time delays.

A numerical routine is implemented in MATLAB to determine the gain values that minimize the the real part of the poles for the transfer function (3.25), associated to the baseline control strategy. In other words, the gains are chosen such that the poles are located in the open left half complex plane and as far as possible from the imaginary axis. This criterion is used to make the transients decay fast during the operation mode described associated to this transfer function. With this procedure, the control gains are chosen as $\gamma_p = 0.14$ and $\gamma_d = 0.61$. These gain values also achieve stable poles in the transfer function (3.30) associated to the proposed control strategy, so these gains are used to conduct simulations for both control schemes and allow for a direct comparison.

The results for this simulation are shown in Figure 4.4, where a comparison is offered between the two control schemes. A significant difference in this simulation compared to that in Section 4.1 is the presence of gear-shifting. Notice that around $t = 16 \text{ s}$ the acceleration of vehicle 4 has a step-like response, which indicates that this vehicle has shifted to a higher gear, thus decreasing its acceleration limit. This step disturbance in the acceleration limit of vehicle 4 is propagated through the coordination layer causing an undershoot in the acceleration of vehicles 1 to 3. Notice in the detailed view for acceleration that the undershoot is less severe when using the proposed control scheme. Overall, in this scenario the acceleration response is smoother when using the proposed algorithm.

In this simulation, the proposed algorithm achieves smaller spacing error for vehicle 4 compared to the baseline approach. However, with the proposed algorithm the spacing error of vehicles 2 and 3 increase during the transient, which is not the case for the baseline algorithm. This is the main disadvantage of the proposed algorithm; not only the spacing error of the slowest vehicle increases during accelerating phases, but also that of the vehicles between the first and the slowest. Still the proposed scheme achieves smoother acceleration and overall smaller spacing errors.

One of the control goals for this platooning problem is disturbance attenuation. A formal analysis of disturbance attenuation or string stability properties as defined in [14] is out of the scope of this thesis. However, the simulation results allow to qualitatively assess how the disturbances in the acceleration limit propagate through the platoon. For the case of the baseline scheme, notice in Figure 4.4 that the undershoot in acceleration of vehicles 1 to 3, between $t = 15 \text{ s}$ and $t = 20 \text{ s}$, can be considered as a string stable behavior because the undershoot attenuates as it propagates from vehicle 1 to vehicles 2 and 3. This attenuation is achieved by the CACC in the lower layer of the baseline control approach.

Assessing string stability for the proposed control scheme is not straightforward. Recall that in the proposed scheme the coordination layer is used to directly limit the desired acceleration for all vehicles in front of the slowest. Hence, disturbances in the acceleration limit of the slowest vehicle are propagated downstream, contrary to the upstream propagation discussed in the previous paragraph. For this reason, it would not be appropriate to apply the string stability definition presented in [14], which deals only with upstream disturbance attenuation.

The acceleration plots to the right of Figure 4.4 illustrate how the step disturbance in $a_{max,4}$ propagates towards vehicles 3, 2, and 1 causing an undershoot that is more pronounced as it propagates downstream. This could be regarded as a string unstable behavior in downstream direction. In spite of this, the proposed algorithm exhibits an asymptotically stable response with adequate performance in terms of platoon cohesion, since the transient spacing error is in the order of centimeters. It is worth mentioning that the aforementioned disturbance amplification is only present in the operation mode where the vehicles in front of the slowest are being restricted by the coordination layer.

The simulation described before is repeated now for a timegap of $h = 1$ s. The values for the gains γ_p and γ_d are not modified because these still achieve stable poles in (3.26) in spite of the larger timegap. This time the desired cruising speed is set higher, $v_{des} = 100$ km/h, but the initial conditions are not altered. This higher cruising speed allows for a longer period of acceleration during which the transient performance can be observed.

Figure 4.5 illustrates the results of the simulation with a timegap of 1 s. Compared to the simulation with $h = 0.3$ s, in this case the spacing error reaches larger magnitudes during the transient regardless of the control scheme. Consequently, the undershoot in the acceleration of vehicles 1 to 3 is more pronounced. With both control algorithms platoon cohesion is guaranteed, but the proposed algorithm achieves smaller spacing errors.

Studying the plots at the bottom of Figure 4.5, the oscillations in acceleration that have been mentioned various times throughout this report can be clearly observed. For the case of Zeger's control scheme, the step disturbance in the acceleration limit of vehicle 4 induces oscillations in the acceleration of vehicles 1 to 3. During the accelerating period, vehicle 4 is periodically switching between driving at its limit and following the input prescribed by the CACC. This oscillatory behavior is inadequate for passenger comfort and fuel efficiency. For the previous reason, in this scenario the proposed algorithm outperforms the baseline scheme.

To reduce the oscillations in acceleration when using the baseline approach, the control gains γ_p and γ_d should be chosen small, but in that case the spacing error would have a larger amplitude during the transient. The baseline algorithm faces a compromise between smooth acceleration and small spacing error. This compromise is not there for the proposed control algorithm.

To offer a quantitative assessment of the simulation results, two simple indices are defined that allow for a more objective comparison of the performance achieved by the control strategies. The first index intends to quantify platoon cohesion by measuring the worst spacing error among the platoon members, as follows:

$$\max_i \|e_i(t)\|_{\mathcal{L}_2} = \max_i \left(\sqrt{\int_0^{t_f} |e_i(t)|^2 dt} \right), \text{ for } i \in \mathcal{I} \setminus \{1\}, \quad (4.3)$$

where $\|\cdot\|_{\mathcal{L}_2}$ denotes the \mathcal{L}_2 signal norm and t_f is the time span of the simulation. This index retrieves the maximum over the energy in the spacing error signals e_i . Hence, it captures how large (both positive or negative) and for how long the worst spacing error is. A spacing error with large amplitude results in a higher value for this index, but also a spacing error that takes long to converge to zero.

The second performance index is based on the \mathcal{L}_2 signal norm of the difference between the

Table 4.1: Performance indices for simulations with a 4-vehicle platoon.

Timegap	$\max \ e_i(t)\ _{\mathcal{L}_2}$		δ_{a_1, a_4}	
	Baseline	Proposed	Baseline	Proposed
$h = 0.3$ s	0.789	0.761	0.270	0.264
$h = 1.0$ s	3.89	2.51	0.555	0.511

acceleration of the platoon leader and that of the slowest vehicle, as follows:

$$\delta_{a_1, a_k} = \|a_1(t) - a_k(t)\|_{\mathcal{L}_2} = \sqrt{\int_0^{t_f} |a_1(t) - a_k(t)|^2 dt}, \quad (4.4)$$

where k corresponds to the index of the slowest vehicle in the platoon and t_f is the time span of the simulation. Evidently, this performance index captures how dissimilar the acceleration of vehicle 1 is from that of vehicle k throughout the simulation. The longer the period of time for which a_1 is different from a_k , the higher the value of the index δ_{a_1, a_k} . This index can be regarded as a proxy for the amount of over and undershoot in the acceleration of vehicle 1 with respect to that of vehicle k , as well as how long it takes to correct the overshoot or undershoot.

Table 4.1 collects the values for the performance indices defined in (4.3) and (4.4) computed for the simulations in figures 4.4 and 4.5. The index $\max \|e_i(t)\|_{\mathcal{L}_2}$ indicates that, in these simulation scenarios, the proposed algorithm achieves better performance in terms of spacing error. Notice from figures 4.1 and 4.4 that with the baseline control scheme the vehicle with the worst spacing error is the one with the lowest acceleration limit, vehicle 4 in this case. On the other hand, for the proposed control scheme, vehicle 2 has the worst spacing error, but this is not as large as the error obtained for vehicle k with the baseline strategy. Regarding the index δ_{a_1, a_4} associated to the transients in acceleration, the proposed scheme outperforms the baseline. This implies that the proposed algorithm achieves less undershoot, shorter settling time, or a combination of both.

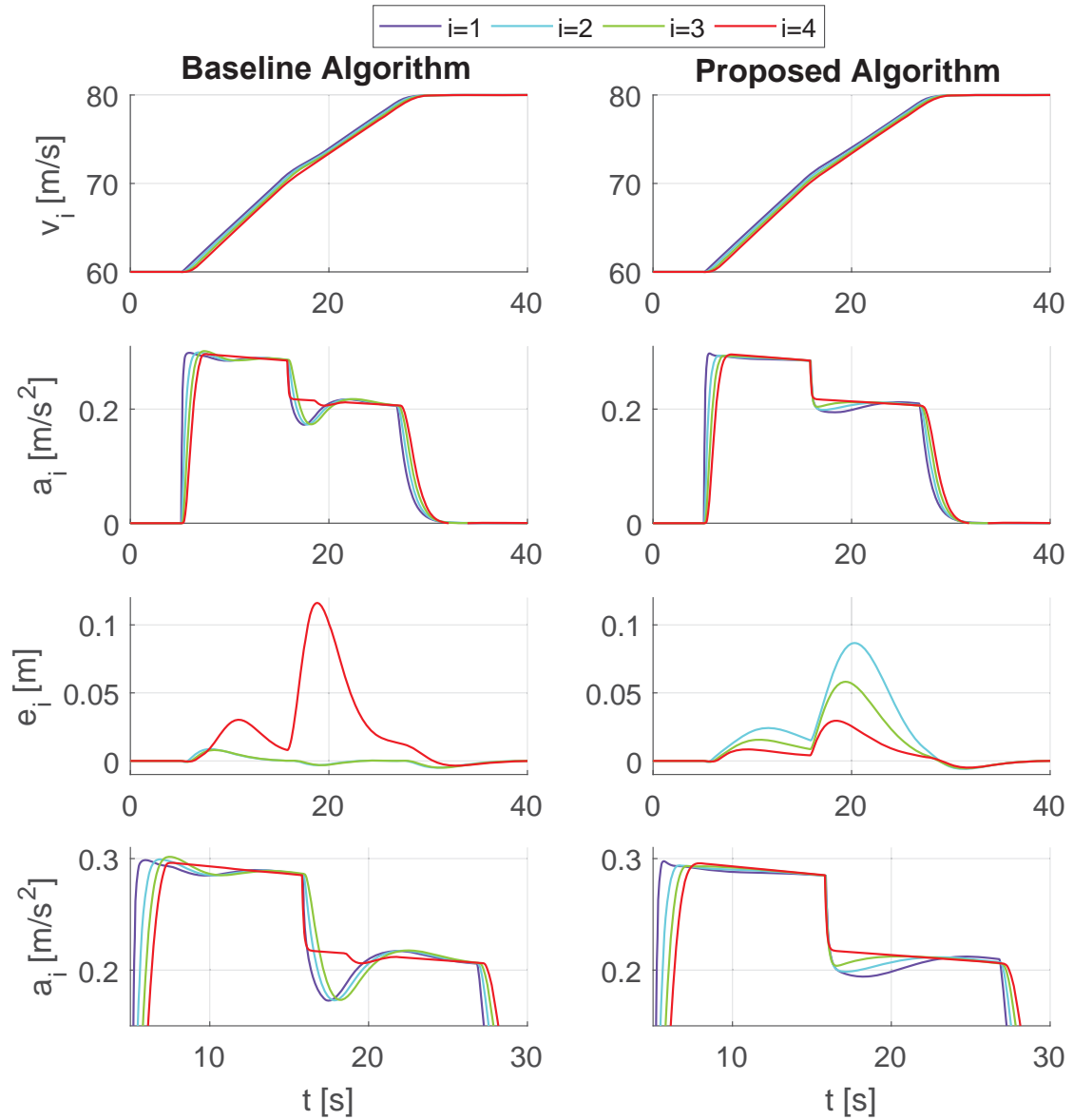


Figure 4.4: Time response for velocity, acceleration, and spacing error of a 4-vehicle platoon. The plots to the left correspond to the baseline control scheme. The plots to the right correspond to the proposed control scheme. The plots at the bottom are detailed views of the acceleration response. The timegap is set to $h = 0.3$ s, and the control gains to $\gamma_p = 0.14$ and $\gamma_d = 0.61$.

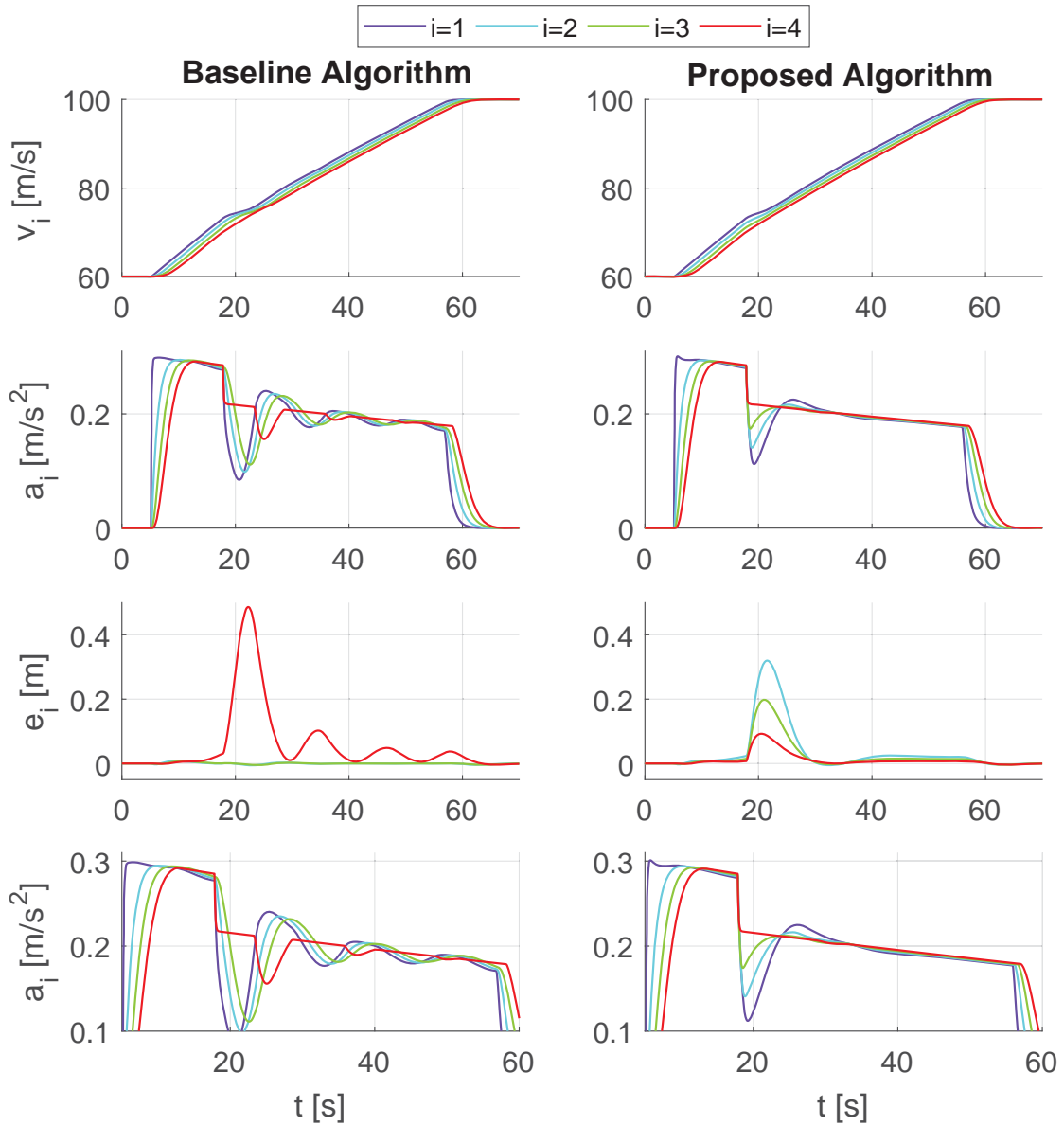


Figure 4.5: Time response for velocity, acceleration, and spacing error of a 4-vehicle platoon. The plots to the left correspond to the baseline control scheme. The plots to the right correspond to the proposed control scheme. The plots at the bottom are detailed views of the acceleration response. The timegap is set to $h = 1$ s, and the control gains to $\gamma_p = 0.14$ and $\gamma_d = 0.61$.

4.2.2 10-vehicle platoon

Large platoons pose a difficult scenario for the control algorithms analyzed in this report. For this reason, simulations considering a platoon of 10-vehicles are presented in this section. For the simulations discussed next, the last vehicle in the platoon has lower acceleration capabilities because of its higher mass. The mass distribution is chosen as

$$\begin{aligned} m_i &= 20 \cdot 10^3 \text{ kg}, \text{ for } i = \{1, \dots, 9\} \\ m_{10} &= 40 \cdot 10^3 \text{ kg}. \end{aligned} \tag{4.5}$$

The difficulty with large platoons lies on how the gains γ_p and γ_d should be tuned. For the baseline algorithm, the stability of the transfer function (3.25) can be used as a reference to tune the gains, but this applies only for small values of timegap. For example, for a 10-vehicle platoon, with a timegap of $h = 0.3 \text{ s}$, the gains $\gamma_p = 0.0162$ and $\gamma_d = 0.2$ achieve stable poles in (3.25) that are located as far as possible from the imaginary axis. On the other hand, when the timegap is set to $h = 1 \text{ s}$, the gains $\gamma_p = 0.0014$ and $\gamma_d = 0.06$ minimize the real part of the poles, which are all stable. Nevertheless, the simulations for these two parameter sets show very distinct performance.

Figure 4.6 illustrates the performance of the baseline control strategy for a 10-vehicle platoon with the two values of timegap mentioned in the previous paragraph and the corresponding gain values. For the case with $h = 0.3 \text{ s}$, the spacing error of vehicle 10 is not too large during the transient and the undershoot in the acceleration of vehicles 1 to 9 is not too pronounced. However, for a timegap of 1 s , vehicle 10 has a large transient spacing error, sufficiently large for another vehicle to cut in if this were a real life scenario. For the timegap of 1 s it is possible to reduce the transient spacing error e_{10} by choosing higher gains, but this tuning should be done carefully otherwise oscillations appear in the acceleration of vehicles 1 to 9 which dampen out very slowly, similar to the case illustrated in Figure 4.5.

The 10-vehicle platoon scenario is simulated now using the proposed control strategy. For the simulation with $h = 0.3 \text{ s}$ the control gains are chosen equal to those used in the simulation in Figure 4.6, i.e., $\gamma_p = 0.0162$ and $\gamma_d = 0.2$. However, for the case with $h = 1 \text{ s}$, the gain values are not chosen equal to those in Figure 4.6. Instead, the gains are set to $\gamma_p = 0.0162$ and $\gamma_d = 0.2$, i.e., the same tuning used for the case with $h = 0.3 \text{ s}$. This illustrates that with the proposed control strategy it is not always necessary to re-tune the control gains when changing the value of the timegap. The results for these simulations are shown in Figure 4.7.

Comparing the simulations in figures 4.6 and 4.7, it can be seen that the proposed algorithm achieves less undershoot in the acceleration of vehicles 1 to 9 in the period when vehicle 10 is driving at its limit. Notice that when using the proposed algorithm vehicles 2 to 10 have an overshoot in velocity with respect to the desired cruising speed. This overshoot is explained by the increase in spacing error of those vehicles, which requires them to keep accelerating after the leader has reached v_{des} . This overshoot forces vehicles 2 to 9 to brake once they have regulated their spacing error. During this overshoot period, the upstream string stability properties of the proposed algorithm can be clearly observed, in particular for the simulation with $h = 1 \text{ s}$. In the plots to the right of Figure 4.7, it can be seen that the amplitude of the velocity overshoot does not increase indefinitely as the index of the vehicle increases. In fact, the overshoot increases from vehicles 2 to 5 and then attenuates for the following vehicles. A similar attenuation can be observed for the undershoot in acceleration around $t = 60 \text{ s}$. This attenuation is achieved by the CACC in the lower layer of this approach.

Notice also that the proposed algorithm achieves smaller transient errors. For the simulation with timegap of 1 s , the spacing errors are certainly not negligible but they are much smaller compared to those obtained with the baseline scheme. This clearly indicates that the proposed control strategy is more versatile than the baseline approach because the former achieves platoon cohesion for larger platoons and for larger values of timegap, without causing sustained oscillations in the acceleration of the vehicles.

Table 4.2: Performance indices for simulations with a 10-vehicle platoon.

Timegap	$\max \ e_i(t)\ _{\mathcal{L}_2}$		$\delta_{a_1, a_{10}}$	
	Baseline	Proposed	Baseline	Proposed
$h = 0.3 \text{ s}$	21.7	28.8	0.533	0.584
$h = 1.0 \text{ s}$	468	80.2	1.263	1.060

The performance indices defined in (4.3) and (4.4) are computed for the simulations in figures 4.6 and 4.7; the values for these indices are collected in Table 4.2. Notice that for the simulations with a timegap $h = 0.3 \text{ s}$, the baseline control scheme achieves lower values for the indices, i.e., it outperforms the proposed scheme, which was not the case for the simulations with 4 vehicles. In order to improve the performance of the proposed scheme for the scenario with $h = 0.3 \text{ s}$, the control gains need to be adjusted. On the other hand, for a timegap $h = 1 \text{ s}$ the proposed scheme achieves better indices than the baseline, especially for the index associated to spacing error. With proper tuning, the proposed control scheme can achieve smaller spacing errors than the baseline without causing inadequate transients in acceleration.

Simulations with non-zero initial conditions, i.e., when the vehicles start with some spacing error or different velocities, are also executed. The results indicate that both control schemes can handle initial-condition perturbations, which confirms the global asymptotic stability result obtained in Chapter 3. However, for the sake of brevity simulation results with non-zero initial conditions are not illustrated here.

The various simulation results presented in this chapter illustrate the advantages and limitations of the control strategies analyzed in this report. Although stable responses were observed in all the simulation scenarios, the performance varies significantly and degrades as the platoon size increases or the timegap is chosen higher. Nevertheless, compared to the baseline algorithm, the proposed control strategy can provide platoon cohesion for a wider range of timegap values and platoon sizes.

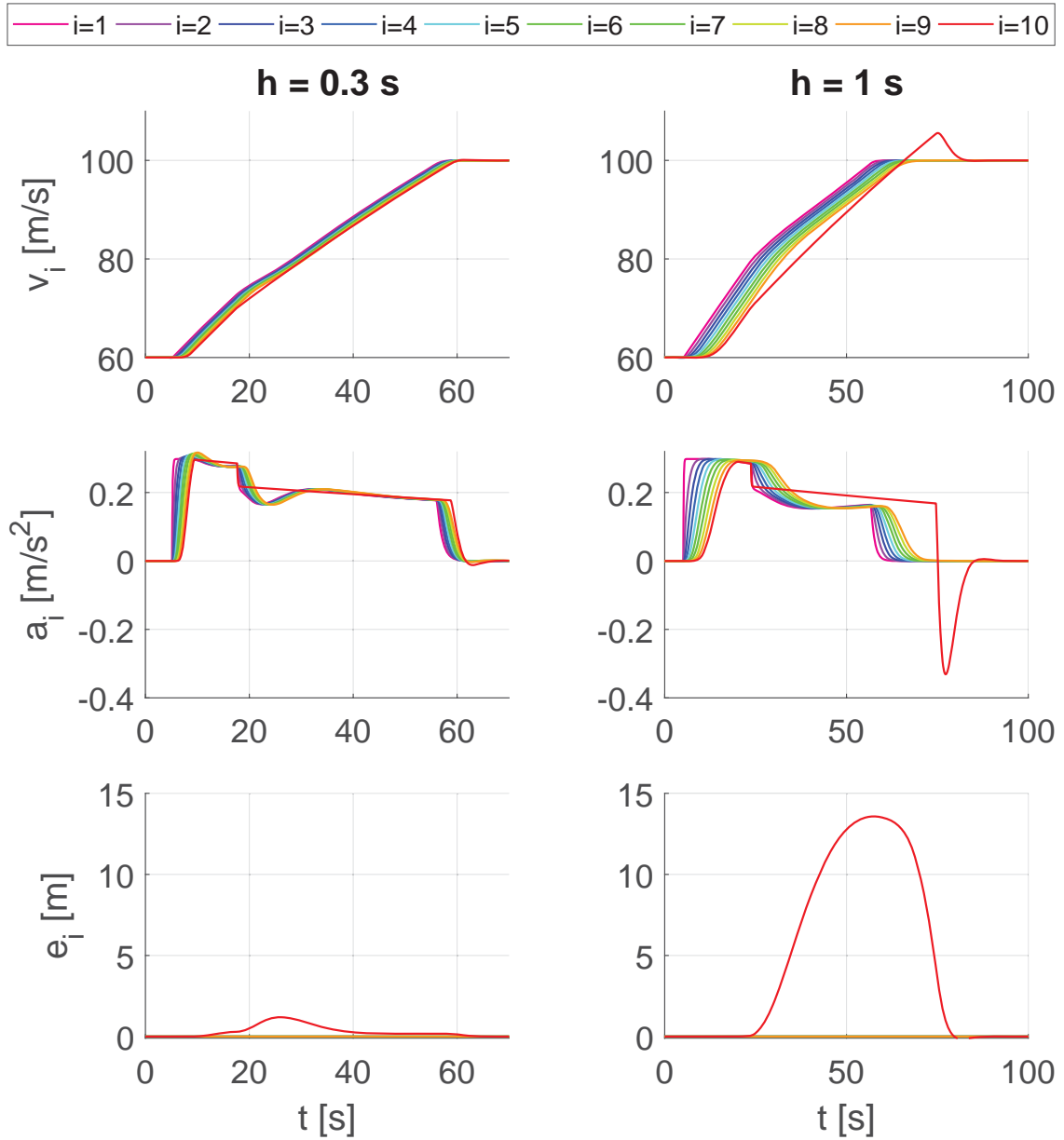


Figure 4.6: Time response for velocity, acceleration, and spacing error of a 10-vehicle platoon using the baseline control scheme. The control gains are set differently for each value of timegap h to achieve smooth accelerations.

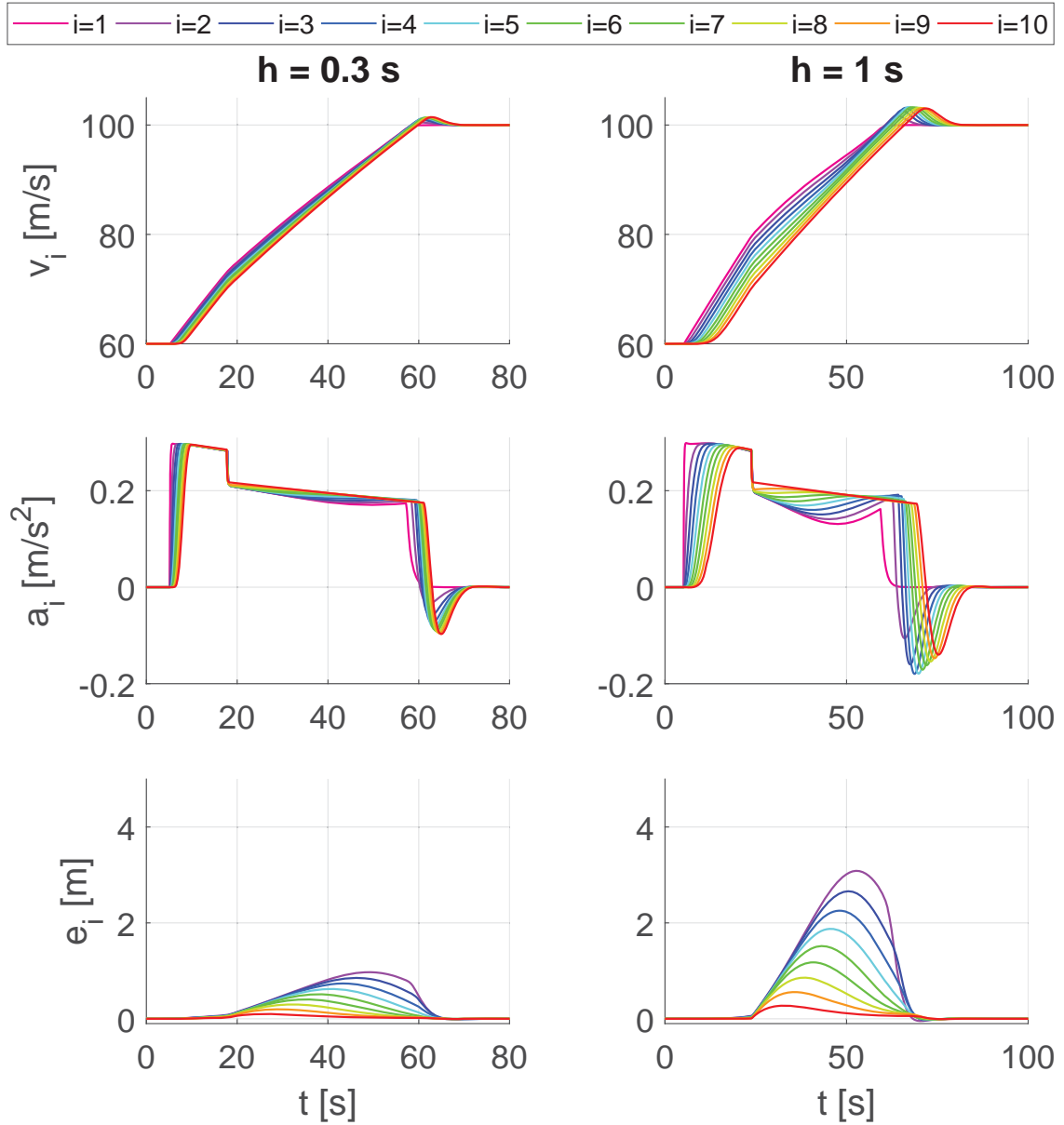


Figure 4.7: Time response for velocity, acceleration, and spacing error of a 10-vehicle platoon using the proposed control scheme. The control gains are set equal for both values of timegap h .

Chapter 5

Conclusions and recommendations

This report has addressed the problem of vehicular platooning subject to heterogeneous and dynamic acceleration limits. A literature survey was conducted to identify existing solutions for vehicle platooning subject to some sort of heterogeneity in the vehicles' dynamics or constraints in the input. Few publications on CACC consider heterogeneous constraints in the acceleration, but only one study addresses the implications of acceleration limits in platoon cohesion, i.e., the multi-layer control strategy in [23].

Chapter 3 thoroughly analyzes the control scheme from [23] in order to assess asymptotic stability. To this end, a piecewise affine modelling framework was used to translate the non-linearities in the control strategy into state-based switching between various linear dynamics. Then, piecewise quadratic Lyapunov functions were derived based on linear matrix inequalities and numerical routines for semi-definite programming. Using this methodology, global asymptotic stability was proven for 3-vehicle platoons. Furthermore, parametric studies were conducted to have a reference of which parameter combinations lead to asymptotic stability.

A classical frequency domain technique was also used in an attempt to derive a simple criterion to tune the control gains. This analysis allowed to identify an important limitation: with the baseline multi-layer strategy platoon cohesion and oscillation-free accelerations are mutually exclusive requirements, in particular for the case of large platoons or large timegaps. Overcoming this limitation motivated an intensive design process to propose an alternative control strategy.

After several iterations, a multi-layer control scheme was derived that is able to mitigate the aforementioned limitation without adding too much complexity and preserving a distributed control approach. The tools used to analyze the baseline approach were applied also to the proposed algorithm, focusing primarily on illustrating the advantages of this proposal and also the limitations.

Due to the complexity of the piecewise affine models, the stability analyses were limited to platoons of 3 vehicles. However, computer simulations were used to confirm the stability results and extend the analysis to platoons with more vehicles. Moreover, a complex simulation model was used to evaluate the robustness of the control schemes in face of gear-shifting and time delays in communication, actuation, and sensing. The simulations presented here offer a useful comparison of the stability properties of the control schemes. Furthermore, the strong influence of the timegap and the control gains on the performance was discussed. The stability analyses and simulation results allow to conclude that the newly proposed multi-layer CACC scheme overcomes limitations of the baseline CACC strategy in [23]. With the proposed control scheme, the phase lag in actuation that is present in the baseline control scheme is eliminated, such that the vehicles in front of the slowest react sooner to changes in the spacing error of the slowest vehicle. In this way, platoon cohesion can still be achieved for larger platoons and for a wider range of timegaps, without compromising the transient acceleration performance.

Recommendations

During the extensive research project that culminated in this thesis report, various areas of opportunity for future research were identified. The most relevant and pressing ones are discussed next.

The proposed control strategy exhibits a stable response in simulations, provided the control gains are chosen appropriately. However, the disturbance attenuation properties of this approach are not adequate in the downstream direction. To this end, a formal definition for string stability that encloses both upstream and downstream disturbance attenuation is required to evaluate platooning strategies with bidirectional topologies, such as the one proposed in this work. Then, the proposed control scheme could be adjusted to achieve downstream disturbance attenuation. A possible approach could be to introduce a dynamic control law in the coordination layer, as opposed to the static feedback proposed in this report. In other words, it might be possible to design a filter to be introduced in the definition for the coordination variables such that the transfer function from the desired acceleration of vehicle i to the desired acceleration of vehicle $i - 1$ satisfies some disturbance attenuation criterion for the applicable operation modes.

The non-linear dynamics arising from the control schemes discussed here required complex modelling and analysis tools. A scalable analysis methodology is required if one intends to address the stability properties of arbitrarily large platoons. A possible direction is to apply \mathcal{L}_2 -gain and small gain theories for piecewise affine systems. This would allow to analyze the platoon dynamics as a collection of simple piecewise affine systems connected among themselves, instead of assessing the dynamics as a single PWA system with an unmanageable amount of subsystems.

In this research, only one type of heterogeneity was addressed, i.e., the acceleration limit. However, as identified in the literature survey, several vehicle parameters might vary among platoon members. Hence, it would be fruitful to combine the multi-layer control strategies described here with other control laws designed to handle other source of heterogeneity. In this regard, the multi-layer structure of the control strategies allows to easily integrate other CACC techniques designed to handle different heterogeneities or schemes with more complex communication topologies.

An additional recommendation concerns the model used in this research for the acceleration limit of the vehicles. Although several factors were considered in the equation dictating the acceleration limit, it was assumed that the maximum engine torque is constant. This is not the case for real combustion engines, in which the maximum output torque depends on the engine speed. It would be interesting to include a realistic engine map that relates the maximum engine torque with the engine speed in the simulation models. Similarly, the limitation in braking force could be included in the model and the multi-layer control strategies could be adjusted to address this limitation in deceleration capabilities.

A final recommendation is to conduct experiments with real vehicles to evaluate the robustness of the proposed control scheme in face of unmodelled dynamics and external disturbances, such as measurement noise. This would reveal the weak points of the control design and provide further inspiration to develop a solution that could reach maturity in the coming years.

Bibliography

- [1] European Transport Safety Council. Prioritising the Safety Potential of Automated Driving in Europe. Technical report, European Transport Safety Council, 2016. Retrieved August 29, 2018 from https://etsc.eu/wp-content/uploads/2016_automated_driving_briefing_final.pdf.
- [2] F. Gao, S. E. Li, Y. Zheng, and D. Kum. Robust control of heterogeneous vehicular platoon with uncertain dynamics and communication delay. *IET Intelligent Transport Systems*, 10(7):503–513, 2016.
- [3] Y. A. Harfouch, S. Yuan, and S. Baldi. An adaptive switched control approach to heterogeneous platooning with inter-vehicle communication losses. *IEEE Transactions on Control of Network Systems*, 2017.
- [4] M. Johansson. *Piecewise Linear Control Systems*. Springer-Verlag, Germany, 2003.
- [5] Stephen Jones. Cooperative Adaptive Cruise Control: Human Factors Analysis. Technical report, U.S. Department of Transportation, 2013. Retrieved August 29, 2018 from <https://www.fhwa.dot.gov/publications/research/safety/13045/13045.pdf>.
- [6] M. R. Jovanovic, J. M. Fowler, B. Bamieh, and R. D’Andrea. On avoiding saturation in the control of vehicular platoons. In *2004 American Control Conference (ACC)*, volume 3, pages 2257–2262, 2004.
- [7] Y. Labit, D. Peaucelle, and D. Henrion. SEDUMI INTERFACE 1.02: a tool for solving LMI problems with SEDUMI. In *Proceedings. IEEE International Symposium on Computer Aided Control System Design*, pages 272–277, 2002.
- [8] W. Levine and M. Athans. On the optimal error regulation of a string of moving vehicles. *IEEE Transactions on Automatic Control*, 11(3):355–361, 1966.
- [9] S. E. Li, X. Qin, K. Li, J. Wang, and B. Xie. Robustness analysis and controller synthesis of homogeneous vehicular platoons with bounded parameter uncertainty. *IEEE/ASME Transactions on Mechatronics*, 22(2):1014–1025, 2017.
- [10] J. Lofberg. YALMIP : a toolbox for modeling and optimization in MATLAB. In *2004 IEEE International Conference on Robotics and Automation*, pages 284–289, 2004.
- [11] MathWorks. Symbolic Math Toolbox User’s Guide. Retrieved August 29, 2018 from https://nl.mathworks.com/help/pdf_doc/symbolic/symbolic_tb.pdf, 2018.
- [12] Ellen Van Nunen, Jan Verhaegh, Emilia Silvas, Elham Semsar-kazerooni, and Nathan Van De Wouw. Robust Model Predictive Cooperative Adaptive Cruise Control Subject to V2V Impairments. *2017 IEEE 20th International Conference on Intelligent Transportation Systems (ITSC)*, pages 2013–2020, 2017.

- [13] J. Ploeg, B. T. M. Scheepers, E. van Nunen, N. van de Wouw, and H. Nijmeijer. Design and experimental evaluation of cooperative adaptive cruise control. In *14th International IEEE Conference on Intelligent Transportation Systems (ITSC)*, pages 260–265, 2011.
- [14] J. Ploeg, N. van de Wouw, and H. Nijmeijer. \mathcal{L}_p string stability of cascaded systems: Application to vehicle platooning. *IEEE Transactions on Control Systems Technology*, 22(2):786–793, 2014.
- [15] E. Shaw and J. K. Hedrick. Controller design for string stable heterogeneous vehicle strings. In *46th IEEE Conference on Decision and Control*, pages 2868–2875, 2007.
- [16] S. Sheikholeslam and C. A. Desoer. Longitudinal control of a platoon of vehicles. In *1990 American Control Conference*, pages 291–296, May 1990.
- [17] J. Toth and G. Rodonyi. String stability preserving adaptive spacing policy for handling saturation in heterogeneous vehicle platoons. *IFAC-PapersOnLine*, 50(1):8525 – 8530, 2017.
- [18] C. Wang and H. Nijmeijer. String Stable Heterogeneous Vehicle Platoon Using Cooperative Adaptive Cruise Control. In *IEEE 18th International Conference on Intelligent Transportation Systems*, pages 1977–1982, 2015.
- [19] S. C. Warnick and A. A. Rodriguez. A systematic antiwindup strategy and the longitudinal control of a platoon of vehicles with control saturations. *IEEE Transactions on Vehicular Technology*, 49(3):1006–1016, 2000.
- [20] H. Xing, J. Ploeg, and H. Nijmeijer. Padé Approximation of Delays in Cooperative ACC Based on String Stability Requirements. *IEEE Transactions on Intelligent Vehicles*, 1(3):277–286, 2016.
- [21] M. Yan, J. Song, P. Yang, and Y. Tang. Distributed adaptive sliding mode control for vehicle platoon with uncertain driving resistance. In *36th Chinese Control Conference (CCC)*, pages 9396–9400, 2017.
- [22] M. Zabat, N. Stabile, S. Frascaroli, and F. Browand. The aerodynamic performance of platoons. Technical report, California PATH Program, 1995.
- [23] J. C. Zegers, E. Semsar-Kazerooni, M. Fusco, and J. Ploeg. A multi-layer control approach to truck platooning: Platoon cohesion subject to dynamical limitations. In *5th IEEE International Conference on Models and Technologies for Intelligent Transportation Systems (MT-ITS)*, pages 128–133, 2017.
- [24] J. C. Zegers, E. Semsar-Kazerooni, J. Ploeg, N. van de Wouw, and H. Nijmeijer. Consensus control for vehicular platooning with velocity constraints. *IEEE Transactions on Control Systems Technology*, 2017.
- [25] Y. Zheng, S. E. Li, K. Li, F. Borrelli, and J. K. Hedrick. Distributed model predictive control for heterogeneous vehicle platoons under unidirectional topologies. *IEEE Transactions on Control Systems Technology*, 25(3):899–910, 2017.

Appendix A

Matrices used in the stability analysis of piecewise affine systems

A.1 Continuity matrices

This section describes the procedure suggested in [4] to construct continuity matrices to be used in the search of a continuous PWQLF that proves stability of a PWA system. The continuity matrices must satisfy

$$\begin{bmatrix} x^T & 1 \end{bmatrix} \bar{F}_j \begin{bmatrix} x \\ 1 \end{bmatrix} = \begin{bmatrix} x^T & 1 \end{bmatrix} \bar{F}_k \begin{bmatrix} x \\ 1 \end{bmatrix}, \text{ for } x \in \mathcal{X}_j \cap \mathcal{X}_k, \forall j, k \in \mathcal{J}. \quad (\text{A.1})$$

The continuity matrices can be constructed based on the matrices $\bar{G}_j = [G_j \quad g_j]$ that collect the equations of the hyperplanes that delimit the cells.

Notice that the points on the boundary between two adjacent cells \mathcal{X}_j and \mathcal{X}_k simultaneously satisfy $G_j x + g_j \geq 0$ and $G_k x + g_k \geq 0$. If care is taken to construct the matrices \bar{G}_j in such a way that they contain information related to the same hyperplane in the same row (i.e., the first row of all matrices \bar{G}_j corresponds to the same hyperplane, the second row to another hyperplane, and so on), then the following is true:

$$G_j x + g_j = G_k x + g_k \geq 0, \forall x \in \mathcal{X}_j \cap \mathcal{X}_k, \forall j, k \in \mathcal{J}, \text{ with } \mathcal{X}_j \cap \mathcal{X}_k \neq \emptyset, \quad (\text{A.2})$$

which explains why matrices G_j and g_j can be used as a basis for the continuity matrices \bar{F}_j .

The structure for the continuity matrices \bar{F}_j is the following:

$$\bar{F}_j = \begin{bmatrix} F'_j & f'_j \\ I_{(n_x)} & 0_{(n_x \times 1)} \end{bmatrix}, \text{ for } j \in \mathcal{J}, \quad (\text{A.3})$$

with $F'_j \in \mathbb{R}^{m \times n_x}$, $f'_j \in \mathbb{R}^m$, where m corresponds to the number of rows in the matrices \bar{G}_j , i.e., the number of hyperplanes that bound the corresponding region \mathcal{X}_j . The submatrix $I_{(n_x)}$ corresponds to the identity matrix of dimension $n_x \times n_x$, which gives full column rank to \bar{F}_j .

The blocks F'_j and f'_j are constructed using the matrices G_j and g_j , applying the following procedure:

- Set $[F'_j \quad f'_j]$ equal to $[G_j \quad g_j]$.

- Replace with a row of zeros those rows in $[F'_j \quad f'_j]$ that have a positive element in the last column.

The procedure above guarantees that the matrices \bar{F}_j have the so-called zero interpolation property, which means that $f'_j = 0$ for $j \in \mathcal{J}_0$. This property allows to construct a continuous piecewise quadratic Lyapunov function of the form (3.3) having no affine term for those cells that contain the origin [4].

To explain how the matrices \bar{F}_j ensure continuity for the function $V(x)$ defined in (3.3), consider two quadratic functions of the form $\bar{x}^T \bar{P}_j \bar{x}$ and $\bar{x}^T \bar{P}_k \bar{x}$, with $\bar{P}_j = \bar{F}_j^T T \bar{F}_j$ and $\bar{P}_k = \bar{F}_k^T T \bar{F}_k$, where the abbreviated notation $\bar{x} = [x^T \quad 1]^T$ is used. Furthermore, $T \in \mathbb{R}^{(n_x+m) \times (n_x+m)}$ is a symmetric matrix. Then, in view of (A.1), the following equalities are satisfied:

$$\bar{x}^T \bar{P}_j \bar{x} = \bar{x}^T \bar{F}_j^T T \bar{F}_j \bar{x} = \bar{x}^T \bar{F}_k^T T \bar{F}_k \bar{x} = \bar{x}^T \bar{P}_k \bar{x}, \text{ with } \bar{x} = \begin{bmatrix} x \\ 1 \end{bmatrix}, \text{ for } x \in \mathcal{X}_j \cap \mathcal{X}_k, \forall j, k \in \mathcal{J}. \quad (\text{A.4})$$

A.2 Cell bounding matrices and the S-procedure

This appendix describes the procedure proposed in [4] to arrive at cell bounding matrices E_j and \bar{E}_j that satisfy (3.12). These matrices are used for the S-procedure in the LMIs presented in (3.9) and (3.10), which is explained at the end of this appendix.

For $j \in \mathcal{J}_0$, the matrices \bar{E}_j are constructed as follows:

- Set $\bar{E}_j = \bar{G}_j = [G_j \quad g_j]$.
- Replace with a row of zeros those rows in \bar{E}_j whose element in the last column is different from zero.

The previous algorithm removes from \bar{E}_j the information of those hyperplanes that have an offset term. This achieves the zero interpolation property in matrices \bar{E}_j for $j \in \mathcal{J}_0$, which means these matrices have only zeros in their last column. As explained in [4], this property allows the LMIs in (3.9) to be strict. The matrix E_j , which is used in (3.9), is a sub-matrix of the respective \bar{E}_j that corresponds to the first n_x columns of \bar{E}_j .

For the indices $j \in \mathcal{J}_1$, the matrices \bar{E}_j are constructed as follows:

- Set $\bar{E}_j = [G_j \quad g_j]$.
- If the cell \mathcal{X}_j is an unbounded polyhedron, then the matrix \bar{E}_j is augmented with the row $[0_{(1 \times n_x)} \quad 1]$.

The matrices \bar{E}_j are used for the S-procedure in the LMIs in (3.9) and (3.10), which relaxes the conditions for the individual quadratic functions in (3.3), not forcing them to be positive or strictly decreasing outside of the cell where they are used. To explain how this relaxation is achieved, consider the following LMI from (3.9):

$$P_j - E_j^T U_j E_j > 0, \quad j \in \mathcal{J}_0. \quad (\text{A.5})$$

The previous LMI implies $x^T P_j x > x^T E_j^T U_j E_j x$ for any $x \in \mathbb{R}^{n_x}$. As the matrix U_j is required to have only non-negative elements and \bar{E}_j is constructed to satisfy $E_j x \succeq 0$ for $x \in \mathcal{X}_j$, then

$$x^T E_j^T U_j E_j x \geq 0, \text{ for } x \in \mathcal{X}_j. \quad (\text{A.6})$$

The expression $x^T E_j^T U_j E_j x$ might be negative outside of \mathcal{X}_j , so the function $x^T P_j x$ is also allowed to be negative outside of \mathcal{X}_j . A similar reasoning explains how the S-procedure achieves the desired relaxation for other LMIs in (3.9) and (3.10).

Once the LMIs (3.9) and (3.10) are solved, the term $x^T E_j^T U_j E_j x$ defines a quadratic surface that divides the state space in two, and the cell \mathcal{X}_j is contained entirely in one side of the surface. The corresponding quadratic function $x^T P_j x$ is positive for all points on one side of the quadratic surface, including possible points that lie outside of \mathcal{X}_j . This implies that the LMIs are, in general, conservative.

Appendix B

Additional parametric stability studies

In this appendix, the results of additional parametric stability analyses are presented. PWQLFs are attempted to be found for the PWA system corresponding to the baseline control scheme using the vehicle parameters presented in Section 3.3.2.

Parametric study varying the acceleration limit of the vehicles

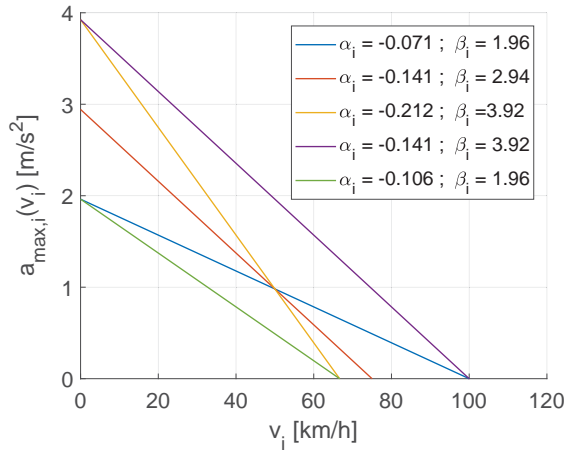


Figure B.1: The five linear functions $a_{max,i}(v_i) = \alpha_i v_i + \beta_i$ used to represent the acceleration limit of the vehicles

The purpose of this study is to confirm if stability of the PWA system can be proven while varying the parameters that define the acceleration limit of the vehicles, but also using different ordering of the vehicles in the platoon. In other words, in this study it is not always the case that the slowest vehicle is at the rear of the platoon.

For this study, the timegap is fixed to $h = 0.3$ s and the driveline time constant is fixed to $\tau = 0.1$ s. The control gains γ_p and γ_d are chosen as 0.1 and 0.5, respectively, and other parameters are set to the values in Table 3.3. These parameters achieve stable eigenvalues for the system matrices in the PWA model. The acceleration limit for the three vehicles in the platoon is defined with

one of the five linear functions presented in Figure B.1. These linear functions have the form $a_{max,i}(v_i) = \alpha_i v_i + \beta_i$. The parameter β_i , indicating the maximum acceleration from rest, is chosen between $0.2g$ and $0.4g$, with $g = 9.81 \text{ m/s}^2$. The parameter α_i is chosen between -0.2 and $-0.07s^{-1}$. For these values of α_i the stability conditions presented in Section 3.3.1 are satisfied.

As shown in Figure B.1, three of the linear functions intersect at $v_i = 50 \text{ km/h}$. This intersection is intentionally designed to verify if stability can be proven even when the vehicle with the lowest acceleration limit is not the same at all driving speeds.

The study consists of 375 iterations, which consider all possible combinations of the acceleration limits in Figure B.1, including cases where the three vehicles have the same function for acceleration limit. The study is conducted for three different values of desired cruising speed, i.e., $v_{des} \in \{40, 50, 60\} \text{ km/h}$.

The study reveals that the LMIs are feasible for any of the combinations of acceleration limits considered here, as long as the desired cruising speed v_{des} is set within the capabilities of all the vehicles in the platoon. In other words, for the LMIs to be feasible, the desired cruising speed should not exceed the point where the maximum acceleration of one of the vehicles has reached zero. This is of course a logical result, but it also means that the desired equilibrium for the PWA system, i.e., the origin of the state space, should be contained in some region (or at the border between some regions) for which the origin is indeed the equilibrium of the local dynamics.

The parametric study described above was conducted also for the PWA model corresponding to the proposed control scheme from Section 2.3. The results are consistent with those corresponding to the PWA model for the baseline control scheme: the functions for the acceleration limits do not have a significant role in the feasibility of the LMIs, provided the desired cruising speed v_{des} is feasible for all vehicles.

Although not being a formal proof, the results presented in this section indicate that the parameters related to the acceleration limit of the vehicles do not play a key role when trying to find a PWQLF to prove the stability of the system.

Parametric study for a 4-vehicle platoon

In Section 3.3.2 the results of a parametric stability study are described, which consists of looking for a PWQLF for the PWA model of a 3-vehicle platoon using several points of the design space $\gamma_p \times \gamma_d \times h \times \tau$. This study is repeated but now for the PWA model corresponding to a 4-vehicle platoon with the control scheme in [23]. The results are condensed in Figure B.2. In this figure, the dashed line indicates the boundary in the design space for which the parameters achieve stable subsystems in the PWA model. Due to the large number of regions in the PWA model, in this study only combinations of parameters that lead to stable subsystems were assessed, which explains why in Figure B.2 all dots and crosses lie to one side of the dashed line. The results of this study are consistent with those in Section 3.3.2: for most points in the design space that achieve stable subsystems it is possible to find a PWQLF that proves stability of the origin. However, some exceptions were found, especially for the larger values of h and τ , which supports the conclusion that the control strategy in [23] is applicable only for a limited range of values of timegap and driveline constant.

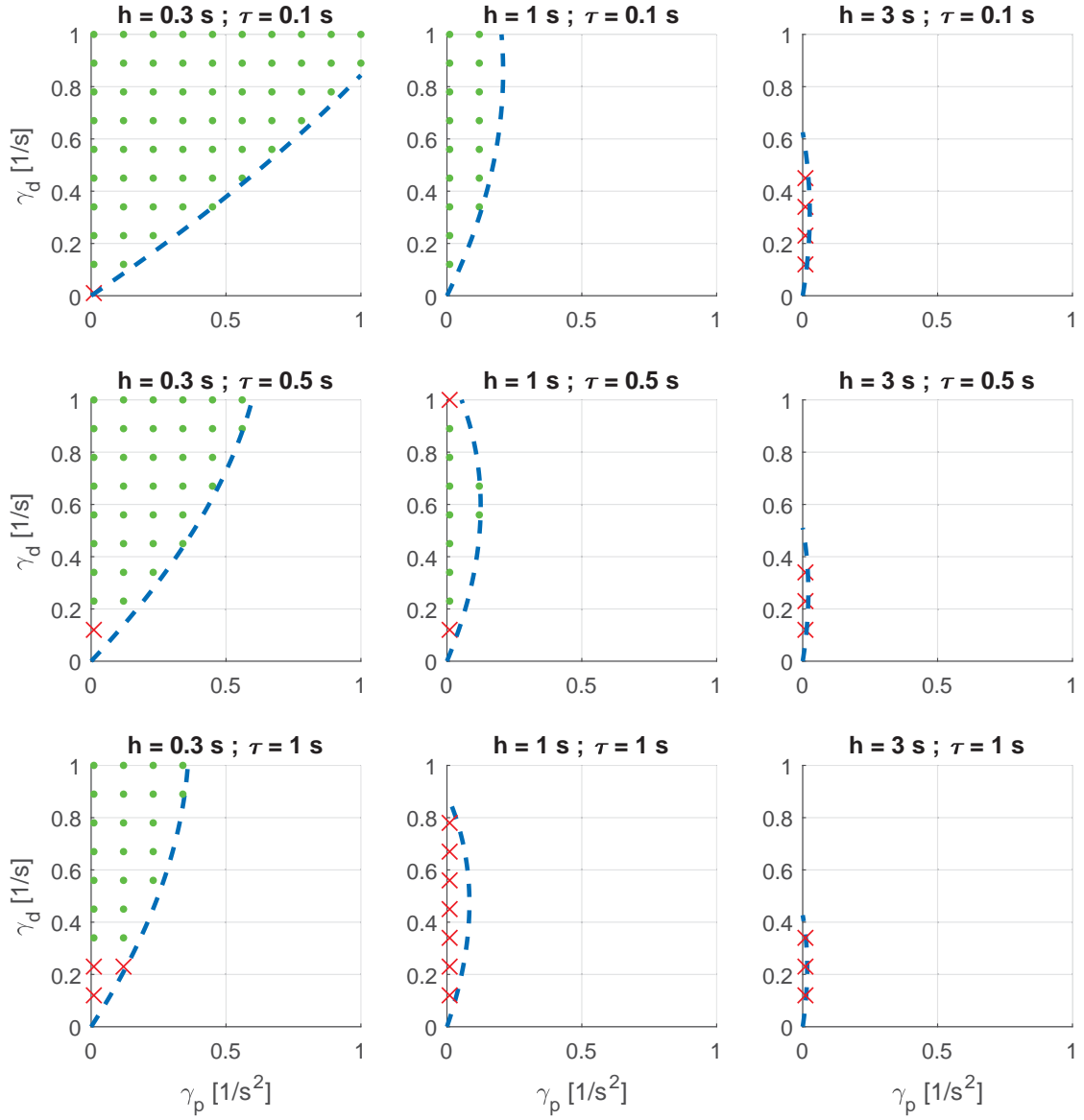


Figure B.2: Parametric stability analysis for a 4-vehicle platoon subject to the control scheme in [23], varying γ_p , γ_d , h , and τ . The green dots indicate points in the design space for which the LMIs (3.9) and (3.9) are feasible. The red dots indicate parameter combinations that lead to infeasible LMIs. The dashed line bounds the region for which (marginally) stable eigenvalues are obtained for all the subsystems in the PWA model.

Appendix C

Other attempts to improve the baseline multi-layer CACC strategy

In this appendix, some additional ideas are presented which were explored during this research project in an attempt to improve the performance and scalability of the multi-layer CACC strategy from [23]. The limitations and disadvantages of these solutions are also discussed to motivate why in the end the preferred alternative is the one presented in Section 2.3. The upcoming sections present also stability analyses based on piecewise affine models and piecewise quadratic Lyapunov functions. It is assumed that the reader is familiar with these concepts, which are explained in Section 3.1.

C.1 A non-linear feedback in the coordination layer

As discussed in Chapter 4 the multi-layer CACC strategy proposed in [23] can cause an oscillatory behavior in the acceleration of the vehicles during transient phases. Depending on the values of the control gains chosen for the coordination layer, the oscillations might dampen out or increase in amplitude. In this section, a solution to mitigate this undesired effect is proposed.

Recall that the control strategy in [23], employs information signals in the upper layer defined as:

$$Ky_i(t) = a_{max,i}(v_i(t)) - \gamma_p e_i(t) - \gamma_d \dot{e}_i(t), \quad \forall i \in \mathcal{I} \setminus \{1\}, \quad (\text{C.1})$$

where the gains γ_p and γ_d are assumed to be positive. Since the spacing error and its time derivative might have negative values, the variable y_i might end up being larger than $a_{max,i}$. In such case, with Zeger's control approach the platoon leader might accelerate beyond the limit of the slowest vehicle in the platoon (recall that, thanks to the coordination layer, vehicle 1 does not accelerate above $\xi_2 = \min[y_2, \dots, y_n]$). This phenomenon has been observed in simulations and seems to be related to the undesired oscillations in the acceleration of the vehicles.

To address the issue described before, the variables y_i are re-defined with the following non-linear expression similar to a one-sided spring:

$$y_i(t) = a_{max,i} - \max[0, \gamma_p e_i + \gamma_d \dot{e}_i], \quad \forall i \in \mathcal{I} \setminus \{1\}. \quad (\text{C.2})$$

The max function in (C.2) guarantees $y_i \leq a_{max,i}, \forall t$. Assuming $a_{max,i}$ to be a linear function of v_i , expression (C.2) is piecewise-linear, which allows to analyze the stability of the platoon

dynamics based on piecewise quadratic Lyapunov functions. The desired acceleration for vehicle 1 is still defined with expression (2.14), and for vehicles 2 to n is defined as in (2.5).

The proposed expression in (C.2) does not suffice to prevent the undesired oscillations in acceleration. This is illustrated with a simulation example later in this section. Hence, an additional term is included in the information variables y_i , as follows:

$$y_i = a_{max,i} - \max [0, \gamma_p e_i + \gamma_d \dot{e}_i + (u_{i-1}(t - \theta_c) - a_{max,i})], \forall i \in \mathcal{I} \setminus \{1\}. \quad (C.3)$$

where u_{i-1} is the control input of the preceding vehicle, which is known to the host vehicle thanks to the wireless communication link and is subject to the time delay θ_c . The vehicle preceding the slowest member should not drive with an acceleration above the limit of the latter (i.e., it is desirable to achieve $u_{k-1} \leq a_{max,k}$, assuming vehicle k is the slowest), otherwise the spacing error of the slowest member might (temporarily) increase. To this end, expression (C.3) decreases the acceleration level allowed for the platoon leader whenever the vehicle in front of the slowest is accelerating too much. Simulation results comparing the effect of expressions (C.2) and (C.3) are presented next.

The simulation scenario consists of a ten-vehicle platoon, where the last vehicle has a lower acceleration limit than the rest (parameters are chosen as in [23], including communication and actuation delays). The platoon starts driving at 70 km/h and the desired cruising speed is set to 100 km/h, which allows for a sufficiently long transient to illustrate the benefits of the proposed strategy. Figure C.1 shows the time response for acceleration and spacing error of this simulation. When using expression (C.2), the acceleration of vehicles 1 to 9 keep oscillating during the transient phase, while vehicle 10 periodically goes in and out of saturation. Notice also that the acceleration of vehicle 9 exceeds that of vehicle 10 in various moments (see the detailed view at the bottom of Fig. C.1). On the other hand, when using expression (C.3), the oscillations in the acceleration fade out and vehicle 9 eventually drives with a lower acceleration than vehicle 10.

After confirming an adequate response through simulations, the stability of the closed-loop platoon dynamics is analyzed using a piecewise affine (PWA) model. As a first attempt, the stability analysis is conducted with the following assumptions. The last vehicle in the platoon has an acceleration limit that is sufficiently low compared to the limits of the predecessors and the initial spacing errors are sufficiently small. This means that only vehicle n might reach its acceleration limit. Additionally, the platoon leader receives information from the last vehicle at all times, i.e., $\xi_2(t) = \min [y_2, \dots, y_n], \forall t > 0$. Furthermore, the function $a_{max,i}$ is assumed to be linear; the communication and actuation delays are neglected.

To explain how expression (C.3) is represented in a PWA model, notice that (C.3) is equivalent to:

$$y_i = \min [a_{max,i}, a_{max,i} - (\gamma_p e_i + \gamma_d \dot{e}_i + u_{i-1} - a_{max,i})], \forall i \in \mathcal{I} \setminus \{1\}, \quad (C.4)$$

With the assumptions mentioned before and because of the coordination layer in this approach, the expression for the control input of the platoon leader is:

$$\begin{aligned} u_{ref,1}(t) &= \min [u_1, y_n] \\ &= \min [u_1, a_{max,n}, a_{max,n} - (\gamma_p e_n + \gamma_d \dot{e}_n + u_{n-1} - a_{max,n})], \end{aligned} \quad (C.5)$$

where $u_1 = k_v(v_{des} - v_1)$. Expression (C.5) translates into three hyperplanes which divide the state space into 6 regions. The saturation of vehicle n is represented with another hyperplane, which results in a PWA system with a total of 12 regions, regardless of the platoon size.

For a platoon of ten vehicles, using the parameters from the simulation presented in Fig. C.2, a piecewise quadratic Lyapunov function for the PWA system can be found by solving linear matrix inequalities as explained in Section 3.1. However, when choosing a larger timegap for the spacing policy (e.g., $h = 1$ sec), the LMIs turn out to be infeasible. Similar to the results discussed in Section 3.3, the dynamics for one of the subsystems in this PWA model can become unstable

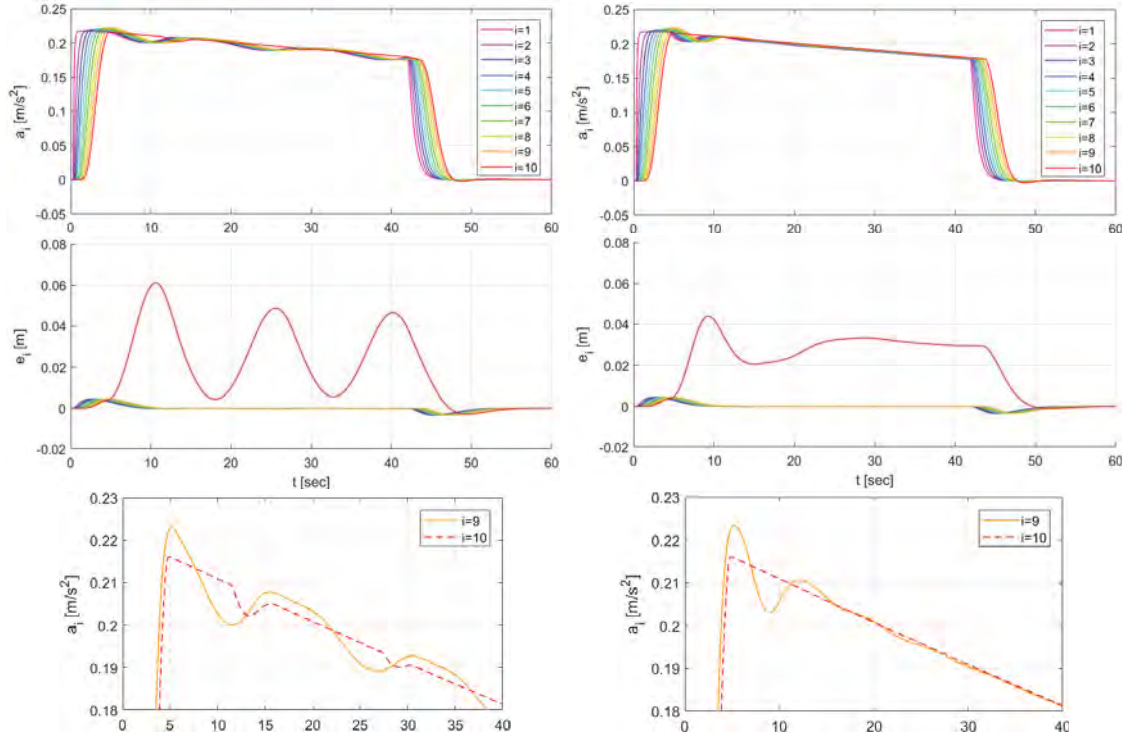


Figure C.1: Time response for acceleration and spacing error of a ten-vehicle platoon. The plots to the left correspond to the simulation with expression (C.2), while the plots to the right correspond to expression (C.3).

depending on the platoon length, the timegap, the time constant of the driveline dynamics, and the control gains γ_p and γ_d . In such case, the stability analysis based on piecewise quadratic functions is not conclusive.

The modification proposed here achieves some improvement with respect to the baseline control strategy. However, it is still not suitable to be scaled to platoons of any size and the stability is still dependent on the timegap. A different control approach is described in the next section which aims to tackle the difficulties described before.

C.2 A dynamic feedback in the coordination layer

To address the limitation discussed before, the feedback law could be re-defined, in the frequency domain, as

$$P(s) = (\gamma_d s + \gamma_p)(hs + 1)^{n-2}. \quad (\text{C.6})$$

This dynamic feedback law would compensate for the phase lag introduced by the spacing policy. However, such a feedback would be difficult to implement in reality because measurements of the high-order derivatives of the spacing error are not available. As an alternative, cascaded lead-filters can be used, as follows:

$$P(s) = (\gamma_d s + \gamma_p) \left(\frac{hs + 1}{\frac{1}{2\pi f} s + 1} \right)^{n-2}, \quad (\text{C.7})$$

with some frequency $f > \frac{1}{2\pi h}$. Substituting (C.7) in (3.26) results in

$$CL(s) = \left(\frac{\frac{1}{2\pi f}s + 1}{hs + 1} \right)^{n-2} \frac{1 - (hs + 1)^{n-1}}{\left(\frac{1}{2\pi f}s + 1 \right)^{n-2} (\tau s + 1)s^2 + \gamma_d s + \gamma_p}. \quad (\text{C.8})$$

Assuming the gains γ_p, γ_d are kept constant, the value of f should increase as n increases in order to achieve stable poles in (C.8). Of course, in practice, the higher the value of f , the higher the amplification of high-frequency measurement noise. Notice also that the order of the filter proposed in (C.7) is higher as the platoon size increases, which might lead to large computation time in a real implementation and also requires more complex PWA models for the stability analysis.

The dynamic feedback proposed before does not compensate for communication delays. Although not discussed here, the stability of the closed-loop transfer function in (3.25) considering time delays could be assessed with graphical methods, such as inspecting the Nyquist plot for the open-loop transfer function, as suggested in [20].

To evaluate the performance of this proposal, a simulation is conducted using the multi-layer CACC strategy with the dynamic feedback law in (C.7). The same scenario described in Section C.1 is used here. In this simulation the timegap is set to $h = 0.3 \text{ sec}$. Figure C.2 shows the time response for acceleration and spacing error. The simulation is performed using two different frequencies for the low-pass filters in (C.7): $f = 1 \text{ Hz}$ and $f = 2 \text{ Hz}$ (these values achieve stable poles in (C.8) for the chosen gains: $\gamma_p = 0.1, \gamma_d = 0.5$). When using $f = 2 \text{ Hz}$, the oscillations in the acceleration of the vehicles decay faster, but the acceleration of vehicle 1 shows a large spike. The spikes in the acceleration a_1 occur when vehicle 10 goes in and out of saturation. This switching introduces high-frequency harmonics in the spacing error e_{10} , which are amplified by the feedback law, thus causing the spikes in the control input for vehicle 1.

The simulation presented before is repeated, but this time for a timegap $h = 0.5 \text{ sec}$ (the plots are not shown here). In this case, spikes in a_1 are observed even when using $f = 1 \text{ Hz}$ in the low-pass filters. Increasing the timegap to $h = 1 \text{ sec}$ results in even larger spikes which cause an unstable behavior. To regain stability, the frequency f or the gains γ_p and γ_d must be reduced. However, the poles in (C.8) become unstable when f is set sufficiently low. This indicates that the dynamic feedback proposed here is not suitable for any timegap h .

It was observed in simulations that, as the slowest vehicle is located further back in the platoon, the spikes in the control input of vehicle 1 increase in amplitude. This leads to conclude that this dynamic feedback is not suitable for platoons with an arbitrary number of vehicles.

From the various attempts to design a feedback law for the multi-layer CACC, it can be concluded that regulating the spacing error of the saturated vehicle at the rear of the platoon just by changing the input to the platoon leader is not an effective solution and leads to the limitations discussed before. An alternative would be to use the coordination layer to also change the input for the vehicles between the slowest and the leader. This would achieve a faster reaction to the changes in spacing error of the saturated vehicle. However, this approach would interfere with the string stability properties of the nominal CACC, which are still present (to some extent) when the coordination layer only affects the input of the platoon leader.

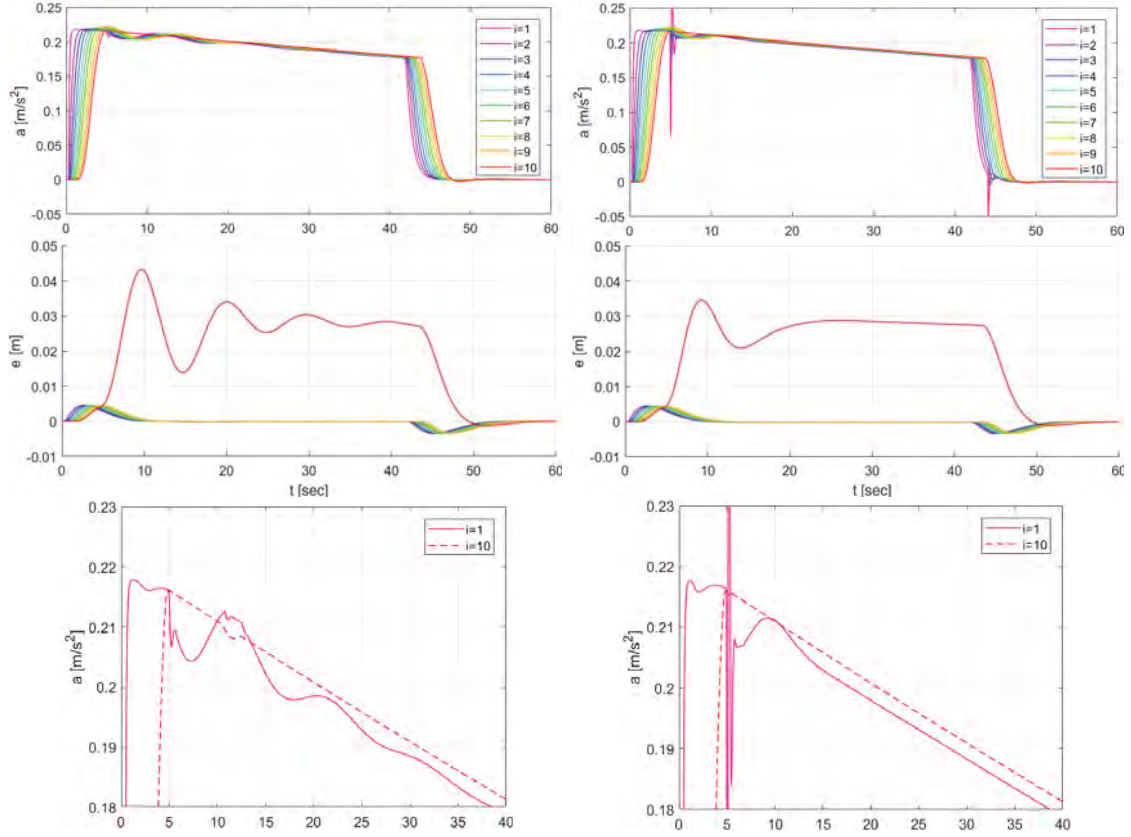


Figure C.2: Time response for acceleration and spacing error of a ten-vehicle platoon subject to the multi-layer CACC strategy with a dynamic feedback law. The plots to the left correspond to the case of a low-pass filter with $f = 1 \text{ Hz}$, while the plots to the right correspond to a low-pass filter with $f = 2 \text{ Hz}$.

C.3 Designing a full state-feedback for the coordination layer

A prior report described a couple of ideas for an output-feedback law to be used in the coordination layer of the multi-layer CACC, this in order to prevent the undesired oscillations in the acceleration of the vehicles, which were observed during the transient periods in simulations. Those ideas were generated while keeping in mind the particular application for this control strategy, i.e., a vehicle platooning problem in which each vehicle has access only to its own states and a single signal is communicated in between contiguous vehicles. This time the problem is approached in a more generic way to be able to apply a different design tool.

It is assumed that the states of all vehicles (i.e., spacing error, velocity, acceleration, and the desired acceleration prescribed by a nominal CACC [13]) are available to construct a full state-feedback in the coordination layer. This feedback is then used to limit the desired acceleration of the platoon leader, while the vehicles between the leader and the slowest continue to use the nominal CACC. Recall that the goal of this multi-layer strategy is to maintain platoon cohesion (i.e., guarantee small spacing errors during accelerating periods) in face of heterogeneous and dynamic acceleration limits in the vehicles.

The coordination variable that is used to limit the desired acceleration of vehicle 1 is defined as

in [23]:

$$\begin{aligned}\xi_i(t) &= \min[y_i(t), \xi_{i+1}(t)], \text{ for } i \in \{2, \dots, n-1\} \\ \xi_n(t) &= y_n(t),\end{aligned}\tag{C.9}$$

where the scalar variable y_i contains the acceleration limit of vehicle i and a feedback term, as follows:

$$\begin{aligned}y_i(t) &= a_{max,i}(v_i) - \delta_i(t) \\ \dot{\delta}_i(t) &= 2\pi f \left(-\delta(t) + K_i(t) (x_1^T, \dots, x_i^T)^T + k_i(t) \right), \text{ for } i \in \{2, \dots, n\}, \\ x_1(t) &= (v_1, a_1)^T \\ x_i(t) &= (e_i, v_i, a_i, u_i)^T\end{aligned}\tag{C.10}$$

where e_i , v_i , a_i , and u_i are the spacing error, velocity, acceleration, and desired acceleration of vehicle i , respectively. The term $\delta(t)$ is the output of a low-pass filter with some cut-off frequency f (the reason for including this filter is explained later on). The variable $K_i(t)$ is a vector of gains associated to the states of vehicles 1 to i , while $k_i(t)$ is an affine term. While designing this feedback, it is assumed that the values for K_i and k_i can switch depending on the current operation mode of the platoon.

The feedback law proposed in (C.10) is a general definition that encloses the less flexible feedback law proposed in [23], which specifies a feedback term $\delta_i(t)$ that depends only on the spacing error $e_i(t)$ and its time derivative $\dot{e}_i(t)$, together with constant gains: $K_i = K$, $k_i = 0$, $\forall i \in \{2, \dots, n\}$, $\forall t > 0$.

The design of the state-feedback proposed in (C.10) is based on a piecewise affine (PWA) system that describes the various operation modes of the closed-loop dynamics of the vehicle platoon. Each mode is described by linear dynamics and the switching between these modes is based on linear functions of the states (i.e., hyperplanes in the state space). However, attempting to design all the gains $K_i(t)$ and terms $k_i(t)$ at the same time would require a PWA system with an unmanageable amount of operation modes (i.e., several regions in the state space). As a first attempt to evaluate this control approach, the procedure presented below focuses on designing only the gains $K_n(t)$ and the term $k_n(t)$, while making some assumptions that allow for a simple PWA system.

The first assumption for the vehicle platoon is that vehicle n is the one with the lowest acceleration limit (i.e., $a_{max,n}(t) < a_{max,i}(t)$, $\forall t > 0$, $i \in \{1, \dots, n-1\}$). This allows to assume that the information communicated to vehicle 1 through the coordination variable ξ_2 originates in vehicle n (i.e., $\xi_2 = y_n$). Furthermore, it is assumed that the limit of vehicle n is sufficiently small compared to the limits of the other vehicles. This means that only vehicle n might reach its acceleration limit at some point in time. This is a reasonable assumption because, thanks to the coordination layer, the leading vehicle would be driving slightly below $a_{max,n}$. Then, because of the CACC in the lower layer of this strategy, the desired acceleration for vehicles 2 to $n-1$ is set below $a_{max,n}$, provided the initial spacing errors for these vehicles are small.

With the assumptions stated above, the closed-loop platoon dynamics subject to the multi-layer CACC can be modelled with a PWA system that consists of a state space partitioned into four regions delimited by two hyperplanes. The first hyperplane indicates a switching in the desired acceleration of vehicle 1, as follows:

$$u_{ref,1}(t) = \min [k_v(v_{des} - v_1), \xi_2],\tag{C.11}$$

where the first argument of the min function is a simple cruise controller (with some gain $k_v > 0$, and v_{des} a desired cruising speed), and $\xi_2(t) = a_{max,n}(v_n) - \delta_n(t)$ (because of the aforementioned assumptions). Notice that, thanks to the low-pass filter associated to the feedback term $\delta_n(t)$ [see (C.10)], the equation of the hyperplane associated to (C.11) is independent of the choice of $K_n(t)$ and $k_n(t)$, which is crucial for the design procedure described below.

The second hyperplane in the PWA model denotes the saturation in the desired acceleration of vehicle n :

$$u_{ref,n}(t) = \min [u_n , a_{max,n}(v_n)], \quad (C.12)$$

where u_n is the desired acceleration prescribed by the CACC and the acceleration limit $a_{max,n}$ is described with a linear function (i.e., $a_{max,n}(v_n) = \alpha_n v_n + \beta_n$, with some constants $\alpha_n < 0$, $\beta_n > 0$).

The PWA system in question can be written as:

$$\begin{cases} \dot{x}(t) = A_j x(t) + b_j + B_j w(t) \\ w(t) = -K_{(n,j)} x(t) - k_{(n,j)} \end{cases}, \text{ for } x(t) \in \mathcal{X}_j, j \in \mathcal{J} = \{1, \dots, 4\}, \quad (C.13)$$

where $x = (x_1^T, \dots, x_n^T, \delta_n)^T$ is a lumped state vector, A_j are the system matrices, b_j are affine terms, and B_j are the input matrices. The scalar input $w(t)$ is the state feedback that needs to be designed. The sets \mathcal{X}_j correspond to the different regions of the state space (i.e., unbounded polyhedra); the subscript j denotes the index of the region. Notice that the input $w(t)$ is a piecewise-affine state-feedback because the gain vectors $K_{(n,j)}$ and affine terms $k_{(n,j)}$ might change depending on the region \mathcal{X}_j . Furthermore, the input $w(t)$ affects only the controller state $\delta_n(t)$, as defined in (C.10), and $B_j = B, \forall j \in \mathcal{J}$.

To design the PWA state-feedback $w(t)$ in (C.13), the procedure described in [4] is used, which relies on solving a bilinear matrix optimization problem. The idea is to solve a set of bilinear matrix inequalities (BMIs) while finding an upper bound for the following cost function:

$$J(x_0, w(t)) = \int_0^\infty (x(t)^T Q x(t) + w(t)^T R w(t)) dt \quad (C.14)$$

with Q and R positive definite matrices, and some initial state $x_0 = x(0)$, assuming the system reaches the equilibrium $x(\infty) = 0$. The BMIs that must be solved are [4]:

$$\begin{bmatrix} (\bar{A}_j - \bar{B}_j \bar{K}_{(n,j)})^T \bar{P}_j + \bar{P}_j (\bar{A}_j - \bar{B}_j \bar{K}_{(n,j)}) + Q + \bar{E}_j^T U_j \bar{E}_j & \bar{K}_{(n,j)}^T \\ \bar{K}_{(n,j)} & -R^{-1} \end{bmatrix}, \text{ for } j \in \mathcal{J}, \quad (C.15)$$

with symmetric matrices $\bar{P}_j = \bar{F}_j^T T \bar{F}_j$, where T is an unknown symmetric matrix, and \bar{F}_j are continuity matrices (see Appendix A).

The matrices \bar{A}_j are augmented system matrices containing A_j and b_j (see (3.11)). The matrices $\bar{B}_j = [B_j^T \ 0]^T$ are augmented input matrices. Then, $\bar{K}_{(n,j)} = [K_{(n,j)} \ k_{(n,j)}]$ are augmented gain matrices. Matrices U_j are unknown symmetric matrices with non-negative entries. Finally, matrices \bar{E}_j are region-bounding related to the S-procedure, as described in Appendix A.

A solution to (C.15) provides an upper bound for (C.14), as follows [4]:

$$J(x_0, w(t)) \leq \inf_{T, U_j} [x_0^T \ 1] P_{j0} \begin{bmatrix} x_0 \\ 1 \end{bmatrix} \quad (C.16)$$

with initial state $x_0 = x(0) \in \mathcal{X}_{j_0}$, with $j_0 \in \mathcal{J}$. Optimization problems involving BMIs are in general non-convex [4]. The linearization method proposed in [4] is used to address this optimization problem, as described next.

The idea is to provide some initial gain matrices $\bar{K}_{(n,j)}^0$ for which (C.15) can be solved (i.e., substitute $\bar{K}_{(n,j)} = \bar{K}_{(n,j)}^0$, and solve the resulting linear matrix inequalities for matrices \bar{P}_j and U_j). Then, substituting $\bar{P}_j = \bar{P}_j^0 + \delta \bar{P}_j$ and $\bar{K}_{(n,j)} = \bar{K}_{(n,j)}^0 + \delta \bar{K}_{(n,j)}$ in (C.15) and neglecting the cross-terms $(\delta \bar{K}_{(n,j)})(\delta \bar{P}_j)$, linear matrix inequalities are obtained with $\delta \bar{P}_j$, $\delta \bar{K}_{(n,j)}$, and U_j as unknowns. This set of LMIs is solved while minimizing the function $\bar{x}_0^T (\delta \bar{P}_{j_0}) \bar{x}_0$, where $\bar{x}_0 = [x_0^T \ 1]^T$. An additional constraint is included to guarantee a valid linearization: $\|\delta \bar{P}_j\| \leq \alpha \|\bar{P}_j^0\|$.

This linearization method is repeated until no further improvement can be achieved in the cost function.

The procedure discussed above leads to a PWA state feedback that is in general discontinuous at the boundary between regions (i.e., $K_{(n,p)}x + k_{(n,p)} \neq K_{(n,q)}x + k_{(n,q)}$, for $x \in \mathcal{X}_p \cap \mathcal{X}_q$, with $p, q \in \mathcal{J}$). A continuous state feedback is preferred because in that case the stability of the PWA system for the resulting closed-loop dynamics can be proved without having to account for Fillipov solutions that might arise from the discontinuity in the dynamics at the boundary between regions. Hence, as suggested in [4], the unknown matrices $\delta\bar{K}_{(n,j)}$ are redefined as $\delta\bar{K}_{(n,j)} = S\bar{F}_j$, where S is an unknown vector and \bar{F}_j are continuity matrices as defined previously.

A major limitation in the design procedure explained before is that one must be able to provide an initial state feedback for which (C.15) can be solved. Fortunately, a possible choice for the initial matrices $\bar{K}_{(n,j)}^0$ can be obtained from the original multi-layer CACC in [23], which corresponds to a continuous output-feedback without affine terms (i.e., $K_{(n,j)}^0(t) = K_n^0$ and $k_{(n,j)}^0(t) = 0$, $\forall j \in \mathcal{J}, \forall t > 0$). This is the starting point for the bilinear matrix optimization problem that leads to a piecewise-affine, full state-feedback.

To provide an illustrative example, the design procedure described above is applied to the PWA system that describes a 10-vehicle platoon, where vehicle 10 has a significantly lower acceleration limit. The control gains for the CACC in the lower layer and other vehicle parameters are taken from [23] (communication and actuation delays, as well as the aerodynamic drag, are neglected to allow for linear systems in the PWA model; no gear-shifting is considered here). The time-gap for the spacing policy is set to $h = 0.3s$. An initial state must be chosen, which in this case is set to $v_i = 60km/h$, $a_i = u_i = 0m/s^2$, $e_i = 0m$, and $\delta_{10} = 0$. The desired cruising speed is set to $v_{des} = 100km/h$.

The initial state-feedback for the iterative procedure is chosen based on the output-feedback proposed in [23], so that the dynamics of the controller state $\delta_{10}(t)$ in the first iteration are given by:

$$\dot{\delta}_{10}(t) = 2\pi f(-\delta_{10}(t) + \gamma_p e_{10}(t) + \gamma_d \dot{e}_{10}(t)), \quad (C.17)$$

with $f = 10Hz$, gains $\gamma_p = 0.02$, $\gamma_d = 0.25$, and $\dot{e}_{10}(t) = v_9 - v_{10} - ha_{10}$. These values are chosen because they lead to feasible LMIs in (C.15). The matrix Q is chosen such that the weight associated to the state e_{10} is equal to 1, while the weight associated to the other states is 0.01. The weight associated to the input $w(t)$ is chosen as $R = 1$.

After around 40 iterations of the linearization method described before, four gain vectors $\bar{K}_{(10,j)}$ and four matrices \bar{P}_j are obtained. With the resulting PWA state-feedback, the upper bound for the cost function (C.14) computes to $J(x_0, w(t)) \leq \bar{x}_0^T \bar{P}_3 \bar{x}_0 = 3.86 \cdot 10^3$, while the bound obtained using the initial output-feedback is $\bar{x}_0^T \bar{P}_3^0 \bar{x}_0 = 15.05 \cdot 10^3$. In this example the initial conditions correspond to a point in region \mathcal{X}_3 , which is why matrices \bar{P}_3 and \bar{P}_3^0 are used for the computation of the upper bound. The response for acceleration and spacing error of the 10-vehicle platoon is shown in Figure C.3, where a comparison is offered between the initial output-feedback (C.17) and the optimized state-feedback.

From Figure C.3, it is evident that the magnitude of the spacing error is lower when using the optimized state-feedback. Notice in the detailed view for acceleration that, with the initial output-feedback, vehicle 10 accelerates up to its limit and keeps driving in saturation until the predecessors reach the desired velocity. On the other hand, when using the optimized state-feedback, vehicle 10 reaches its acceleration limit at around $t = 5s$, but then it goes out of saturation at around $t = 22s$. This happens because the state feedback is setting a desired acceleration for vehicle 1 that eventually makes vehicle 10 to accelerate below $a_{max,10}$, so vehicle 10 ends up driving in CACC mode. Although not illustrated here, depending on the chosen weight matrices Q and R , the state-feedback resulting from the optimization procedure might cause vehicle 10 to drive significantly below $a_{max,10}$, which of course increases the time required to reach the desired velocity.

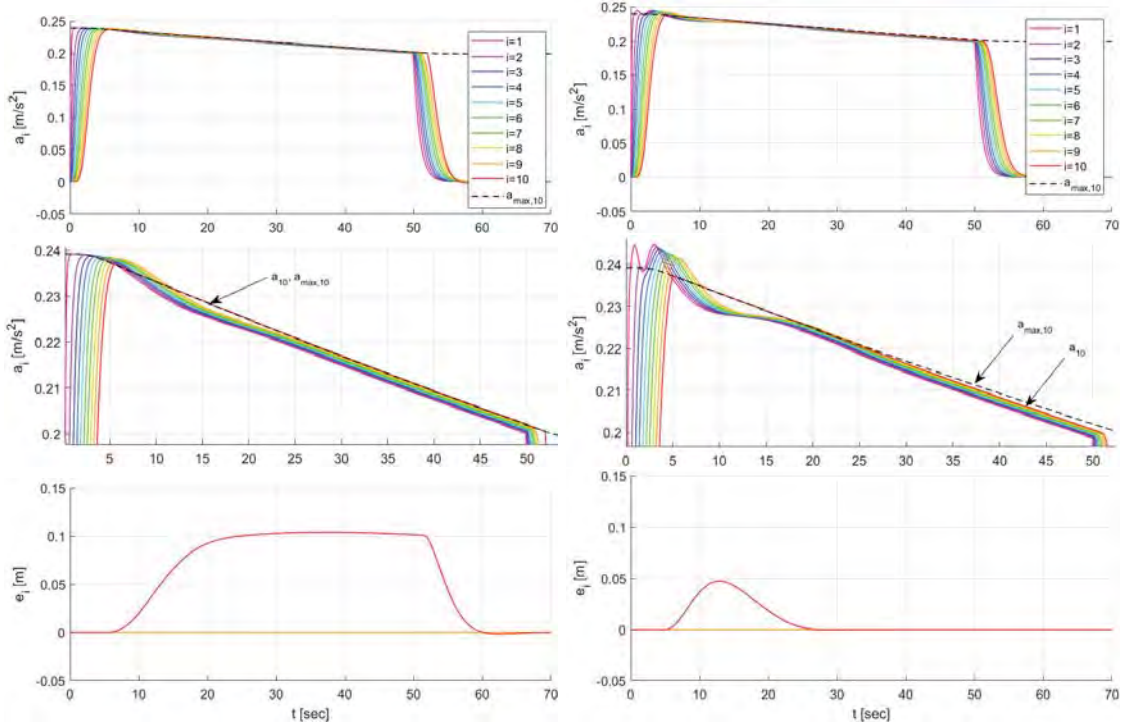


Figure C.3: Time response for acceleration and spacing error of PWA system describing a ten-vehicle platoon. The plots to the left correspond to the simulation with the output-feedback in (C.17), while the plots to the right correspond to the simulation with the PWA state-feedback obtained through bilinear matrix optimization.

Unfortunately, from the simulation example presented before, little benefit arises from the optimized state-feedback, compared to the output-feedback from [23]. Moreover, when trying to design a state-feedback for the simulation scenario described before but using a larger timegap, $h = 1s$, it was not possible to find a value for the gain vectors $\bar{K}_{(10,j)}^0$ based on the output-feedback (C.17) that makes the LMIs in (C.15) feasible, so that one has no starting point for the bilinear matrix optimization. It might be possible to find a suitable initial feedback through some other procedure, but it can be concluded that finding the initial feedback is harder as the platoon size or the timegap increase.

An additional disadvantage of the state-feedback proposed here is related to the implementation in a real vehicle platoon. The feedback signal is, in general, a function of the states from all the vehicles in front of the slowest. To implement this state-feedback in a distributed fashion, a coordination variable could be used that is communicated downstream from vehicle p (assuming vehicle p is the slowest) towards vehicle 1. The states of the vehicles multiplied by their associated gains are added to this coordination variable as it travels downstream, such that in the end vehicle 1 receives a variable equal to $K_{(p,j)}x(t) + k_{(p,j)}$. Additionally, vehicles 1 to $p-1$ should be informed of what are the control gains associated to their states (i.e., the relevant gains in vectors $\bar{K}_{(p,j)}$), as well as the operation mode of the platoon (i.e., which region \mathcal{X}_j is currently applicable). Furthermore, if at some point in time the vehicle with the lowest acceleration limit changes from index p to a different index q , then the gain vector $\bar{K}_{(q,j)}$ for the state-feedback would need to be communicated to vehicles 1 to $q-1$, because in general $\bar{K}_{(p,j)} \neq \bar{K}_{(q,j)}$.

From the discussion in the previous paragraph, it can be concluded that the performance improvement offered by the state-feedback proposed here is outweighed by the difficulties associated to the implementation and the fact that an initial feedback that makes (C.15) feasible is needed.

